KU Leuven

Faculty of Bioscience Engineering

Doctoraatsproefschrift nr. 1078 aan de faculteit Bio-ingenieurswetenschappen van de KU Leuven

MODELING AND BIOPHYSICAL CHARACTERISATION OF THE PRIMARY GUSHING MECHANISM IN BEER

Interaction between gaseous carbon dioxide and Class II hydrophobins

Sylvie DECKERS

Supervisors:
Prof. G. Derdelinckx, KU Leuven
Prof. C. Michiels, KU Leuven

Members of the Examination Committee:
Prof. Em. A. Maes, KU Leuven, Chair
Prof. J. Martens, KU Leuven
Prof. J.A. Delcour, KU Leuven
Prof. M. De Maeyer, KU Leuven
Prof. H. Neven, KU Leuven
Prof. M. Linder, VTT Research Centre, Tietotie, Finland
Dr. J. Titze, University College Cork, Cork, Ireland

Dissertation presented in partial fulfilment of the requirements for the degree of Doctor of Bioscience Engineering

February 2013

ISBN 978-90-8826-285-2
Wettelijke depot D/2013/11.109/12

A mes parents,
A mon frère,
A Jean-Pol et Maria

Dankwoord

Omwille van de gevoeligheid en de emotie gebonden aan de nodige justheid van de gebruikte woorden heb ik, voor dit dankwoord, liever mijn moedertaal gebruikt. VONDEL waarvan ik de taal tijdens de twee eerste jaren van mijn Ph.D., met assiduiteit geleerd heb zal me dit wel niet kwalijk nemen.

Cette thèse de doctorat est le résultat de plusieurs années de travail scientifique en équipe et je voudrais remercier les personnes qui y ont contribué. Ce travail représente également 4 années de ma vie qui resteront inoubliables.

Tout d'abord, je tiens à remercier Monsieur H. Neven, instigateur de la Chaire Hydrophobine visant l'étude et la compréhension du gushing primaire et Monsieur J-M. Rock pour son soutien permanent.

Ensuite je tiens à exprimer ma profonde gratitude à mon promoteur le Professeur Guy Derdelinckx. Malgré les nombreuses discussions étayées régulièrement de l'expression "St….. Ingenieure", je tiens à lui adresser toute ma reconnnaissance pour son encadrement, son expérience, son écoute, ses conseils,… bref tout ce qui m'a permis d'évoluer et de grandir tant d'un point de vue professionnel que d'un point de vue personnel. Merci également pour les moments de "détente" autour d'un verre, d'un délicieux repas et sans oublier ses petites piques sur le Standard. Mais grâce à sa disponibilité, ses qualités pédagogiques et scientifiques, j'ai beaucoup appris à ses côtés et je lui adresse un grand merci.

Merci au Professeur Em. Hubert Verachtert pour son implication constante pendant 4 ans : que ce soit par ses suggestions, ses questions pertinentes, ou sa relecture des articles et du manuscript.

Je remercie également les communautés cisterciennes trappistes de Belgique anisi que la famille Moortgat (Brasserie Duvel-Moortgat) et la Malterie Cargill pour leur intérêt scientifique et leur participation. Sans eux, je n'aurais pu réaliser cette thèse. Merci à Hedwig (Neven) et Dimitri (Staelens) (Duvel), Jean-Marie (Rock) et Anne-Françoise (Pypaert) (Orval), Dominique (Denis), Pierre (Etienne), Xavier (Pirlot) et Paul (Arnott) (Chimay), Sébastien (Frère), Steven (Vangoidsenhoven) et Vincent (Loriau) (Cargill) pour leurs participations actives aux réunions, que je redoutais mais qui furent toujours un très bon exercice. Merci à Antonio (Fumanal) et Jorge (Roehrich) (La Zaragozana), à Karl (Dingemans) (malterie Dingemans), à Peter (De Schouwer) et à Geert (Van D'huynslager) (Boortmalt) pour les échantillons et équipements fournis.

Merci également aux Professeurs Chris Michiels, Jan Delcour, Johan Martens, Marc Hendrickx et Paul Proost, et au Dr Geert Baggerman pour leurs conseils ainsi que pour m'avoir permis de travailler dans leur laboratoire et d'utiliser les équipements nécessaires à la réalisation de ce travail. Merci aux Dr Kurt Gebruers et Yannick Lorgouilloux, de m'avoir encadrée, conseillée et soutenue tout au long de cette thèse et dans les moments difficiles mais aussi pour leur aide scientifique et pratique et leur regard critique sur le projet. Merci au Professeur Marc De Maeyer et son assistant Tom Venken pour leur collaboration éclairée sur la partie consacrée à la modélisation.

Merci à l'American Society of Brewing Chemists d'avoir reconnu le travail accompli en m'attribuant le prix Brian William Scholarship et de m'avoir permis de me faire connaître sur le plan international.

Merci à mes collègues du laboratoire et à mon étudiant, Lennert Vissers.

Merci à Christa pour toutes les tâches administratives, qu'elle a toujours accomplies avec sérieux et avec le sourire.

Merci à l'équipe féminine du RCS Nivellois de m'avoir permis d'évacuer le stress et la pression de temps en temps.

Merci à mes parents et mon frère de m'avoir soutenue tout au long de cette période.

Merci à vous tous et aux personnes que j'aurais malencontreusement oubliées, qui de près ou de loin, ont contribué à la réalisation de ce travail. Ce fut une expérience des plus enrichissantes tant au point de vue humain que professionnel.

Encore MERCI à toutes et tous! Et vive le Standard qui comme ma recherche m'a procuré les pires déceptions et les joies les plus intenses!

Abstract in Dutch

Het “gushing” fenomeen is omschreven als het spontaan en ongecontroleerd overschuimen van gecarbonateerde dranken bij het openen van niet geschudde flessen. Gushing wordt alleen gedetecteerd na het bottelen en leidt tot grote economische en imago schade. Een mechanisme gekend als secundaire gushing is goed omschreven en is het gevolg van de aanwezigheid van externe anorganische stoffen of van technische proces tekortkomingen. Primaire gushing is echter veel nadeliger en een gedetailleerd mechanisme staat nog steeds ter discussie, al is wel geweten dat proteïnen zoals klasse II hydrofobinen, ontstaan door schimmelbesmettingen, verantwoordelijk zijn. Ondanks 25 jaar onderzoek is het proces niet volledig begrepen al werd verondersteld dat hydrofobinen belletjes van CO_2 kunnen stabiliseren. Hoe dit geschiedt en in hoevere zulke structuren stabiel zijn is niet geweten. Dit werd het vraagstuk van ons onderzoek.

De twee partners nodig voor gushing zijn klasse II hydrofobinen en CO_2. Het klasse II hydrofobine HFBI werd geëxtraheerd uit het mycelium van opgekweekte *Trichoderma reesei* MUCL 44908, opgezuiverd door RP-HPLC, gedetecteerd door MALDI-TOF en geïdentificeerd door Edman sequentiebepaling. Standaard bruisend water werd gebruikt als koolzuurbron. De fysico-chemische eigenschappen van klasse II hydrofobinen en van CO_2 werden uitvoerig bestudeerd. Door moleculaire dynamische simulatie werd gevonden dat moleculen van CO_2 aan de hydrofobe patch van klasse II hydrofobinen binden. Dit heeft geleid tot het voorstellen van een gedetailleerd mechanisme voor de vorming van nanobellen die door hydrofobinen gestabiliseerd worden. Dit geschiedt in stappen: *migratie* van hydrofobinen naar de interfase vloeistof-gas, *contaminatie* door het gas (contact met zuivere CO_2 atmosfeer), *concentratie* en daarna *kristallisatie, schudden* met als gevolg verstoring van het koolzuurevenwicht (wet van Henry) in de gesloten fles, terugkeer naar het evenwicht door de *vorming van gesloten nanobellen* (wet van Young-Laplace). Een ongeopende fles bevat dan CO_2 gasnanobellen gestabiliseerd door een kristallijne laag van klasse II hydrofobine. Deze strukturen worden gekenmerkt door een geometrische waarde als het volume wordt bepaald door de kritische diameter van CO_2 bij een bepaalde druk in de fles. De ontploffing van de bellen, *i.e.* “nanobomb effect”, kan worden beschreven door de wet van Avogadro maar vooral door de wet van Boyle-Mariotte want de temperatuur speelt slechts een kleine rol. De invloed van temperatuur op primaire gushing past niet met deze theorie in praktijk. Inderdaad schuimt er veel meer vloeistof uit de fles dan dat kan worden voorspeld door verhoging van de temperatuur bij opening. Dit geeft aan dat naast de chemische binding, veel CO_2 met elkaar verbonden wordt door een lage energiebinding die door trillingsenergie kan worden doorbroken.

Daar klasse II hydrofobinen CO_2 gasbelletjes kunnen stabiliseren, wat leidt tot partikels met een bepaalde diameter bij atmosferische druk, werd er gezocht naar een detectie methode gebaseerd op dynamische lichtverstrooiing (DLS). De detectie van zulke nanopartikeltjes met DLS maakt het mogelijk primaire gushing (hydrofobine) te onderscheiden van secundaire gushing (*b.v.* kieselghur). Het is gebaseerd op de aanwezigheid van 100 nm partikeltjes die worden gevormd in het overschuimen na rust onder gesatureerd CO_2 (1 bar) wanneer hydrofobinen aanwezig zijn. De 100 nm is de kritische diameter van CO_2 bij atmosferische druk. De methode toont duidelijk aan of de gushing primair of secundair is. Deze detectie methode werd ook gebruikt om de aanwezigheid van hydrofobinen aan te tonen in gerst en mout en kan duidelijk niet-gecontamineerde grondstoffen onderscheiden van gecontamineerde. Het doel is deze methode aan te bevelen bij de industrië om de goede resultaten te bevestigen.

Het werk doet ten slotte suggesties om primaire gushing te voorspellen en/of op te lossen.

Abstract

The gushing of carbonated beverages is defined as a spontaneous wild and uncontrolled overfoaming upon opening of non-shaken bottles. As overfoaming is detected after bottling this results in significant economic and image losses to the producer. A mechanism referred to as secondary gushing is well understood and is due to the presence of external inorganic material or technical shortcomings. On the other hand, the very disastrous primary gushing mechanism is still under discussion although it is known it is related to the presence of fungal proteins, the Class II hydrophobins. Despite 25 years of research, several parts of the puzzle are still missing. Recent reviews on the phenomenon indicate that hydrophobins may stabilize gaseous CO_2 bubbles without explaining however how this occurs and how coated bubbles are made and gain stability.

We studied how the two main factors, Class II hydrophobins and CO_2 interact to induce gushing. Class II hydrophobin HFBI was extracted from the mycelium of *Trichoderma reesei* MUCL 44908 with a Tris/HCl buffer, purified by RP-HPLC, detected by MALDI-TOF and identified by Edman amino acid sequencing. Sparkling water was used as source of CO_2. Considering the physico-chemical properties of both Class II hydrophobins and CO_2 and by performing molecular dynamics simulation, it was observed that CO_2 molecules interact with the hydrophobic patch of Class II hydrophobin and a detailed mechanism formation of coated CO_2 bubbles, the stabilized nanobubbles, was proposed. It occurs in several steps : *migration* of hydrophobins to the liquid-gas interface, *contamination* by contact with pure CO_2 atmosphere, *concentration* followed by *crystallization*, *shaking* causing imbalance of Henry's equilibrium in the closed recipient, re-equilibrium resulting in the *nanobubble formation* by closing due to the lateral forces (Young-Laplace forces). Finally, the closed bottle contains gaseous CO_2 nanobubbles stabilized by a crystalline layer of Class II hydrophobin. These solid structures are characterized by a consistent geometric value as their volume is determined by the critical diameter of CO_2 at the pressure in the bottle. The explosion of the bubble, *i.e.* the "nanobomb effect", can be described by Avogadro's law and even by Boyle-Mariotte's law since temperature has a small influence. Nevertheless, primary gushing behavior in function of temperature does not fit with this theory in practice. Indeed, much more liquid than could be predicted is expelled from the bottle by increasing the liquid temperature at the opening. This indicates that beside the chemical binding, a lot of CO_2 is linked by low energy bonds that can be broken just by agitation energy.

Since Class II hydrophobins are able to stabilize gaseous CO_2 bubbles, which must have a critical diameter at atmospheric pressure a method based on the dynamic light scattering was developed. This novel method allows to distinguish primary (hydrophobin) from secondary (kieselghur) gushing. It is based on the presence of 100 nm particles which are formed in the overfoamings after rest under saturated CO_2 (1 bar) only when hydrophobins are present. The 100 nm diameter corresponds to the critical diameter of CO_2 at atmospheric pressure. The method clearly indicates whether the gushing of bottled beer is either primary or secondary. This method was also applied to predict the gushing potential of barley and malt and can distinguish contaminated from non-contaminated raw materials. The target is to further propagate this method in order to confirm at industrial scale the good results obtained.

Finally, the work describes some suggestions in order to prevent and/or to cure primary gushing.

List of abbreviations and list of symbols

Å : Angström

Ala : alanine; Cys : cysteine; Gly : glycine; Ile : isoleucine; Leu : leucine; Val : valine

ASA : accessible solvent area

ASBC : American Society of Brewing Chemists

atm : atmosphere

°C : degree Celsius; K : degree Kelvin

Da : Dalton

DLS : Dynamic light scattering

dw : dry weight

EBC : European Brewing Convention

e.g. : example given

ELISA : Enzyme linked immunosorbent assay

FA : formic acid

FHB : *Fusarium* head blight

FWHM : full width at half maximum

γ : surface tension

h : hour; min : minute; sec : second; ns : nanosecond; ps : picosecond; fs : femtosecond

i.e. : *id est*

J : Joule

kg : kilogram; g : gram; mg : milligram; µg : microgram

λ : wavelength

L : Liter; mL : milliliter; µL : microliter

M : molar; mM : millimolar

m : meter; cm : centimeter; mm : millimeter; nm : nanometer

MΩ : megaohm

MALDI-TOF : Matrix assisted laser desorption ionization – time of flight

MD : molecular dynamics

MOE : molecular operating environment

mol : mole

η : dynamic viscosity of fluid

n.d. : not determined

NMR : Nuclear Magnetic Resonance

N.m : Newton meter

ns-LTP : non specific lipid transfer protein

OPLS AA : Optimal potential for liquid simulation all atom

Pa : Pascal

PCR : Polymerase chain reaction

RP-HPLC : Reverse phase High Performance Liquid Chromatography

rpm : revolution per minute

SDS : sodium dodecyl sulfate

T : temperature

TFA : trifluoroacetic acid

T. reesei : *Trichoderma reesei*

15RPC : reverse phase column with 15 µm diameter beads

Table of contents

Literature review

The history of primary gushing

- The definition of gushing

The first paper describing gushing in beer has been published in **1909** by Kastner, a German brewing scientist (Kastner, 1909). However, the history of gushing (Figure 1) probably dates back to the invention of bottled carbonated beverages by the English chemist Joseph Priestley in **1772** (Pellaud, 2002).

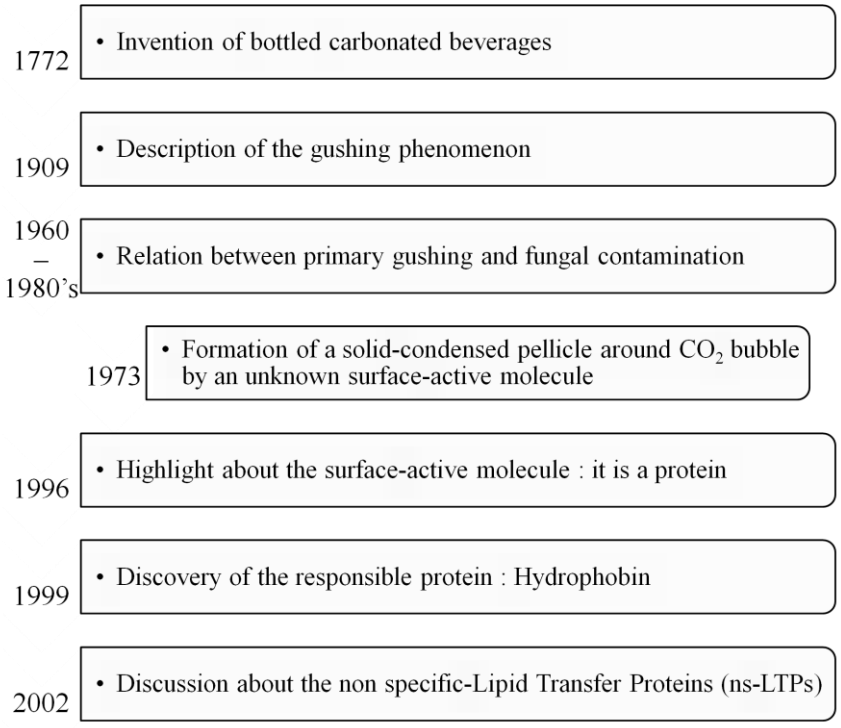

Figure 1: The history of primary gushing.

As a first approach, beer gushing can be described as a strong foam and beer overflow after opening beer bottles without any shaking (Figure 2).

Figure 2: Class II hydrophobins cause gushing. In this experiment, a mycelium extract of *Trichoderma reesei* (*T. reesei*) containing the Class II hydrophobin HFBI was added to a 330 mL bottle of beer and the bottle was shaken for three days prior to opening. The pictures from left to right were taken separately in a few seconds (Shokribousjein *et al.*, 2010).

Although gushing is not a "privilege" of beer and has been observed in other carbonated beverages such as champagne and sparkling wine (Zoecklein, 1999), cider (Wilson *et al.*, 1999), soda and even mineral water (Fischer, 2001), it seems to be most relevant in beer (Pellaud, 2002). Gushing is divided in two types : primary and secondary gushing. Primary gushing is related to contaminated raw material while secondary gushing is due to technical and technological problems (oxalate crystals, filter aids,…) (Pellaud, 2002). Only primary gushing will be reviewed here as the secondary gushing mechanism (solid particles or adsorbed gas residues acting as nucleation site) is well understood.

- The fungal contamination.

Between **1960 and the 1980's**, research mainly focused on the finding of visible causes of gushing such as fungal contamination of raw material by molds (Pellaud, 2002). *Fusarium sp.* and other molds such as *Aspergillus*, *Nigrospora*, *Penicillium*, *Rhizopus* and *Stemphylium* were reported to cause gushing (Flannigan *et al.*, 1982; Gyllang *et al.*, 1981). Nevertheless, contaminated raw material was in general considered as responsible for gushing and some authors reviewed the communities that colonize barley grains extensively (Noots *et al.*, 1998; Laitila, 2007). Their target was to isolate on the one hand microorganisms that can be useful to reduce the damaging communities and on the other hand to identify the ascomycetes described as responsible for primary gushing. Primary gushing is associated with malt prepared from barley at late-harvest time and in wetter seasons and is directly corresponding to the growth of microorganisms on the barley kernels under moist conditions (Flannigan, 2003). In general, filamentous fungi on barley and other cereals are classified as either field or storage fungi (Noots *et al.*, 1998). Field fungi such as *Fusarium* and *Alternaria* colonize the plants and occur outside/inside the grains until harvesting. They are more prevalent when rainfall is more than usual during grain fill and harvest. In the field, barley kernels are already colonized by microbes immediately after ear emergence from the enveloping leaf-sheaths (Flannigan, 2003) and colonization continues throughout the growing season (Noots *et al.*, 1998). At later stages of kernel filling, microbial colonization is restricted to the outer parts of the developing kernels, between the testa and the outer epidermis (Figure 3).

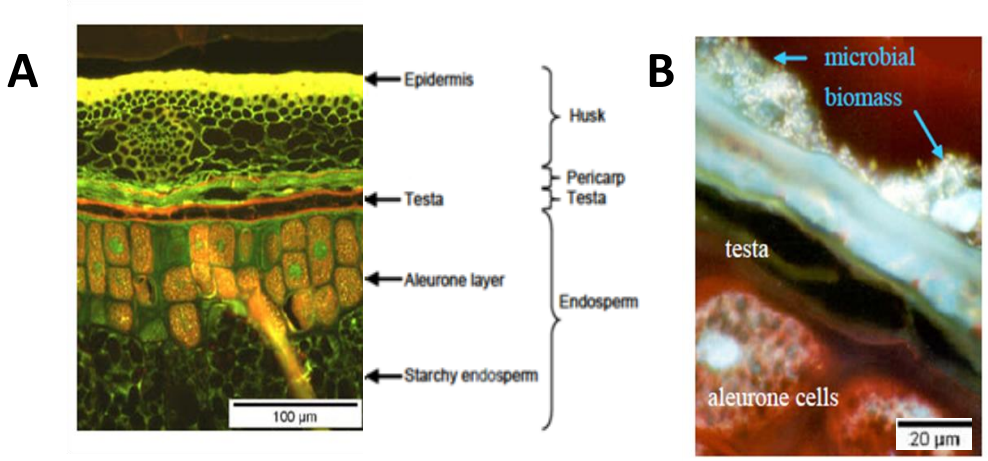

Figure 3: Location of the contaminant on the grain (Adapted from Laitila, 2007). **A**: Barley grain structure where the three cutin layers (between the husk and pericarp, between the pericarp and testa, and between the nucellus and endosperm) are stained red by Oil Red O. **B**: The microbial biomass is located in a pericarp cell (*i.e.* outside the testa layer and below the husk).

Occasionally, and in particular if the testa for some reason is injured, invasion of the endosperm is caused by fungi such as *Fusarium sp.* (Laitila, 2007). If grain is stored at the proper moisture content and temperature, field fungi do not further develop, as they do not grow at a water activity below 0.90 (Noots *et al.*, 1998). On the other hand, storage fungi such as *Aspergillus* and *Penicillium* are usually present in dust and air of the storage environment and can also be found in different farm and malting equipments (Laitila, 2007). They invade grains or seed during storage but are usually not present in any serious extent before harvest. Small quantities of spores of storage fungi may be present on grain going into storage or may be present on spilled grain present in harvest, handling and storage equipment or structures. Under non appropriate storage conditions this low degree of infection increases rapidly leading to significant problems. Although the vegetative forms of molds progressively die upon proper storage, the spores on the grain remain viable and can be activated during condition prevailing during the malting process (Flannigan *et al.*, 1982; Noots *et al.*, 1998). In fact the malting conditions are highly favorable for microbial growth in terms of available nutrients, temperature, moisture content and gaseous atmosphere (Laitila, 2007). The conclusion of this research period according to Professor De Clerck in 1973 was : **"Gushing is due to the moist barley on which too much molds have developed. *Fusarium* are mostly responsible for this phenomenon but it is unclear which *Fusarium* substances play the major role."** (De Clerck, 1973)

- The solid-condensed pellicle

In **1973**, instead of focusing on the molecules responsible for primary gushing, Gardner reviewed gushing with a particular attention to what is known about the stability of supersaturated solutions and bubble formation (Gardner, 1973). In fact, gushing is also characterized by a huge number of tiny bubbles forming throughout the liquid, expanding and rising very rapidly as a consequence of the sudden release of gas (Pellaud, 2002). Gushing does "look like" a nucleation phenomenon. The term nucleation is used to denote any process that leads to the formation of a bubble (Jones *et al.*, 1999). The work required for *de novo* formation of a bubble is given by the equation 1:

$$W = \frac{16\ \pi\gamma^3}{3(P' - P'')^2}$$

(Equation 1) (Gardner, 1973)

where W = work required, γ = surface tension of the liquid, P' = pressure inside the bubble and P'' = pressure in the liquid phase. This equation suggests that spontaneous bubble formation (when W = 0) only occurs at very high supersaturation such as 100 or more. However, in practice, homonucleation cannot occur and be the cause of primary gushing of beer since the supersaturation of the carbonated beverages varies just from 2.0 till 3.0 (Valant, 2005). Consequently it has been suggested that gushing arises when a beer contains many more nuclei than would normally be present. Gardner distinguished three types of nuclei; Type I (solid hydrophobic particles), Type II (gas residues adsorbed on solid "support") and Type III (stabilized micro-bubbles). Type I is very different from either Type II or Type III. Type I requires *de novo* formation of a bubble whilst II and III actually depend on pre-existing embryonic bubbles. In practice bubble-forming nuclei (Type II or III) usually consist of preformed gas residues and are the most likely type to occur in gushing beer. The appearance of a bubble requires a gas residue as a void in the liquid. The nucleus may be in the form of a small bubble, or of a solid carrying adsorbed gas. How are the nuclei formed? When gas bubbles are shaken, they will rise to the surface under their own buoyancy; the smallest rise the most slowly. As there is no supersaturation in the closed bottle such bubbles will tend to redissolve. As the bubbles rise through the beer they will collect surfactants at the gas-liquid interface. The nature of the surface layer formed as the rising bubbles contract will determine whether or not nuclei formation will occur. If the surface layer forms a "solid-condensed" pellicle, which is "porous" to carbon dioxide, the gas will redissolve. In contrast, if the surface layer forms a solid-condensed pellicle which is impervious to carbon dioxide, the gas will be effectively insulated from the bulk of the liquid. However, in practice the degree of agitation to which a beer is exposed may appear to be small, but no carbonated beverage is ever truly stationary.

Thus nuclei formation will be slow and an "induction-period" could be necessary before a sufficient excess of nuclei is built-up for gushing to become apparent. Gardner concluded his review by the following sentences : "**The concept of gushing as a nucleation process is reasonable, but there is no clear indication of which of the nuclei type actually occurs in gushing beer. However, gushing beers must contain surfactants capable of forming a rigid surface layer at the bubble-liquid interface"** (Gardner, 1973).

- A protein

Triggered by the concern over the contamination of the 1993 and 1994 barley crops with molds, Casey conducted a literature search in **1996** in order to better understand the phenomenon of gushing as the presence of certain mold species (*Fusarium*, *Rhizopus*, *Aspergillus*, *Alternaria*, *Penicillium*) is intimately linked to the production of gushing factors. As mentioned by Gardner, primary gushing results from the use of mold-infected malt and is due to the presence of high numbers of Type III microbubbles which are believed to be the nucleation sites. They consist of surface-active materials forming a solid-condensed pellicle around CO_2 insulating it from the bulk liquid (Gardner, 1973). The new insight was that the surface-active material is a protein, produced as a mold metabolite, but the precise identity of the compound had yet to be characterized or identified. However, chemically the gushing factor had the following traits. It was soluble in water, in aqueous methanol and ethanol and water saturated butanol, but was insoluble in acetone, ether and chloroform. It gave a positive reaction with ninhydrin and Cu-Folin reagents, but gave no sugar reaction when tested with anthrone. It had a specific absorption at 1650 cm^{-1} and 1545 cm^{-1} in the IR spectrum and an estimated molecular weight of 15,000 Da (dalton). Amino acid analyses revealed high levels of hydrophobic amino acid residues. Gushing activity was retained at acid and neutral pH values after heating for two hours at 100°C and destroyed by treatment with pepsin or trypsin. Casey concludes his literature search by the following sentences. ***"Primary gushing results from the use of mold infected malt. Although the identity of the gushing factor has yet to be determined, there is a considerable evidence suggesting it is a protein produced directly by contaminating mold species. This factor is surface-active and stabilizes microbubbles of CO_2 by forming a solid-condensed pellicle around it and insulating it from the bulk of the liquid. There is currently no explanation accounting for the tendency of gushing beer to form stable microbubbles"*** (Casey, 1996).

- The hydrophobin

The protein factor inducing gushing was finally identified in **1999** when hydrophobins were incriminated as responsible for beer primary gushing (Haikara *et al.*, 1999). An immunological method for determining the presence of hydrophobins and thus the sensitivity to gushing for a beverage was also developed. In this method, the hydrophobin determination is performed by using an immunological reaction between a hydrophobin antigen and an antibody (Haikara *et al.*, 1999). The first gene encoding for this typical molecules was called *hfb* gene in **1991** due to the high content of hydrophobic amino acids (Wessels *et al.*, 1991).

Hydrophobins are extracellular surface-active proteins produced by most of filamentous fungi and by edible mushrooms (Linder *et al.*, 2005; Linder, 2009). They are small globular proteins with a molecular mass between 7 and 15 kDa and a diameter between 2 and 3 nm. These human safe compounds are produced by Ascomycetes and Basidiomycetes at different stages of fungal life (vegetative hyphae, sporulating, fruiting body) (Linder *et al.*, 2005). Hydrophobins have important functions in fungi. They are needed for aerial growth (Figure 4) and for adhering to solid surfaces (Wösten, 2001). They may protect parts of fungi against wetting and dessication, by making the surface of conidia, spores and caps of mushrooms hydrophobic. They cause dispersal of spores (Wösten, 2001).

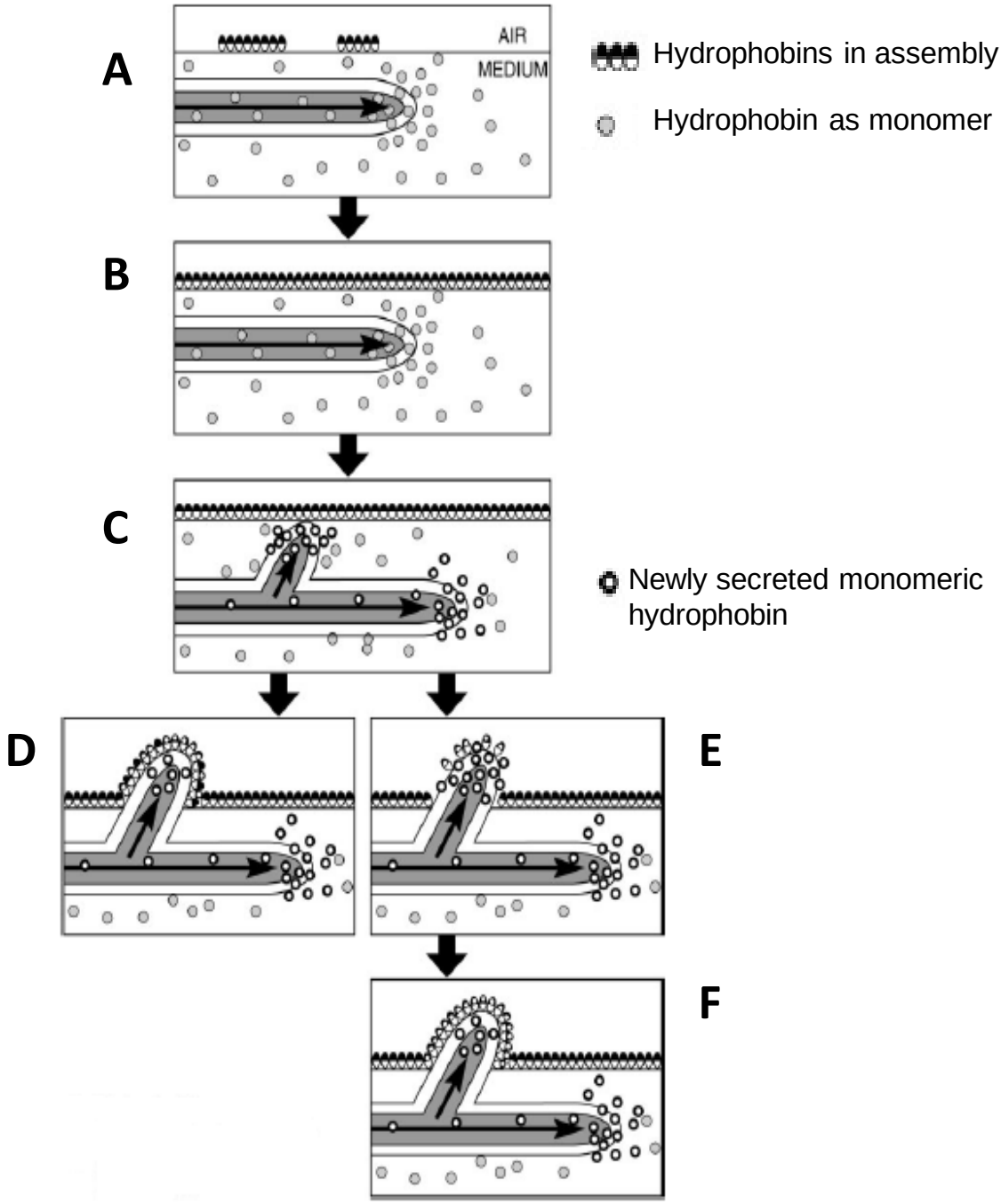

Figure 4 : Model for the formation of fungal aerial structure (Adapted from Wösten, 2001). This model was established by studies with mutant strains where *hfb* gene was deleted. After a submerged feeding mycelium has been formed, the fungus secretes monomeric hydrophobin into the medium (**A**). These monomers self-assemble at the medium-air interface into an amphipathic membrane resulting in a reduced water surface tension (**B**). It has not yet been established what happens when hyphae are confronted with the amphipathic protein layer (**C**). The hyphae may stretch the hydrophobin film enabling intercalation of newly secreted hydrophobin monomers without rupturing the membrane so that the hyphae would never be in contact with the air environment (**D**). Alternatively, the hyphae breaks the hydrophobin membrane and the cell wall contacts the air (**E**). Hydrophobins secreted by such hyphae will self-assemble at the cell wall-air interface. The hydrophilic side of the hydrophobin film faces with the hydrophilic cell wall, while its hydrophobic side is exposed to the air. The hydrophobin films covering the hyphae and the aqueous environment may be fused (**F**) (Wösten, 2001).

Hydrophobins have special arrangements of hydrophobic, hydrophilic and neutral amino acids including 8 cysteine residues. In all hydrophobins, cysteines 2,3 and 6,7 are neighbors and moreover disulfide bridges are formed between cysteines at 1-6, 2-5, 3-4, 7-8 (Figure 5) (Linder *et al.*, 2005).

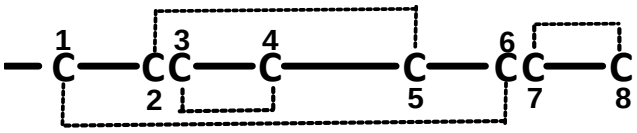

Figure 5: The order of the eight cysteine residues in the hydrophobin primary structures. Cysteines 2,3 and 6,7 are neighbors. They form four intramolecular disulfide bridges as following 1-6, 2-5, 3-4, 7-8.

Based on solubility and sequence comparison, hydrophobins are divided in two classes. Class I hydrophobins (*e.g.* SC3 produced by *Schizophyllum commune*) are produced by both Ascomycetes and Basidiomycetes and their self-assembly is only soluble in strong acids such as formic acid (FA) and trifluoroacetic acid (TFA) (Figure 6 left). Class II hydrophobins (*e.g.* HFBI and HFBII produced by *T. reesei*) are produced only by Ascomycetes and its self-assembly is soluble in 60% ethanol or in 2% hot sodium dodecyl sulfate (SDS) (Figure 6 right) (Linder *et al.*, 2005).

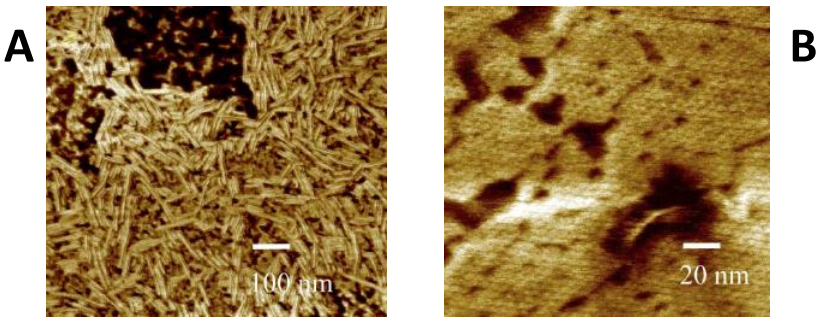

Figure 6: Assemblies of hydrophobins. On the left, an atomic force microscopy image of the self-assembly of the Class I hydrophobin SC3 showing rodlets. On the right, an atomic force microscopy image of an ordered film of the Class II hydrophobin HFBI (Linder *et al.*, 2005)

Differences in behavior are due to differences in tertiary structure. Class II hydrophobins have a hydrophobic patch (about 12 % of the total surface area of the protein) which is made of 2 β-hairpin loops including only aliphatic amino acids. This hydrophobic patch is exposed at the surface and explains the formation of disulfide bridges (Figure 7A and B) regarding the stability of the protein as the hydrophobic amino acid are usually buried in the core of the protein. Amino acid residues forming the hydrophobic patch are conserved among Class II hydrophobins. The patch consists of Val18-Leu19-Leu21-Ile22-Val24 in the first β-hairpin loop, Ala55-Val57-Ala61-Leu62-Leu63 in the second β-hairpin loop and Leu7 (Szilvay, 2007).

Class I hydrophobins are similar to Class II hydrophobins but without α-helix (Figure 7C) and with more amino acids and diversity in amino acid sequences.

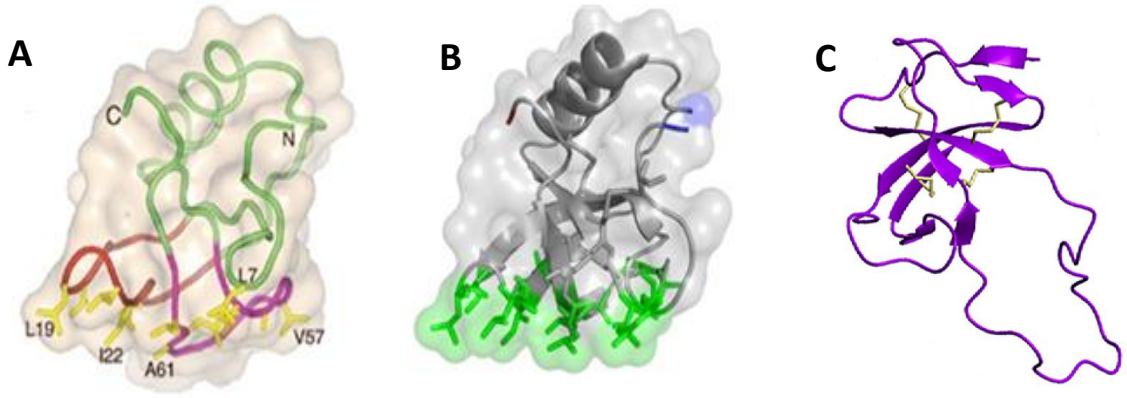

Figure 7: Structural difference between Class I and Class II hydrophobins. **A**: X-Ray Crystal structure of the Class II hydrophobin HFBII in which the two β-hairpins are shown in red and purple. Some aliphatic hydrophobic amino acids of the hydrophobic patch are shown in yellow (Hakanpää *et al.*, 2004). **B**: X-Ray Crystal structure of HFBII in which the hydrophobic patch is shown in green and the α-helix (spirale) and the β-sheets (arrow) are in cartoon representation (Szilvay, 2007). **C**: NMR structure of the Class I hydrophobin EAS produced by *Neurospora crassa* in which the β-sheets (arrow) are in cartoon representation. The long loop on the right side is the main structural difference with the Class II hydrophobins (Bayry *et al.*, 2012).

Different structures of Class I and II hydrophobins lead to different properties. At first this is due to variations in amino acid sequences. Class I have more amino acids (100-125 residues) than Class II (50-100 residues), and are more hydrophobic; they have more β-sheets than Class II which renders them more stable. In contrast, Class II hydrophobins have more tendency towards foaming and are characterized by their specific property to provoke primary gushing.

- Class I hydrophobins : Structural difference with Class II and why they do not induce primary gushing?

During self-assembly at air-water interfaces, Class I proteins show changes in their secondary structure, but such modifications in secondary structure of Class II proteins have not been seen. The soluble state of SC3 (Class I) consists of monomers and oligomers (Scholtmeijer, 2000). During the self-assembly of SC3 at the water-air interface, the soluble state proceeds via an intermediate form with increased α-helical content to the stable β-sheet form (Figure 8 A). The latter form has increased β-sheet content in comparison with the soluble state SC3. After a few hours a typical ultrastructure is observed consisting of a mosaic of 10 nm wide fibrils; these fibrils are known as rodlets. The α-helical state is an intermediate of self-assembly whereas the β-sheet state is the stable end-form (Scholtmeijer, 2000; Wösten and de Vocht, 2000; Wösten, 2001; Wang *et al.*, 2005; Fan

et al., 2006). When assembled at the hydrophobic surface of Teflon, SC3 is trapped in the intermediate α-helical state (Figure 8 B) (Scholtmeijer, 2000; Wösten and de Vocht, 2000; Wösten, 2001; Wang *et al.*, 2005; Fan *et al.*, 2006). Treatment with detergent (2% SDS) at elevated temperatures, however induces the stable β-sheet conformation at the hydrophobic solid surface (Scholtmeijer, 2000) (Figure 8 B). While lowering of surface tension by traditional surfactants is attained within a few seconds, it takes minutes to hours in the case of Class I hydrophobins. It is explained by the fact that hydrophobins lower the water surface tension only after self-assembly which is accompanied by conformational changes in the molecule (Wösten, 2001). The thickness of the interface films of Class I is higher than with Class II (10 nm and just a few nm, respectively). It has to be noted that Class I hydrophobins interact with the interface with the loop comprised between cysteines 3 and 4 (Fan *et al.*, 2006) which is a structural difference between Class I and Class II hydrophobins. In fact, Class I does not contain an α-helix but contains two large disordered regions so that the sequence between cysteines 4 and 5 is shorter in Class I hydrophobins (Kallio *et al.*, 2007). This made the structure of Class I hydrophobins as strong and rigid as a fiber while Class II hydrophobins form an elastic structure (Figure 6 A for Class I and B for Class II).

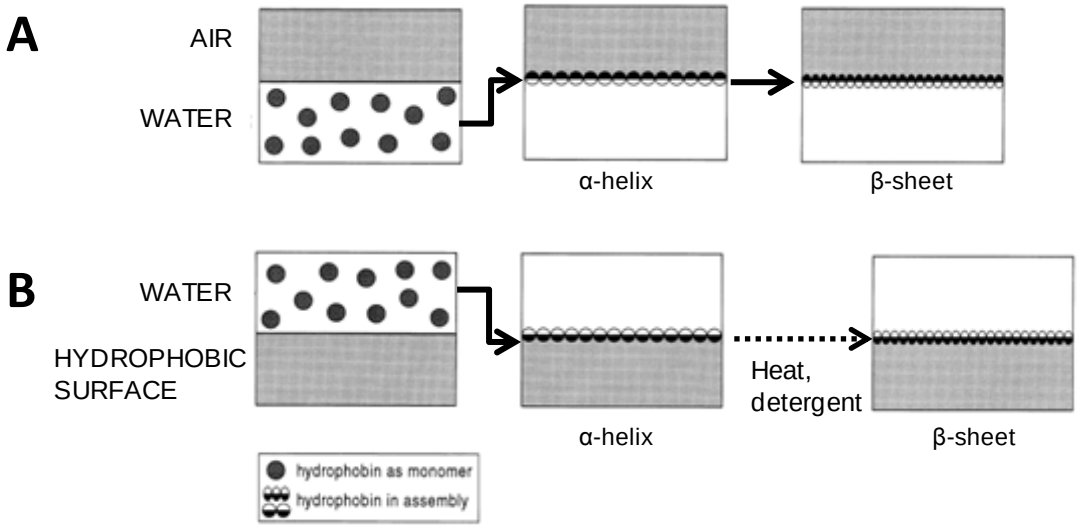

Figure 8: Model for self-assembly of Class I hydrophobin at interfaces. **A**: At air-water interface, the soluble state proceeds via an intermediate form with increased α-helical content to the stable β-sheet form. **B**: At a hydrophobic surface, SC3 is trapped in the intermediate α-helical state. Treatment with detergent at elevated temperature induces the stable β-sheet conformation (Adapted from Wösten and de Vocht, 2000).

- What about non-specific Lipid Transfer Proteins (ns-LTP)?

Besides Class II hydrophobins produced by barley pathogens, a typical molecule produced by barley shows close similarities with the hydrophobins and has been questioned in **the beginning of the 21st century** regarding its gushing inducing property (Hippeli and Elstner, 2002). This molecule is called non-specific lipid transfer protein (ns-LTP) and has been proposed to carry out the task of transferring lipids within the cells (Chasan, 1991) due to the presence of a hydrophobic cavity. ns-LTPs are abundant water-soluble proteins of the aleurone layer from barley grain endosperm with molecular masses of 9 kDa (ns-LTP1) and 7 kDa (ns-LTP2) and with an isoelectric point of 9.0 (Chasan, 1991; Sossountzov *et al.*, 1991; Kader, 1997; Dubreil *et al.*, 1998; Douliez *et al.*, 2000; Jégou *et al.*, 2000; Gorjanovic *et al.*, 2005). Cereal seed ns-LTP1s show high sequence homologies including the presence of eight cysteine residues at conserved locations which form four intramolecular disulfide bridges (Sossountzov *et al.*, 1991; Heinemann *et al.*, 1996; Kader, 1997; Gorjanovic, 2007). Barley grain ns-LTP1 consists of 91 amino acid residues; 64 are identical to wheat, 57 to rice and 49 to maize ns-LTP1 (Gorjanovic, 2007). ns-LTP1 are proteins with a folding involving only α-helices and turns. This fold is characterized by a four-helix bundle surrounded in part by a C-terminus formed by turns. The most interesting feature of this fold is the presence of a large internal cavity (Figure 9) (Heinemann *et al.*, 1996; Dubreil *et al.*, 1998; Douliez *et al.*, 2000; Gorjanovic *et al.*, 2005; Oshchepkova *et al.*, 2009). The surface of this cavity is covered with the side chain of hydrophobic residues provided by the hydrophobic faces of the amphipathic helices and by the C-terminal region. Most of the hydrophobic residues involved in the formation of the hydrophobic cavity are conserved (Douliez *et al.*, 2000; Gorjanovic, 2007).

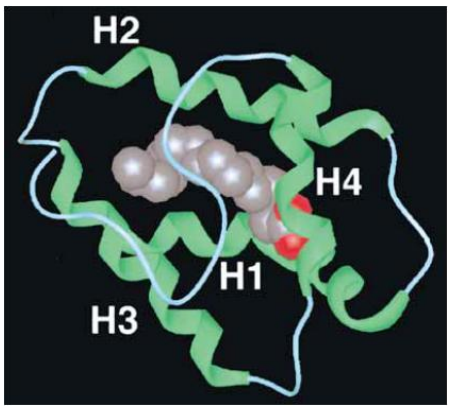

Figure 9: Structure of barley ns-LTP1 complexed with palmitic acid. The four α-helices denoted H1-H4 and represented by a green spirale form a large internal cavity. The surface of this cavity is covered with the side chain of hydrophobic residues and allows the complexation with hydrophobic molecules such as palmitic acid shown in sphere representation (Douliez *et al.*, 2000)

The original postulation that they are involved in intracellular transport of the lipids between compartments, based on their ability to bind lipids in vitro, was contrasted by finding that they are extracellular secretory proteins (Gorjanovic, 2007). So it is not clear which specific role they play (Lindorff-Larsen *et al.*, 2001). Novel roles have been suggested for plant LTPs: participation in cutin formation, embryogenesis, defense reactions against phytopathogens, symbiosis, and the adaptation of plants to various environmental conditions (Kader, 1996). Several ns-LTP genes in barley are upregulated in response to infection by various strains of fungal pathogens (Kader, 1997; Gorjanovic *et al.*, 2005). ns-LTPs isolated from various plants were shown to be active against different fungal and bacterial pathogens with various degrees of specificity, but it was demonstrated that not all ns-LTPs possess antimicrobial properties and protective function (ns-LTPs from maize and wheat were devoid of antimicrobial activity) (Gorjanovic *et al.*, 2005; Gorjanovic, 2007). The antimicrobial activity of the ns-LTP1s is not related to the lipid transport ability, but to their basic nature and the presence of amphipathic α-helices. Clustered distribution of basic and hydrophobic residues is a common characteristic of antimicrobial proteins in general. The positively charged residues on the ns-LTP1 surface may bind to the negatively charged membrane surface, while hydrophobic domains could be inserted into the cell membrane bilayer (Kader, 1997; Gorjanovic, 2007). Barley can be infested with different microorganisms during growth, ripening, harvesting and storage. The ns-LTP1 gene is then upregulated in response to infection, particularly with *Fusarium*, resulting in an increased production of the protein compared to what is the case in uninfected grains (Gorjanovic, 2007; Marion and Bakan, 2009; Lutterschmid *et al.*, 2011). It is hypothesized that gushing occurs when the barley grain ns-LTP1 level exceeds a threshold value (Gorjanovic, 2007). However, Hippeli and Hecht (2009) detected lower amounts of ns-LTP1 in bottles of gushing beer than in non-gushing beer of the same brand (Hippeli and Hecht, 2009; Lutterschmid *et al.*, 2011). Also, it was shown that ns-LTPs were not gushing inducers (Zapf *et al.*, 2006; Lutterschmid *et al.*, 2011) but in contrast were able to reduce the gushing volume induced by Class II hydrophobins (Lutterschmid *et al.*, 2011).

- What about other foam-proteins?

This part will focus on the foam-proteins as gushing is visualized as an overfoaming. Together with protein Z, ns-LTP1 has been identified as the major protein of beer and beer foam (Gorjanovic *et al.*, 2005). ns-LTP1 contributes to foam formation while protein Z confers foam stability (Sorensen *et al.*, 1993; Douliez *et al.*, 2000; Jégou *et al.*, 2000; Gorjanovic *et al.*, 2004). For a protein to have good foamability it must be capable of rapid adsorption and unfolding at the surface. In order to offer good foam stability, the protein must form a strong, flexible and cohesive film in order to reduce gas permeability and to inhibit coalescence and disproportionation. A single protein may not necessarily combine both attributes. Proteins with good foamability tend to be flexible, amphipathic and relatively small. This means that they diffuse rapidly to the gas-liquid interface, display strong adsorption and rapidly lower interfacial tension. Proteins displaying good foam stability form an adsorbed film that is resistant to mechanical deformation, can pack densely and are able to cross-link and aggregate (Bamforth, 2004). Their resistance to high temperature and to malt and yeast protease may explain their survival during malting and brewing (Lindorff-Larsen and Winther, 2001; Gorjanovic *et al.*, 2004; Gorjanovic *et al.*, 2005). However, barley grain ns-LTP1s display poor foaming properties (Jégou *et al.*, 2000). The structural and chemical modifications that barley grain ns-LTP1s undergo during the malting and brewing process result in increased foaming potential of the corresponding beer protein (Sorensen *et al.*, 1993; Bech *et al.*, 1995; Douliez *et al.*, 2000; Jégou *et al.*, 2000; Gorjanovic, 2007). ns-LTP1s undergo a structural maturation including glycation through Maillard reaction in malting (kilning step) and unfolding on heating during the brewing process (wort boiling) (Figure 10) (Douliez *et al.*, 2000; Gorjanovic *et al.*, 2004; Marion and Bakan, 2009). However a significant part of the ns-LTPs remains in the native form (Gorjanovic *et al.*, 2004). The Maillard reaction includes the initial condensation reaction between proteins and reducing sugars to form Amadori intermediate rearrangement products (Bobalova and Chmelik, 2007) and is favored by high-temperature treatment (Jégou *et al.*, 2000). The most reactive groups are the α-NH_2-terminal amino acids and the ε-NH_3^+ of the side chain of lysine residues (Jégou *et al.*, 2000). Arginine (guanidino group) is also a potential site (Gorjanovic, 2007; Hippeli and Hecht, 2009). The glycation is heterogeneous and can be due to the presence of both glucose and maltose in barley malt (Jégou *et al.*, 2000; Bobalova and Chmelik, 2007; Gorjanovic *et al.*, 2007). The unfolding occurs during wort boiling but only when all the disulfide bonds are reduced (Jégou *et al.*, 2000; Gorjanovic; 2007). The mechanism of the reduction of the disulfide bonds during the mashing has not been identified yet but probably involves the thioredoxin and/or glutathione oxido-reducing pathways (Marion and Bakan, 2009).

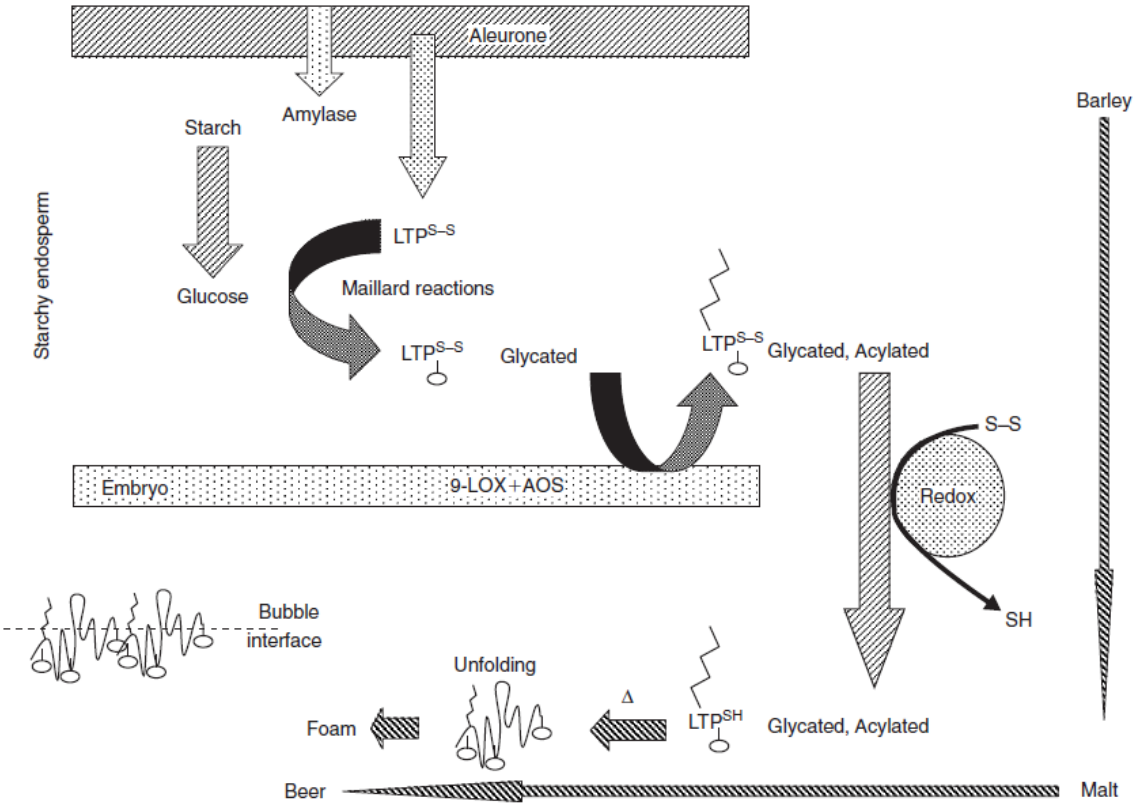

Figure 10: Structural maturation of LTP1 from a non-foaming protein to a foaming protein during the malting and brewing processes. During germination of barley, amylase secreted by the aleurone layer cells into the starchy albumen provides glucose and maltose needed for glycation of the LTP1 during the kilning step of malting. During germination of barley or extraction of malt, LTP1 or glycated LTP1 from the aleurone cells are acylated by the enzyme complex from the embryo. On mashing, the non-reduced LTP^{S-S} is reduced to LTP^{SH} by a redox system from malt. The disulfide bond reduction and boiling promote protein unfolding during brewing. The glycated, acylated and unfolded beer LTP1 displays higher foaming properties than the corresponding non-modified protein from barley (Marion and Bakan, 2009).

Regarding the gushing foam, it is not exceptionnaly stable but is formed very effectively and instantly (Linder, 2009). Also, if Class II hydrophobin is added to sparkling water, gushing is observed as a liquid jet and not as overfoaming. Gushing is observed as overfoaming when proteins are present in the beverage and the foam is formed by protein adsorption at the bubble surface when the bubbles ascend to the surface . So the responsible for gushing has to be able to create nucleation sites for the formation of CO_2 bubble. As described by Gardner (1973), gushing is induced by bubbles stabilized by a pellicle avoiding the redissolution of CO_2 in the liquid. Regarding the properties of hydrophobins and of the ns-LTP, hydrophobins are the best candidate on a theoretical and a practical point of view.

Aims of this study

The systematic uncontrolled beer degassing at bottle opening, the involvement of organic material originating from contaminating molds and the hypothesis that this organic material forms a solid pellicle around CO_2 bubbles in contaminated carbonated beverages such as beer are the basic statements that describe the mechanism of primary gushing.

Indeed, several studies all together assumed pieces of the puzzle, but the biophysical details of the gushing mechanism remain unexplained. In fact, it is assumed that Class II hydrophobins, produced by Ascomycetes, are able to stabilize CO_2 bubble. However, the detailed mechanism of the formation of CO_2 bubble and its stabilization by Class II hydrophobins are not yet described. Also what happens at the bottle opening is not described. The main objective is to improve the comprehension of the primary gushing mechanism at the molecular level.

In **Chapter I**, the production, the extraction, the purification, the detection and the identification of the Class II hydrophobin HFBI produced by *T. reesei* was adapted in the laboratory. This step was necessary to obtain the two main factors responsible for primary gushing : Class II hydrophobin (produced in the laboratory) and solubilize CO_2 (available via sparkling water).

In **Chapter II**, the physical properties of CO_2 and the physico-chemical properties of Class II hydrophobins are reviewed in details and a molecular dynamics simulation is performed in order to describe a theoretical model for primary gushing mechanism.

In **Chapter III**, the thermodynamic aspects of primary gushing are approached.

In **Chapter IV,** a method based on the particle size analysis is developed to detect primary gushing in carbonated beverages; this technique is based on the statements and observations of Chapter II.

In **Chapter V**, the method developed in the Chapter IV is combined with a gushing test in order to predict the primary gushing potential of raw materials (*i.e.* predict the primary gushing potential of barley and malt).

Chapter I

Production of the Class II hydrophobin HFBI

As Class II hydrophobins were identified as responsible for primary gushing, the Class II hydrophobin HFBI from *T. reesei* was produced at lab-scale in shaken-flasks. It was extracted by a Tris/HCl buffer containing 1% SDS and the purification was performed by reversed phase chromatography. MALDI-TOF and N-terminal amino acid sequencing were used for detection and identification respectively. Finally the quantification was performed by Nanodrop 1000 spectophotometer. The yield was 14 mg pure HFBI from mycelium (26 g dw), derived from 1 L of culture.

I.1. Introduction

In 1999, Class II hydrophobins were identified as responsible for primary gushing (Haikara *et al.*, 1999). In the first part of this study and further, in order to study this phenomenon, we produced a Class II hydrophobin at lab-scale. As shown by the amount of publications (Askolin *et al.*, 2001, 2004, 2005; Bailey *et al.*, 2002; Hakanpää *et al.*, 2004, 2006a, 2006b; Kisko *et al.*, 2005, 2008; Linder *et al.*, 2002; Nakari-Setälä *et al.*, 1996, 1997; Paananen *et al.*, 2003; Szilvay *et al.*, 2006, 2007a, 2007b), the hydrophobins HFBI and HFBII from *T. reesei* are the most studied and described Class II hydrophobins. In this work, we produced and investigated further the Class II hydrophobin HFBI. This was necessary in order to obtain in a pure form the two main factors (CO_2 and Class II hydrophobin) responsible for gushing. The mature HFBI protein is composed of 75 amino acids and has a predicted molecular weight of 7,533 Da (Nakari-Setälä *et al.*, 1996; Neuhof *et al.*, 2008). HFBI is located on the cell wall of the mycelium and has a role in hyphal development, *i.e.* it enables *T. reesei* to grow into the air out of liquid cultures (Askolin *et al.*, 2005).

As a production yield is known (Askolin *et al.*, 2001) and as it has the same gushing potential as hydrophobin HFBII (Sarlin *et al.*, 2005), the hydrophobin HFBI was chosen even if it is less suitable for a continuous production than the hydrophobin HFBII which is secreted in the medium culture. However, a small amount (3 µg/L) suffices to induce primary gushing (Sarlin *et al.*, 2005).

The characteristics of these proteins give them a potential for many applications and the large-scale processes of production and isolation were studied. As the *hfb1* gene is only expressed on glucose-containing medium (Nakari-Setälä *et al.*, 1997), the production was done with glucose as carbon source. In 2001, Askolin *et al.* purified the HFBI hydrophobin from the cell walls of the *T. reesei* strain by a simple three-step method; extraction with 1% SDS at pH 9.0, removal of SDS by precipitation, and hydrophobic interaction chromatography. In this study, the method published by Askolin et *al.* (2001) was followed and adapted to the available equipment in the laboratory. The hydrophobic interaction chromatography was replaced by reverse-phase chromatography on a Source 15RPC column composed of spherical particles of polystyrene-divinyl benzene (Source 15RPC Product data sheet, GE Healthcare). As the reverse-phase column, more hydrophobic than those used for hydrophobic interaction chromatography, leads to stronger interaction, a non-polar organic solvent such as acetonitrile is needed for successful elution followed by ultraviolet detection at 215 (peptide bonds) and 280 nm (aromatic residues) (Reichelt *et al.*, 1998).

The detection and the mass determination of the hydrophobin produced was performed by MALDI-TOF (Matrix-Assisted Laser Desorption/Ionization Time-of-Flight). The analytes are mixed with a saturated solution of ultraviolet-absorbing matrix and the matrix/analytes mixture is applied to a target plate (Jonsson, 2001). The solvent evaporates and the matrix and the analytes co-crystallize so that the analyte molecules are surrounded by the matrix molecules (Kaufmann, 1995; Vinh, 1999; Jonsson, 2001). A laser beam provides light that is absorbed by the aromatic matrix molecules. Energy is subsequently transferred to the analyte that becomes desorbed into the gas phase (Vinh, 1999; Jonsson, 2001). The TOF device measures the flight time of ion accelerated out of an ion source into a field-free drift tube to a detector and determines the mass as light ions arrive at the detector earlier than heavy ones (Vinh, 1999; Jonsson, 2001).

After purification and mass determination, the next analysis performed is the determination of the amino acid sequence by Edman degradation, *i.e.* labeling the amino-terminal residue and cleaving it from the peptide without disrupting the peptide bonds between the other amino acid residues.

The quantification of purified hydrophobin HFBI was performed by a Nanodrop 1000 spectrophotometer (NanoDrop Technologies, Wilmington, DE, USA).

I.2. Materials and Methods

I.2.1. Materials and Chemicals

The strain *T. reesei* MUCL 44908 was purchased from BCCM/MUCL (Agro) Industrial Fungi & Yeasts Collection (Louvain-la-Neuve). Bacteriological peptone and yeast extract were purchased from Oxoid (Hampshire, England). Glucose monohydrate, $MgSO_4.7H_2O$ and $CaCl_2.2H_2O$ were purchased from ChemLab (Zeldegem, Belgium). KH_2PO_4 and Tris base were purchased from Sigma-Aldrich (Bornem, Belgium). $(NH_4)_2SO_4$, formic acid (FA) and trifluoroacetic acid (TFA) were purchased from Acros Organics (Geel, Belgium). $CoCl_2.6H_2O$, $MnSO_4.H_2O$, $ZnSO_4.7H_2O$ and $FeSO_4.7H_2O$ were purchased from Merck (Darmstadt, Germany). Sodium dodecyl sulfate (SDS) and KCl were purchased from Applichem GmbH (Darmstadt, Germany). HCl (37%), H_3PO_4 and acetonitrile gradient grade (ACN) were purchased from VWR (Leuven, Belgium). De-ionized water (18.2 MΩ cm) was produced with a Millipore system (Molsheim, France). Source 15RPC column (6.4 × 100 mm) was purchased from GE Healthcare (Diegem, Belgium). α-cyano-4-hydroxy cinnamic acid matrix and Protein Standard I were purchased from Brüker Daltonics (Bremen, Germany). The Protein I standard was composed of insulin, ubiquitin I, cytochrome C and myoglobin and covered a mass range from 5,000 till 17,500 Da.

I.2.2. Methods

- Culture of *T. reesei* and production of HFBI

T. reesei was cultivated in a 1L shaken-flask at 25°C for 4 days, with agitation at 200 rpm. The 300 mL culture medium consisted of glucose (40.0 g/L), peptone (4.0 g/L), yeast extract (1.0 g/L), KH_2PO_4 (4.0 g/L), $(NH_4)_2SO_4$ (2.8 g/L), $MgSO_4.7H_2O$ (0.6 g/L), $CaCl_2.2H_2O$ (0.8 g/L), $CoCl_2.6H_2O$ (4.0 mg/L), $MnSO_4.H_2O$ (3.2 mg/L), $ZnSO_4.7H_2O$ (6.9 mg/L), and $FeSO_4.7H_2O$ (10.0 mg/L) (Askolin *et al.*, 2001; Bailey *et al.*, 2002; Kovacs *et al.*, 2008). Phosphoric acid was used to adjust the pH to 4.5-5.0 (Askolin *et al.*, 2001). After 30 h, 25 mL of a glucose solution (240.0 g/L) was added to the culture medium. After 96 h, the culture medium and the biomass were separated by centrifugation (8,000 × g for 25 min at 6°C; Beckman model J2-21) (Askolin *et al.*, 2001) and the biomass was used further to extract hydrophobin HFBI.

- Extraction of HFBI

The hydrophobin HFBI was extracted from the wet mycelium (approximately 40.0 g) with 25 mL of a 170 mM Tris/HCl buffer (pH 9.0) containing 1% SDS at room temperature for 1 h with occasional mixing. The mycelium was then separated and discarded by centrifugation (8,000 × g for 25 min at 6°C; Beckman model J2-21). SDS was precipitated as water-insoluble potassium dodecyl sulfate by adding 10 mL of a 2 M KCl solution and discarded by centrifugation (8,000 × g for 25 min at 6°C; Beckman model J2-21) to obtain a crude mycelium extract (Askolin *et al.*, 2001). The dry weight (dw) of the biomass was determined by placing 40 g of wet mycelium at 105°C for 24h till a constant weight is obtained.

- Purification of HFBI

The crude mycelium extract was filtered on hydrophilic polyestersulfone filter (Millipore) and loaded (0.5 mL) on a reverse phase column, Source 15RPC. The elution was done with a linear gradient of ACN in de-ionized water containing 0.1% TFA (from 0 to 60% in 20 min) at a flow rate of 1 mL/min and was monitored by ultraviolet detection at 215 and 280 nm. The chromatographic procedures were performed on an ÄKTA Purifier system equipped with an ultraviolet-detector and controlled by Unicorn software (GE Healthcare, Uppsala, Sweden). Fractions of 1 mL were collected during all the purification.

- Detection of HFBI.

The detection was performed by MALDI-TOF with an Ultraflex II instrument in linear mode and an α-cyano-hydroxy cinnamic acid matrix and by comparison with the molecular weight (7,533 Da) (Neuhof *et al.*, 2007). The fractions collected were dried in a vacuum centrifuge (Univapo 150 Ech and Multitrap, Sanyo) and redissolved in 50 µL de-ionized water containing 5% ACN and 0.5% FA. The samples were vortexed and then sonicated for 5 min in an ultrasonic bath (Branson 2510). The matrix (a spatula tip) was placed in 200 µL of de-ionized water containing 50% ACN and 0.5% FA and sonicated for 5 min. 1 µL of sample was placed on the target plate (MTP 384 ground steel) and mixed with 1 µL of matrix solution. 0.5 µL of Protein I standard was placed on the target plate and mixed with 0.5 µL of matrix solution for calibration.

- Identification of HFBI

The fraction in which HFBI was detected was further submitted for N-terminal amino acid sequencing. This was performed by automated Edman degradation on a capillary protein sequencer (Procise 491 cLC, Applied Biosystems).

- Quantification of HFBI

The protein concentrations in purified fractions were quantified by measuring the absorbance at 280 nm using a Nanodrop 1000 spectrophotometer (NanoDrop Technologies, Wilmington, DE, USA). As there is no tryptophan in the aminoacid sequence of hydrophobin HFBI, an extinction coefficient of 10 is assume. The blank sample was a solution of de-ionized water containing 53% ACN and 0.1% TFA.

I.3. Results and Discussion

The culture was stopped after 96 h cultivation and approximately 40 g wet mycelium (20 % dw) were obtained from a 300 mL culture which is similar to the amount (2.15 kg wet mycelium/15 L) obtained by Askolin *et al.* (2001).

The extraction of HFBI from the cell wall was performed with a buffer at pH 9.0 containing 1% SDS (Askolin *et al.*, 2001). However, HFBI was rather susceptible to N-terminal asparagine deamidation at high pH (Askolin *et al.*, 2001). By storing and purifying HFBI at pH lower than 6-7, the deamidation could be prevented but short treatments at high pH did not alter the sample significantly (Askolin *et al.*, 2001).

The RP-HPLC (reverse phase – high pressure liquid chromatography) chromatogram generated during purification of crude mycelium extract is shown (Figure 11).

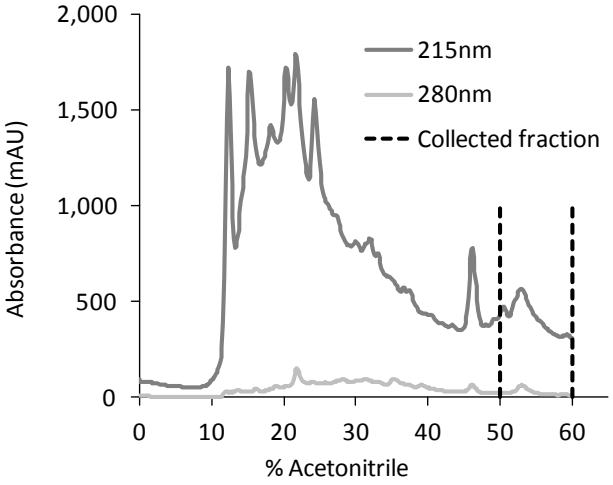

Figure 11: RP-HPLC chromatogram of a crude mycelium extract containing the hydrophobin HFBI. The detection at 215 and 280 nm are shown in dark and light gray, respectively. The dashed lines show the region in which the hydrophobin is eluted.

Different fractions were analyzed by MALDI-TOF. The comparison of the measured molecular weights with that predicted for the hydrophobin HFBI (7,533 Da) suggested the hydrophobin was present in the 50-60 % ACN fractions (53 %) (Figure 12) (Neuhof *et al.*, 2007). Peaks are visible for wavelengths 215 and 280 nm between 50-60 % ACN (Figure 11). The hydrophobin HFBI obtained is pure as no other molecules are detected with MALDI-TOF.

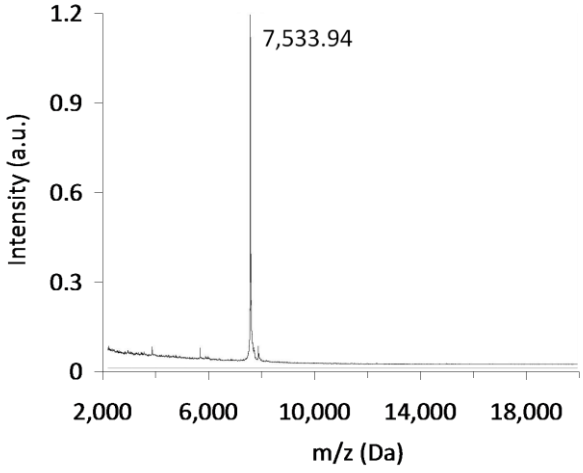

Figure 12: MALDI-TOF mass spectrum analysis of the fraction collected at 53% ACN.

The molecule eluting at 53 % ACN and having the same molecular weight than the hydrophobin HFBI was identified by N-terminal amino acid sequencing. The following sequence where X represents unidentified amino acid, was obtained: XXXNGNVXPPGL and was compared with the known sequence of HFBI (Table 1). Although the first three and the eighth amino acids, represented by X, could not be identified, a BLAST search (Altschul *et al.*, 1997) (http://blast.ncbi.nlm.nih.gov/Blast.cgi) for this sequence resulted in only one match: hydrophobin HFBI from *T. reesei*.

Table 1: Comparison of the sequence of HFBI with that experimentally obtained by N-terminal amino acid sequencing. X represents unidentified amino acid, S serine, N asparagine, G glycine, V valine, C cysteine, P proline and L leucine.

HFBI sequence	S N G N G N V C P P G L
Experimental sequence	X X X N G N V X P P G L

After purification, the concentration of HFBI was determined and the yield calculated was 14 mg pure HFBI per 1 L of culture (Table 2). By RP-HPLC, Askolin *et al.* (2001) determined that 0.17 g HFBI is bound on 28 g dry weight of mycelium per 1L of culture. As 26 g dry weight of mycelium per 1L of culture is obtained in this work, we considered that the initial (100%) amount of HFBI bound on the mycelium is 0.15g. It was determined that the buffer extraction extract 57% of the bound hydrophobins which corresponds to 0.097g (Askolin *et al.*, 2001) and 0.086g (this work). In this work, RP-HPLC was used to purified HFBI and 0.014g per 1L of culture was quantified by Nanodrop which represents 10% of the initial amount.

Table 2: Comparison and determination of the production yield (%) of HFBI. The concentration of HFBI is shown in g per 1 L of culture. For Askolin, the quantitative analysis was performed by RP-HPLC (Askolin *et al.*, 2001). In this work, the concentration was calculated by comparison with that published by Askolin *et al.* (2001) for all steps except for the pure HFBI which was quantified by Nanodrop microspectrophotometer.

Labo	Strain	Wild/mutant	Mass mycelium	HFBI bound on mycelium		HFBI in mycelium extract (after buffer extraction)		Pure HFBI after chromatography step	
			g/L dry weight	g/L medium culture	%	g/L medium culture	%	g/L medium culture	%
Askolin	*T. reesei* VTT-D-98692	Overexpressed	28	0.49	100	0.28	57	0.14	28
Askolin	*T. reesei* VTT-D-74075	Wild	28	0.17	100	0.097	57	0.048	28
This work	*T. reesei* MUCL 44908	Wild	26	0.15	100	0.086	57	0.014	10

This yield is low regarding that obtained by Askolin *et al.* (2001) (0.048g per 1L of culture representing 28% of the initial amount) and could be explained by different reasons. The initial amount of HFBI is expected to be 0.15g (by similarity with Askolin *et al.*, 2001) but for the current conditions, it can be different. The culture conditions were slightly different. Askolin *et al.* (2001) used a fermentor where the glucose concentration was kept within the limits 10-30 g/L and the production was performed at 29°C. In this study, the production was performed in shaken-flasks at 25°C and the glucose concentration was not controlled. As the *hfb1* gene is expressed when *T. reesei* grows on glucose-containing medium, the fact that the glucose concentration was not controlled could mainly explain the low production yield. Hydrophobins could be partially removed during the filtration before injection on the column. The fact that all HFBI monomers might be unable to interact with the column due to competition with other molecules present in the extract could also explained this low yield. The use of plastic material (centrigure pot, syringe,…) could be an explanation too. A better quantification method such as ELISA test could bring a more precised quantification of the hydrophobin.

Since our objective was only qualitative we limited our scientific work to obtaining pure HFBI in order to further carry out our research.

I.4. Conclusion

The extraction, purification, detection, identification and quantification protocols were adapted to the equipments available in the laboratory in order to characterize the production of pure HFBI. The production was performed at 25°C in shaken flasks without monitoring the glucose concentration. The extraction was not modified. The purification was performed with reversed phase chromatography. The detection was performed by MALDI-TOF and by comparison of the molecular weight of HFBI. The N-terminal amino acid sequencing was carried out as identification. The Nanodrop technology was used for quantification. Although our target was just qualitative, the production yield was determined by similarity with the literature for all the steps before the chromatography separation. The amount of pure HFBI obtained was quantified by the Nanodrop technology. The yield of pure HFBI obtained here is lower than that already published. However, the objective of this part was limited to the production of HFBI in order to obtain pure HFBI to allow the experiments to study the primary gushing mechanism.

Chapter II

Nanobubbles and Nanobombs: Why and How?[1]

Primary gushing is a phenomenon described as wild and uncontrolled overfoaming of carbonated beverages due to the presence of Class II hydrophobins. By molecular dynamics simulation approaches, new insights on the involved mechanism were acquired. A mechanism describing the successive phases of the nanobubble formation is proposed. Class II hydrophobins are able to form and stabilize gaseous CO_2 bubbles. These are called nanobombs as our theory proposes that the many stabilized nanobubbles present in the nanometer size range, explode when opening bottles causing overfoaming.

[1]This chapter is based on the following publications:

Deckers, S.M., Gebruers, K., Baggerman, G., Lorgouilloux, Y., Delcour, J.A., Michiels, C., Derdelinckx, G., Martens, J., Neven, H., (2010). CO_2-Hydrophobin structures acting as nanobombs in beer Part I: a critical review of hypotheses and mechanisms. *Brewing Science* **63**, 54-61.

Deckers, S.M., Venken, T., Khalesi, M., Gebruers, K., Baggerman, G., Lorgouilloux, Y., Shokribousjein, Z., Ilberg, V., Schönberger, C., Titze, J., Verachtert, H., Michiels, C., Neven, H., Delcour, J., Martens, J., Derdelinckx, G., De Maeyer, M., (2012). Combined modeling and biophysical characterisation of CO_2 interaction with Class II hydrophobins: new insight into the mechanism underpinning primary gushing. *Journal of the American Society of Brewing Chemists* **70** (4), 249-256.

II.1. Introduction

Despite the knowledge on primary gushing described in the literature review, gushing – puzzle parts are still missing : how does primary gushing occur?, how to prevent it?, … (Winkelmann and Hinzmann, 2009). These questions remain unanswered due to the fact that mostly all emphasis was put on hydrophobins and not on the true responsible molecule, which is CO_2 (Deckers *et al.*, 2011). This can be deduced from the two following observations : gushing can be reduced by reducing the liquid temperature at the opening and gushing disappears when the carbonated beverages are bottled in polyethylene terephtalate bottles (Data not shown; Ravve and Wilt, 1982) due to CO_2 escaping through the plastic material and to the hydrophobicity of the plastic material. The thermodynamical aspect of primary gushing will be discussed in the Chapter III. To understand gushing, it is necessary to consider the whole process including the physico-chemical properties of both Class II hydrophobins and of CO_2.

Carbon dioxide under its gaseous form is hydrophobic due to the planarity of the molecule and since both dipole moments created by the electronegativity difference between hydrogen and oxygen atoms annihilate each other (Figure 13).

Figure 13: Lewis representation of the CO_2 molecule.

Moreover, the critical diameter of a gas bubble is the most important physical property. During saturation of a liquid or in supersaturated liquid, above the critical diameter, the bubbles grow in size by diffusion till they burst (Figure 14 A) and below it they shrink in size till complete dissolution (Figure 14 B) except if a contaminant is present (Figure 14 C) (Nelson, 2009; Sahu *et al.*, 2006; Deckers *et al.*, 2010).

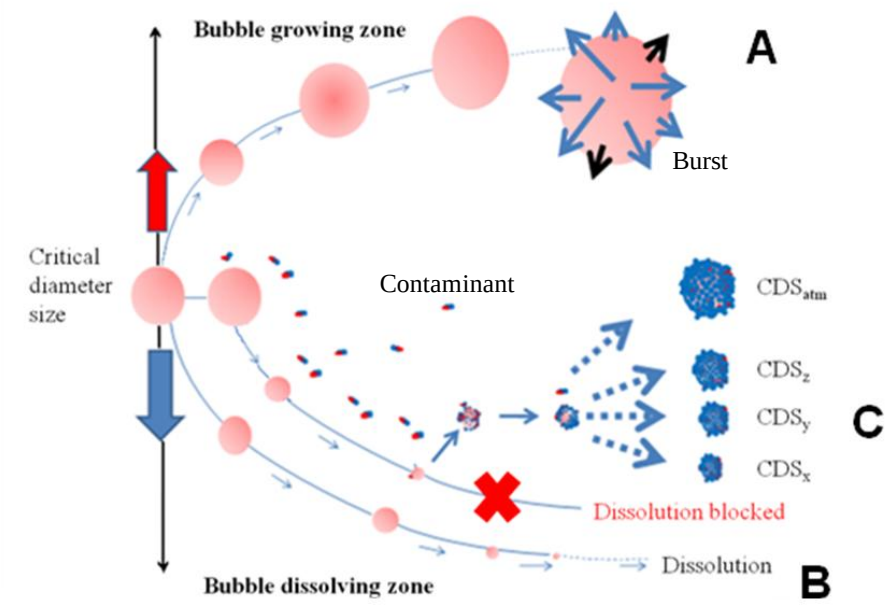

Figure 14: Critical diameter of gas during saturation or in supersaturated liquid (Adapted from Deckers *et al.*, 2010). **A** : the bubble grows in size by diffusion till bursting as its diameter is greater than the critical diameter; **B** : As soon as its diameter is smaller than the critical diameter, the bubble shrinks in size till complete dissolution; **C** : The contaminant prevents the complete dissolution and stabilize the bubble at a diameter (CDS) depending on the pressure. The diameter is CDS_{atm} at atmospheric pressure, CDS_x at pressure x, CDS_y at pressure y, CDS_z at pressure z. The bubble properties are discussed in Chapter III.

The critical diameter is determined by the balance of three "forces": the ambient pressure causing shrinking, the surface tension (Young-Laplace's law) causing also shrinking and the chemical pressure (Henry's law) causing expansion (Nelson, 2009). The Young-Laplace's law binds the local curve at the interface between two media to the pressure difference between these two media and is expressed as following:

$$\Delta P = \frac{2\gamma}{R} \qquad \text{(Equation 2)}$$

where ΔP is the pressure difference, γ is the surface tension and R is the radius of the sphere (Nelson, 2009).

Henry's law states that the solubility of a pure gas in a liquid is directly proportional to the partial pressure of that gas above the liquid as expressed in the following equation:

$$P_i = K_{Hi} C_i \qquad \text{(Equation 3)}$$

where P_i is the partial pressure, K_{Hi} is the Henry's constant, and C_i is the concentration.

For carbon dioxide, the critical diameter at atmospheric pressure is 100 nm (Figure 15) (Nelson, 2009).

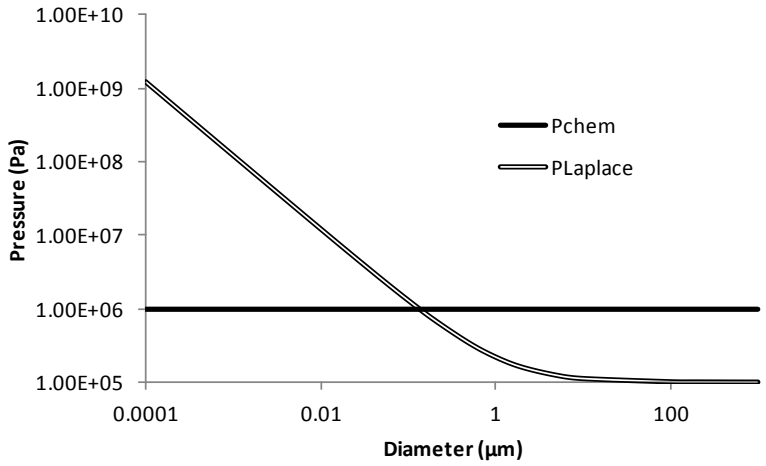

Figure 15: Determination of the CO_2 critical diameter at atmospheric pressure. P_{chem} represents the chemical pressure ($P = K_{H\,CO2} \times C_{CO2}$). $P_{Laplace}$ represents the sum of the ambient pressure and the Young-Laplace's law ($P = P_{atm} + 2\gamma/R$). The critical diameter is determined when $K_{H\,CO2} \times C_{CO2} = P_{atm} + 2\gamma/R$.

Gaseous CO_2 is used in the food industry to produce fizzy beverages such as soda, sparkling water, beer, … In beer production, due to yeast activity ethanol and CO_2 are produced from sugars (Liger-Belair, 2012):

$$C_6H_{12}O_6 \rightarrow 2\ CH_3CH_2OH + 2\ CO_2$$

During this step, the amount of gaseous carbon dioxide produced is allowed to escape but with bottling, by applying a pressure and by injecting gaseous CO_2, the beer can be carbonated by the help of a static mixer which will reduce the size of the bubble below the critical size so that the inside pressure is so high that the gas will diffuse out of the bubble to be dissolved in the beer (Young-Laplace's law). Carbonation can also occur by refermentation in the bottle in which sugar and fresh yeast are added.

When CO_2 dissolves in water the following equilibria are established :

$$CO_2\,(g) \underset{}{\overset{K_H}{\rightleftharpoons}} CO_2\,(d) + H_2O \overset{K_s}{\rightleftharpoons} H_2CO_3 \overset{K_{a1}}{\rightleftharpoons} HCO_3^- + H^+ \overset{K_{a2}}{\rightleftharpoons} CO_3^{2-} + 2H^+$$

where K_H is the Henry's constant, K_s is the hydration constant, and K_{a1} and K_{a2} represent the two dissociation constants of carbonic acid. Henry's law ($P_i = K_{Hi} \times C_i$) states that the solubility of a gas in a liquid is directly proportional to the partial pressure of that gas above the liquid. Carbon dioxide reacts chemically with water molecules to form carbonic acid, an unstable and weak diprotic acid but the reactivity is clearly in favor of dissolved CO_2 as the K_s equals 1.7×10^{-3} at 25°C. However, H_2CO_3 concentration is dependent upon pH. At pH 7.0 about 80 % of carbonic acid is mono-dissociated in HCO_3^- as $pK_{a1} = 6.4$ at 25°C (Pellaud, 2002). The more the CO_2 is dissolved in water, the more the H_2CO_3 is formed and ionized in HCO_3^-. Moreover, increasing the concentration of H^+

results in pH decrease. When the pH is lower than the pK_{a1} value, the equilibria are displaced toward the left side and H_2CO_3 is finally dissolved in CO_2 (Baur *et al.*, 2006; Sahu *et al.*, 2006). In order to obtain a CO_2 concentration of approximately 7 g/L, a pressure is applied to increase the CO_2 solubility as stated by Henry's law (Liger-Belair *et al.*, 2011; Stuart and Craig, 2011). Sparkling water has a final pH value of 4.0 due to the fact that the main species is dissolved CO_2. The beer situation is not so much different. Beer can be considered as a phosphate buffer characterized by a pH value of 4.0 – 4.30. The equilibria are also directed towards the dissolved CO_2. How the dissolved CO_2 molecules interact with the water molecules will be discussed in Chapter III.

What happens when a glass bottle of sparkling beverage is opened?

Carbonated beverages are liquids which are saturated with CO_2, meaning that more CO_2 is dissolved than is sustainable at atmospheric pressure. When such carbonated liquid is in a closed container (bottle or can) a thermodynamic equilibrium (Henry's law) is established between the partial pressure of CO_2 in the gaseous phase above the liquid, and the CO_2 concentration in the liquid (Figure 16; a: equilibrium state before depressurization). When the container is opened, the gaseous phase which is above the liquid will quickly escape because the container is overpressurized (typical pressures in beer bottle are about 4 bar) and the pressure is replaced by one bar of air (with only 382 mg of CO_2/L) pressure. In other words, several grams of CO_2/L in the liquid (commonly 3-9 g CO_2/L) are no longer in thermodynamic equilibrium with the minute concentration of CO_2 in the air. The liquid is supersaturated (Figure 16; b: non-equilibrium state-Supersaturated state) and to attain a new equilibrium, almost all of the excess CO_2 must escape from the liquid (Figure 16; c: equilibrium state after depressurization) (Valant, 2005). There are two ways for CO_2 to escape : the first way (very slow) is through diffusion at the air-liquid interface; the other one is through the formation of bubbles, which will then rise through the liquid and escape into the air. Bubble formation however requires energy for the formation of a curved gas-liquid interface. However individual gas molecules dissolved in the liquid are less ordered than gas molecules in a bubble. Due to this energy barrier for bubble formation, a massive formation of bubble (gushing) is usually not observed when a bottle of beer or other carbonated is opened. Rather, the CO_2 will escape slowly through diffusion.

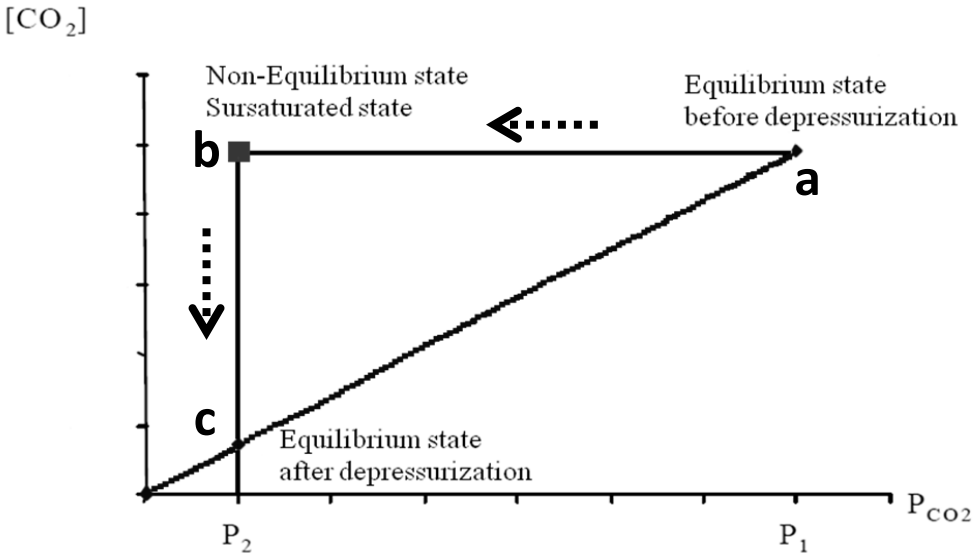

Figure 16: Supersaturation (Adapted from Valant, 2005). The point **a** represents the situation of the closed bottle (i.e. equilibrium state before depressurization). The point **b** is the situation just after the bottle opening; the concentration of dissolved CO_2 is higher than that allowed at pressure P_2 (i.e. sursaturated state). The point **c** represents the equilibrium state after depressurization (i.e. the dissolved CO_2 in excess escaped and reached the concentration allowed by the pressure P_2).

The formation of a bubble is called nucleation. There are four different types of nucleation (Jones *et al.*, 1999). The first one (Type I) is classical homogeneous nucleation. In this type of nucleation, gas bubbles are formed in the bulk solution at high levels of saturation (100 times oversaturated or more) (Figure 17). This type of nucleation does not occur at the saturation level found in carbonated beverages.

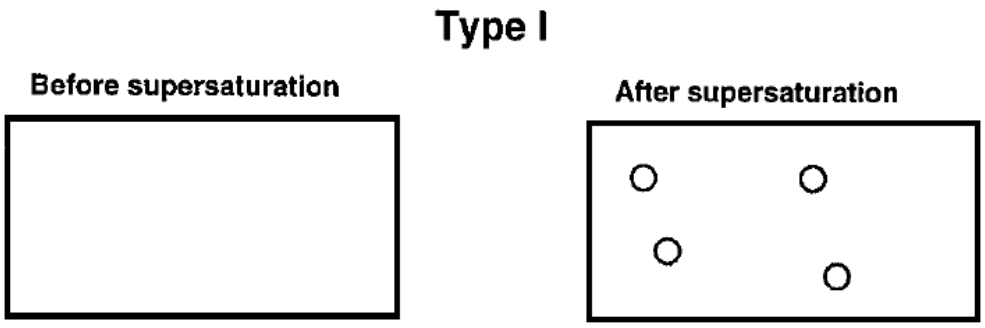

Figure 17: Type I classical homogeneous nucleation, producing gas bubbles in the bulk at high levels of supersaturation of 100 or more (Jones *et al.*, 1999).

The second type (Type II) of nucleation is classical heterogeneous nucleation, due to the presence of another material in the liquid (Figure 18). This catalyst can be a crystal, like oxalate in beer, which then induces what is called secondary gushing. It is known that secondary gushing can be provoked in carbonated liquids by adding sugar or Mentos® candy pastilles.

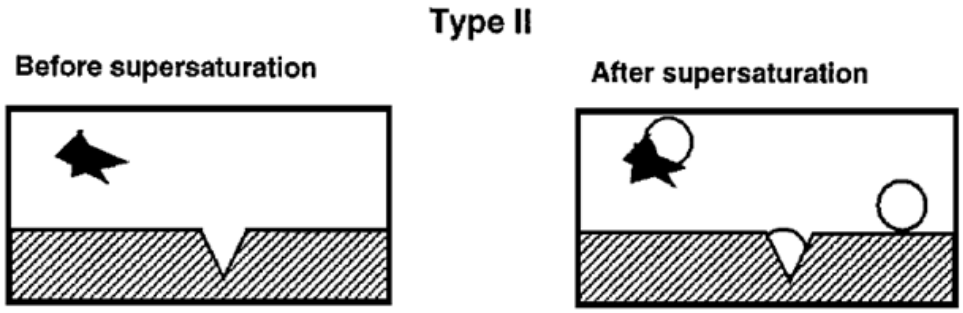

Figure 18: Type II classical heterogeneous nucleation, catalysed by the presence of another material in the liquid (Jones *et al.*, 1999).

The third type (Type III) and the fourth type (Type IV) of nucleation is pseudo-classical and non-classical nucleation respectively and is related to pre-existing gas cavities on surfaces (Figure 19). The difference between Type III and IV is related to the size of the gas cavity. If the size is lower than the critical size, the gas cavity may not grow after supersaturation (Type III). This type of nucleation most probably occurs in primary gushing which is due to the presence of small pressurized gas structure covered by hydrophobins which surround and stabilize them in the bottled beer and which will act as nucleation site for dissolved CO_2. However, how these bubbles are formed, surrounded and stabilized and how will they act as nucleation site remains still unknown. If the gas cavity is higher than the critical size, the gas bubble will grow after supersaturation (Type IV). The Type IV occurs when a beer is poured into a glass. The bubble formation is caused by irregularities in the glass. These can be accidental (minor scratches, impurities like cellulose fiber, …) or deliberate (in many glasses for specialty beers, there are scratches at the bottom of the glass which will cause a constant stream of bubbles to rise to the beer surface) (Figure 20) (Liger-Belair *et al.*, 2008).

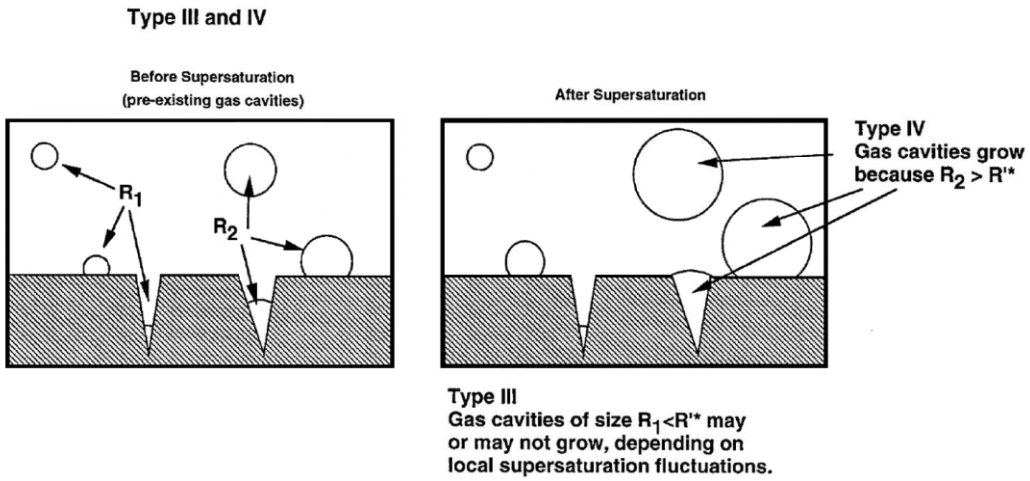

Figure 19: Type III pseudo-classical nucleation and Type IV non-classical nucleation, induced by pre-existing gas cavities. In the Type III, the radius of the pre-existing gas cavities is smaller than the critical radius and in the Type IV, the radius is higher (Jones *et al.*, 1999).

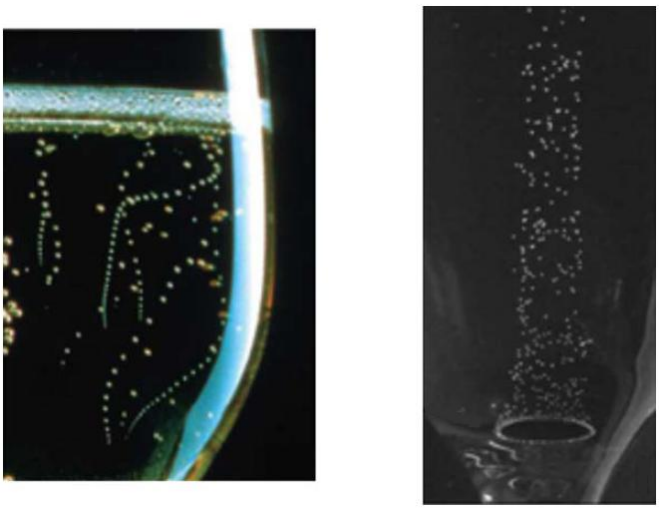

Figure 20: "Natural" effervescence resulting from minor scratches, impurities,… on the left side and artificial effervescence resulting from scratches made by the glass manufacturer on the right side. (Liger-Belair *et al.*, 2008).

As primary gushing is strictly related to Class II hydrophobins (Zapf *et al.*, 2006; Lutterschmid *et al.*, 2011), only the surface properties of Class II hydrophobins will be discussed here.

It has been shown that in solution, hydrophobins associate into multimers (dimers and tetramers) in a concentration-manner dependent (Szilvay *et al.*, 2006; Kallio *et al.*, 2007). HFBII can form tetramers at 10 mg/mL (Hakanpää *et al.*, 2006a). Multimers of hydrophobin are formed in solution, driven by the formation of an energetically more favorable state, parts of the hydrophobic patch becoming concealed from the solvent by multimerization, in comparison to a monomeric hydrophobin where the entire hydrophobic surface area would be exposed to the solvent (Hakanpää *et al.*, 2006b; Kallio *et al.*, 2007). The molecules pack with their hydrophobic patches toward each other, with the contact face being roughly half of the hydrophobic patch (Hakanpää *et al.*, 2004; Kallio *et al.*, 2007). Almost all residues on the dimer interface belong to the first hairpin (Val18, Leu19, Ile22 and Val24). Only Ala61 from the second hairpin participates in the contact, leaving the majority of the hydrophobic residues from the second hairpin exposed to the solvent. If steric factors in the dimer interactions leave a significant part of the hydrophobic surface to be solvated by water, this dimer state can be considered a high-energy state (Hakanpää *et al.*, 2004). Larger hydrophobic interfaces such as the air-water interface could more easily provide a larger water-free environment, and thus produce a low-energy state. Hydrophobin molecules would then preferentially expose their hydrophobic faces to larger interfaces than to each other (Hakanpää *et al.*, 2004; Hakanpää *et al.*, 2006b). For HFBI, there is no strong relationship between multimerization and surface properties as HFBI reaches its lowest surface tension values already at the concentrations where monomers are predominant in solution (Szilvay *et al.*, 2006).

The affinity of a monomer for a multimer is approximately one order of magnitude lower than its affinity for surfaces (Szilvay *et al.*, 2006). It follows that hydrophobins prefer to migrate to interfaces before forming multimers. Experimental data indicate that homotetramerization of HFBI and HFBII is cooperative (*i.e.* the binding of subsequent molecules depends on the binding of the preceding molecules). This expresses that the dimerization of dimers inherently depends on the formation of dimers (*i.e.* tetramers can be formed only if dimers are present) (Szilvay *et al.*, 2006; Kallio *et al.*, 2007). The association is most probably driven by hydrophobic interactions (Kallio *et al.*, 2007; Cox *et al.*, 2007) as the effect of temperature or added salts or solvents are completely in line with the hydrophobic effect dependency (Szilvay *et al.*, 2006).

By adsorption at interfaces, hydrophobins have a surfactant-like behavior (Kisko *et al.*, 2008) and reduce the surface tension of water. At the interface, the water molecules cannot make favorable contact and to minimize the energy, the system will minimize the number of water molecules that need to interact with the surroundings. So, any molecule that can form hydrogen bonds with water on one side and is free of hydrogen bond forming tendencies on the other side will favorably migrate to the interface between air and water. HFBII can reduce the surface tension of water to 28 mJ/m^2 at a concentration of 0.02 mg/mL (Linder *et al.*, 2005; Hakanpää *et al.*, 2004). This property is used by fungi to escape the water environment and to grow in the air (Wösten, 2001). The natural function of hydrophobin is to form amphiphilic layers on the hydrophobic-hydrophilic interfaces. Alignment of hydrophobic surface areas necessitates favorable lateral interactions in the hydrophobin assembly. All the residues involved in lateral interactions are well conserved in Class II hydrophobin sequences and have no other apparent reason for conservation other than the involvement in lateral interactions (Kallio *et al.*, 2007).

Hydrophobins form films at air-water interfaces (Szilvay *et al.*, 2006) and both HFBI and HFBII are strongly interfacially active (Cheung, 2012). HFBII adsorbs strongly to form a compact layer which is consistent with a monolayer of HFBII (Linder, 2009) at the interface, with its hydrophobic patch adjacent to the air phase (Zhang *et al.*, 2011). Hydrophobins form spontaneously highly ordered arrangements at the air-water interface, resulting in a hydrophobin film with elastic properties (Cox *et al.*, 2007) and with hexagonal-like structure (Szilvay *et al.*, 2007b; Kisko *et al.*, 2008; Linder, 2009). The elastic adsorption layer has higher mechanical strength than that of other proteins (Basheva *et al.*, 2011). Specific molecular interactions lead to an ordered network of proteins in the surface films that have a thickness of only one molecule (Szilvay *et al.*, 2007b; Kisko *et al.*, 2008). Hydrophobins form an elastic surface layer formed at the air-water interface. However, at sufficiently low surface concentrations, the interfacial layer is expected to be fluid. Then, a transition from fluid to solid (elastic) interfacial layer is expected with the rise of

hydrophobin surface concentration. The time needed for solidification of the adsorption layer depends strongly on the hydrophobin concentration (Alexandrov *et al.*, 2012). Once adsorbed at the air-water interface, hydrophobin does not desorb indicating that interfacial adsorption is then essentially irreversible (Alexandrov *et al.*, 2012; Cheung, 2012). Once adsorbed at the bubble surface, the addition of other ingredients does not appear to greatly inhibit the surface-stabilising capacity of the hydrophobin protein (Cox *et al.*, 2009). The structure of the protein is essentially unchanged indicating no unfolding of the protein at the interface (Cox *et al.*, 2007; Basheva *et al.*, 2011; Cheung, 2012). Dissociation of HFBI to monomers may not be necessary for surface activity. In fact, there is no strong relationship between the solution association and the surface properties of HFBI. As the monomers and multimers both are surface active, it seems that multimer dissociation to monomers is not required for surface activity. However, the bulk hydrophobin concentration may not be important for self-assembly, as the local concentration at the air-water interface experienced by a hydrophobin molecule can be much higher than the concentration in the bulk solution. This high local concentration could effectively promote monomer association and further self-assembly into the observed hexagonally ordered monolayers. HFBI monomers, as well as dimers and tetramers, are surface active units (Szilvay *et al.*, 2006). The high surface elasticity of membranes of hydrophobins is connected to their tendency to form very stable foams. Even if it is formed very effectively and instantly, the gushing foam is not exceptionally stable. Gushing is therefore more likely to be related to the Class II hydrophobins acting as nucleation sites for the formation of CO_2 bubbles (Linder 2009).

II.2. Materials and Methods

II.2.1. Location of hydrophobins

A bottle (330 mL) of a refermented beer (8.5% alcohol, 9 g/L CO_2) identified as primary gushing beer (36 % overfoaming) was opened at 25°C. All the beverage was collected and centrifuged (Beckman model J2-21) for 10 min at 4,000 × g to remove the yeast. The centrifuged beverage was then placed into a separatory funnel and left to degass for 3 days (Figure 21). After degassing, fractions (Table 3) were collected from the lower part and introduced in sparkling water (7g CO_2/L) at 2°C. All the equipment used was in glass The bottles were then shaken (Bühler SM30, Berlin, Germany) for 3 days at 150 rpm and 25°C (Bühler TH30 incubator hoods, Berlin, Germany). After shaking the bottles were opened to determine the overfoaming. This was at least repeated two times.

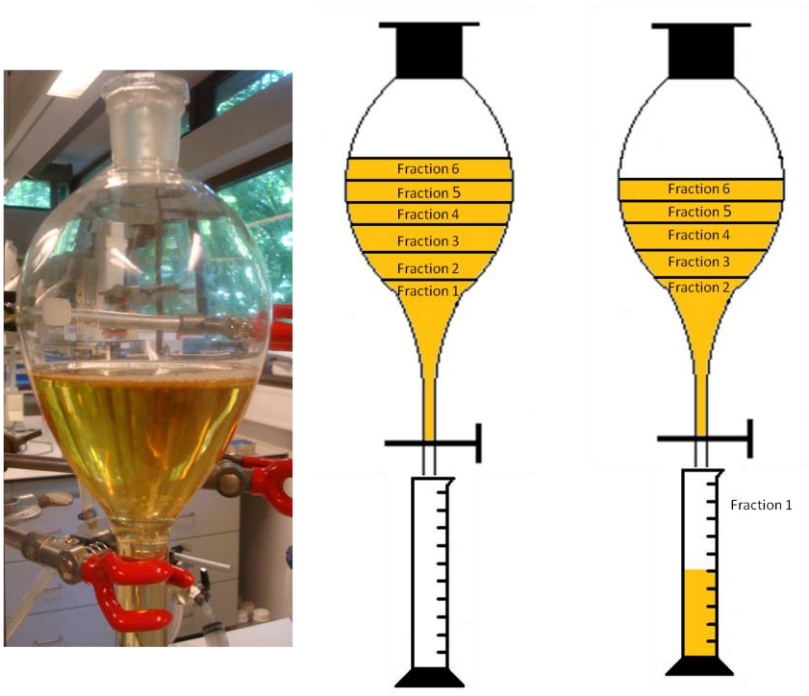

Figure 21: Design of the experiment to localize hydrophobin.

Table 3: The volume of the collected fractions.

Fraction	Volume
Fraction 1	70 mL
Fraction 2	50 mL
Fraction 3	50 mL
Fraction 4	50 mL
Fraction 5	50 mL
Fraction 6	50 mL

II.2.2. Molecular Dynamics (MD)

- MD simulation model parameters

The ultrahigh resolution crystal structure 2B97 (Resolution 0.75 Å; HFBII) was used to simulate the behavior of a Class II hydrophobin as a function of time (Hakanpää *et al.*, 2006a). This crystal structure is a dimeric conformation containing 2 chains, A and B; only chain A was used here. Manganese ions and water molecules were stripped as well. The hydrophobin is a neutral structure, therefore no counterions were added to the system. The correct protonation state of the amino-acids was verified in the MOE molecular operating environment software (Chemical Computing Group, Montreal, Canada). The protein was placed in a dodecahedral box and the distance between the protein and the edge of the box was set to 0.85 mm to ensure that the protein did not interact with its

own periodic image during the MD simulation. Considering these settings, the total volume of the box was approximately 90 nm^3. Ninety carbon dioxide molecules (Calculation 1) were randomly added to the box and the remaining parts were filled with 2525 TIP3P water molecules (Jorgensen *et al.*, 1983). The whole system (protein, water and CO_2) consisted of approximately 9000 atoms.

Calculation 1 : Geometrical properties of the structures in the nanobox

- The critical diameter of CO_2 at 1 bar (*i.e.* opened bottle)

$d_{1bar} = 100\ nm \quad (i.e.\ \ r_{1bar} = 50\ nm)$ (Nelson, 2009)

- Volume of one bubble (V) at 1 bar.

$$V_{1bar} = \frac{4}{3} \times \pi r^3 = 5.24 \times 10^5 nm^3$$ (Equation 4)

- Critical diameter of CO_2 at 4 bar (*i.e.* closed bottle)

Application of the Boyle-Mariotte's law:

$$P_{1bar} \times V_{1bar} = constant \rightarrow P_{1bar} \times V_{1bar} = P_{4bar} \times V_{4bar} \leftrightarrow V_{4bar} = \frac{P_{1bar} \times V_{1bar}}{P_{4bar}} = 1.31 \times 10^5 nm^3$$ (Equation 5)

$$r_{4bar} = \sqrt[3]{3V_{4bar}/4\pi} = 31.5\ nm$$ (Equation 6)

The volume of one CO_2 molecule (V_{CO2}) was estimated to be 0.033 nm^3 using the van der Waals volume. Combining the volume of the bubble (V_{4bar}) and of the CO_2 molecules, the number of CO_2 molecules in one bubble was estimated as follows:

$$Number\ of\ CO_2\ molecules\ in\ one\ bubble = \frac{V_{4bar}}{V_{CO2}} = 3.9 \times 10^6 molecules$$ (Equation 7)

Knowing the surface of the bubble (S_{4bar}), knowing the solvent accessible area of the hydrophobic patch (S_{patch}) of HFBII is 7.4 nm^2 (Hakanpää *et al.*, 2006b) and supposing that only 2/3 of the total surface of the bubble is covered due to steric interaction, the amount of hydrophobin monomers covering the surface of the bubble is determined as follow:

$$S_{4bar} = 4\pi \times r_{4bar}^2 = 1.2 \times 10^4 nm^2$$ (Equation 8)

$$Amount\ of\ monomer\ of\ HFBII\ covering\ one\ bubble = \frac{2}{3} \times \frac{S_{4bar}}{S_{patch}} = 1123\ monomers\ of\ HFBII$$ (Equation 9)

The proportion between CO_2 and HFBII at 4bar then equals:

$$Proportion = \frac{Number\ of\ CO_2 molecules\ in\ one\ bubble}{Amount\ of\ monomer\ of\ HFBII\ covering\ one\ bubble} = 3515 \quad \text{(Equation 10)}$$

It means that there are 3515 CO_2 molecules per monomer of HFBII and that 3515 CO_2 molecules has to be placed in the simulation box at 4 bar. However, to save computational time, less CO_2 molecules (90 molecules) were placed in the simulation box. Moreover, if too much CO_2 molecules are used, an aggregation everywhere would be seen and less CO_2 molecules has to be used to see a concentration effect.

- MD simulation

All simulations were performed using the GROMACS package (version 4.5.3.) (Hess *et al.*, 2008) in conjunction with the OPLS-AA force field (Jorgensen and Tirado-Rives, 1988). Partial charges of the CO_2 molecules were taken from a previous study (Hub and de Groot, 2006). The system was relaxed by executing 2,000 steps of steepest descent and subsequently 2,000 conjugated gradient energy minimization. Two rounds of equilibration were performed, first 100 ps at constant volume and the next 100 ps at constant pressure. All heavy protein atoms were kept fixed with position restraints during the equilibration steps. Next, position restraints were removed and the system was simulated for 100 ns at constant pressure. A snapshot of the system was saved every 4 ps. The simulation temperature was kept constant by coupling protein and solvent separately to an external bath temperature at 298 K and by using a coupling constant of 0.1 ps with the V-rescale thermostat (Bussi *et al.*, 2007). The simulation pressure was kept constant at constant pressure by coupling protein and solvent separately to an external bath pressure at 4 bar by using a coupling constant of 1 ps with the Parrinello-Rahman barostat (Parrinello, 1981). The particle-mesh Ewald method was used calculating the long-range electrostatics (Essmann *et al.*, 1995). A cut-off of 1.4 nm was used for the van der Waals interaction. The LINCS algorithm was used to ensure a 2 fs integration step by constraining all bonds system (Hess *et al.*, 2008).

- Measurements

We calculated the amount of CO_2 molecules per $Å^2$ accessible surface area (ASA) within a sphere of 10 Å near the hydrophobic patch compared to the rest of the protein surface. The following 19 residues were defined as the hydrophobic patch : Gly6, Leu7, Leu12, Val 18 until Val24, Val 54 until Ala58 and Ala61 until Cys64.

II.3. Results

- Location of hydrophobins

As it could be expected from their physico-chemical properties, fraction 6 was mainly responsible for inducing primary gushing (Figure 22). This experiment showed that hydrophobins are localized at the liquid-gas interface.

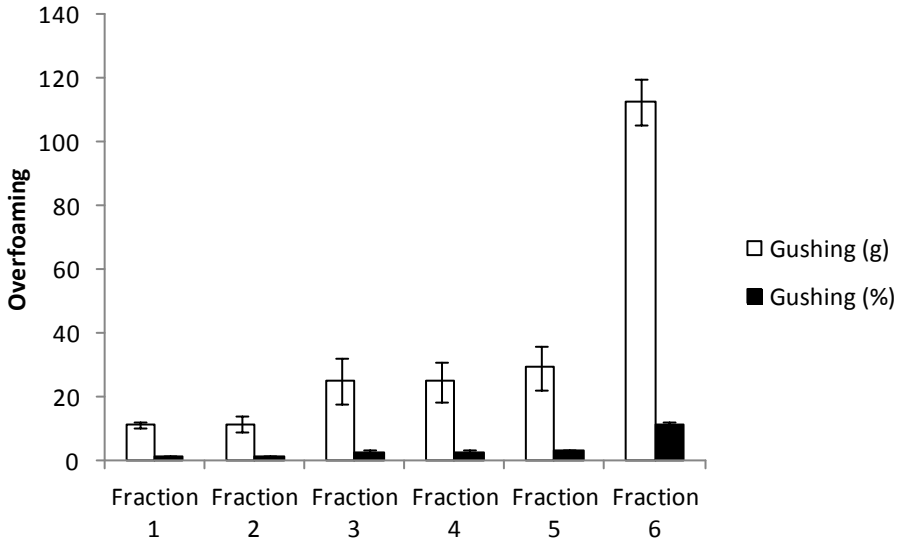

Figure 22: Overfoaming shown by the different fractions collected from the separatory funnel. Fraction 6 is mainly responsible to provoke primary gushing.

- Molecular Dynamics simulation

MD simulations were conducted to study CO_2 clustering at the hydrophobic patch of a Class II hydrophobin in solvent. This patch contains exclusively hydrophobic aliphatic side chains and is formed by two loop regions in the central β-barrel structure. As an initial test to verify the carbon dioxide parameters, 170 carbon dioxide molecules and 2641 water molecules were added randomly to a box of approximately 90 nm^3 and this system was simulated for 100 ns. As expected, the hydrophobic CO_2 molecules quickly diffuse to each other and form both local and global aggregates in the system. An example of this aggregation at 10 ns is shown (Figure 23).

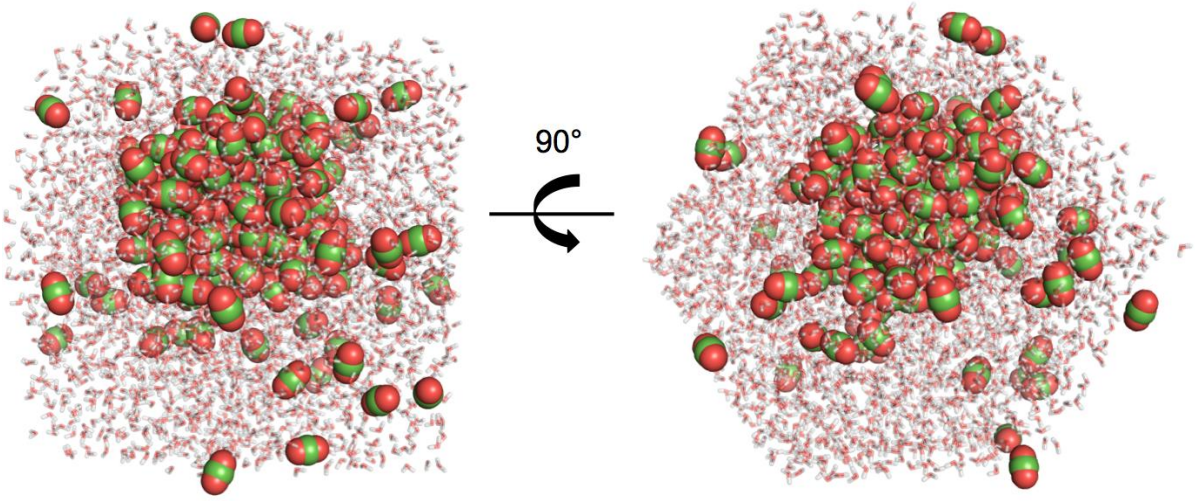

Figure 23: Example of CO_2 aggregation in bubble-like structures. CO_2 molecules are shown as spheres. Water molecules are depicted in sticks representation (Deckers et al., 2012a).

Next, a system with HBII hydrophobin, CO_2 and water molecules was simulated for 100 ns. This simulation was conducted with water molecules without any other components in order to work with the simplest model occuring in nature. Figure 24 graphically displays the amount of CO_2 molecules within the vicinity (10 Å) of the hydrophobic patch. The CO_2 per $Å^2$ ASA amount was followed during the whole trajectory and compared with the rest of the protein. It can be seen that in the vicinity of the hydrophobic patch, the amount of CO_2 molecules per $Å^2$ ASA is more than twice that in the vicinity of the rest of the protein surface. This effect is the strongest after 20 ns simulation time, which can be considered as an equilibration time necessary to cluster the CO_2 molecules on the protein surface.

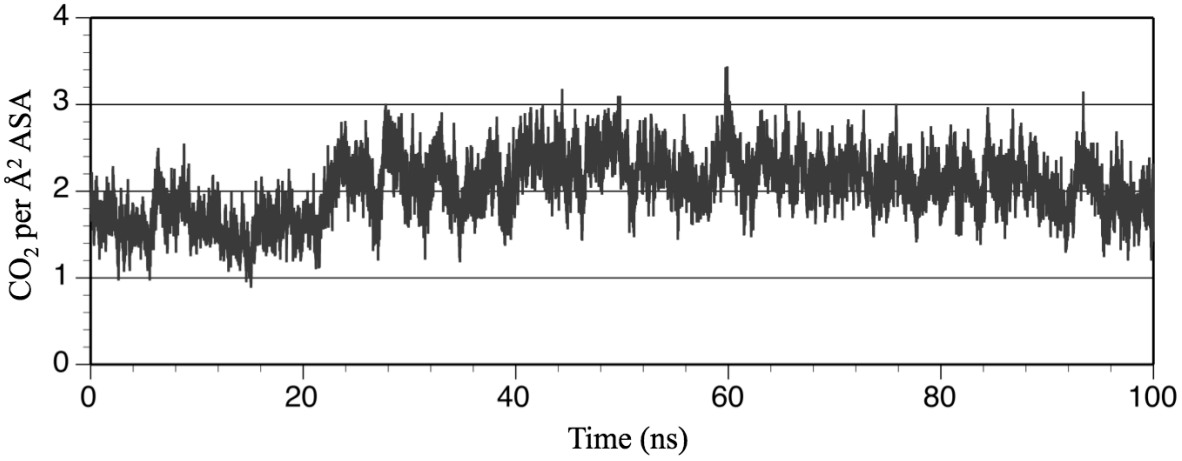

Figure 24: Normalized CO_2 molecules near the hydrophobic patch. Number of CO_2 molecules per square Å in a sphere of 10 Å near the hydrophobic patch as a function of the MD trajectory. The amount of CO_2 molecules per $Å^2$ ASA (Accessible surface area) in the vicinity of the hydrophobic patch is more than twice that in the vicinity of the rest of the protein surface (Deckers *et al.*, 2012a).

The demonstration of the presence of a CO_2 aggregate bound to the hydrophobic patch of the protein during the MD trajectory is shown too (Figure 25). As such, the hydrophobic patch has a tendency to cluster the hydrophobic CO_2 molecules close to the protein surface. It can be hypothesized that this effect could be enhanced when multiple hydrophobins are present and polymerize with each other, thereby increasing the hydrophobic patch area and reducing contact with other parts of the protein. The simulation also shows that CO_2 binding does not happen exclusively at the hydrophobic patch but also on other hydrophobic areas of the protein (Figure 25). Possibly, these areas could be buried upon oligomerization of multiple hydrophobins, thereby reducing binding of CO_2 at these sites. It is of note that during the simulation some CO_2 molecules are occasionally captured in internal cavities of the hydrophobin and stay encapsulated within the protein for multiple nanoseconds.

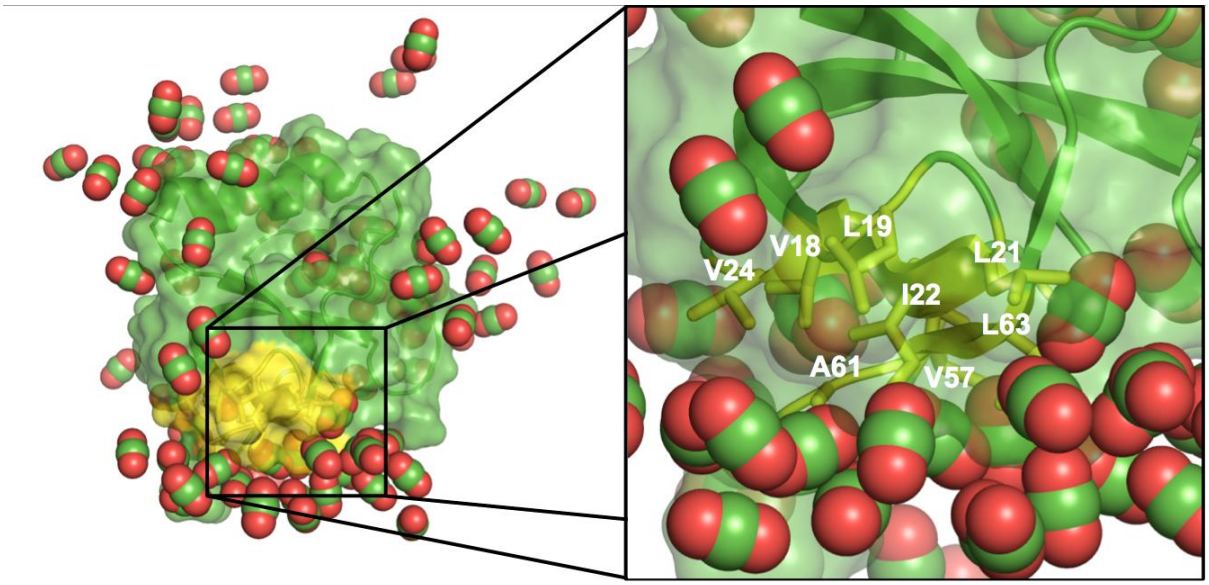

Figure 25: Example of CO_2 clustering near the hydrophobic patch. The residues from the hydrophobic patch are in yellow. CO_2 molecules are shown in spheres representation. Water molecules are omitted for clarity. The inlet represents some of the interacting residues of the hydrophobic patch (yellow) with the CO_2 molecules (shown in spheres representation).

II.4. Gushing model

It was suspected that primary gushing of carbonated beverage could be due to the capacity of Class II hydrophobin to stabilize gaseous CO_2. However it was never well understood how this protein can form and stabilize gaseous CO_2 bubbles although typical information was available in different disciplines of the scientific literature.

II.4.1. Nanobubble formation

Based on the properties of CO_2, the properties of Class II hydrophobin and the results presented above, this part will describe in different successive phases (Figure 26) how Class II hydrophobins can form and stabilize gaseous bubbles which become responsible for primary gushing upon bottle opening. First of all, only 30 % of hydrophobins present on malt are transferred to wort and only 10 % are present in beer (Sarlin *et al.*, 2007). This is sufficient to induce gushing. The hydrophobins can pass through the brewing process and are present in the liquid to be bottled. The hydrophobins present in the liquid become all or in part contaminated by CO_2 during the carbonation process by gaseous CO_2 injection or not contaminated at all if carbonation occurs by refermentation (Figure 26, A). Secondly, due to their surface properties, hydrophobins migrate to the liquid (beer)-gaseous (pure CO_2) interface as in the presence of a hydrophilic-hydrophobic interface; they prefer to move there instead of interacting together (Szilvay *et al.*, 2006 and 2007a) (Figure 26, B). By their presence at the interface, all hydrophobin will become contaminated by CO_2 due to the presence of the pure CO_2 atmosphere in the bottle neck. If the quantity of Class II hydrophobins is sufficient, this will allow the concentration of hydrophobin to reach the critical concentration required for self-assembly of hydrophobins into a crystalline monolayer at this interface (Cox *et al.*, 2007; Szilvay, 2007) (Figure 26, C). Once this structure is formed, if energy (*e.g.* shaking during the transport) is given to the system, the Henry's law equilibrium is imbalanced. This will result in gas exchange between the liquid and the gaseous phase. It also results in the attraction between the hydrophilic glass wall of the bottle and the "hydrophilic" part of the hydrophobin layer (Qin *et al.*, 2007) (Figure 26, D). The hydrophobic part will act as anchorage place or a pit for the nanobubble formation. To return to the equilibrium, the gas will come back inside the liquid where the surface tension is the lowest. The surface tension is in a range of 45 (beer) – 72 (pure water) mJ/m^2 (Bamforth, 2004). However, in presence of hydrophobin, it is reduced to 30 mJ/m^2 (Cox *et al.*, 2007). Due to the reduction of the surface tension by hydrophobin and to the elasticity of the crystalline monolayer formed by this protein, CO_2 molecules accumulate in this structure (Figure 26, E). Finally the bubble stabilized by hydrophobin will be closed by the lateral force resulting from the Young-Laplace's law (Figure 26, F).

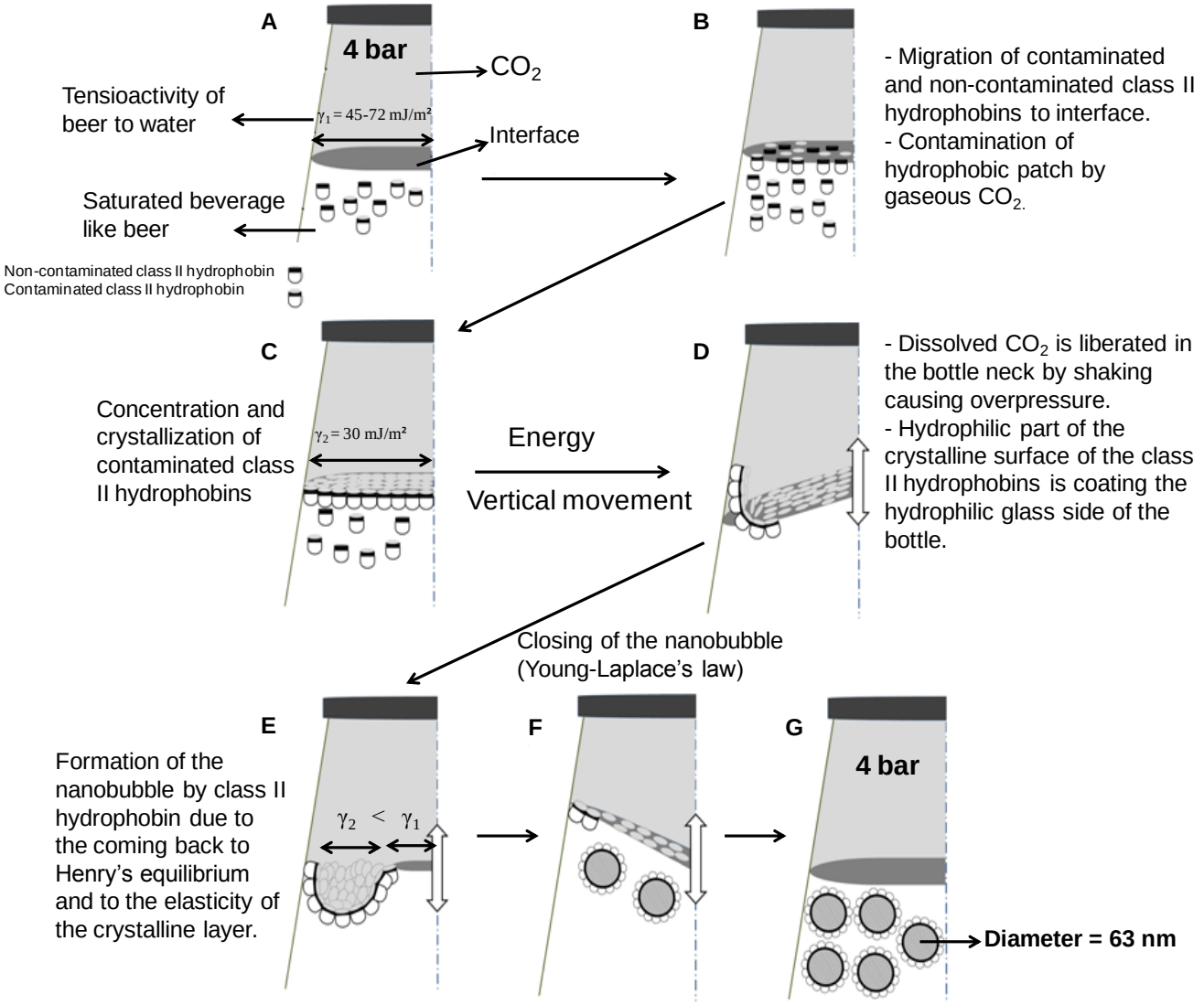

Figure 26: Nanobubble formation by Class II hydrophobin in different successive phases. **A**: Hydrophobins are present in the saturated beer bottle. The surface tension of the saturated liquid is between 45 and 72 mJ/m². The gaseous phase is a pure CO_2 atmosphere. **B**: Due to their surface activity, the hydrophobins migrate to the gas-liquid interface where they become contaminated by CO_2 due to the interaction with the pure CO_2 atmosphere. **C**: At the interface, the contaminated hydrophobins are concentrated and finally reach the critical concentration required to self-assemble into a crystalline layer having elastic properties. The surface tension is therefore reduced to 30 mJ/m². **D**: Due to agitation, the Henry's equilibrium is imbalanced and an overpressure is created in the bottle neck. Also the hydrophilic part of the hydrophobin layer can interact with the hydrophilic glass of the bottle. **E**: To come back to the Henry's equilibrium, gaseous CO_2 will go back into the liquid by the easiest way where the surface tension is at the lowest. Due to the elastic properties of the hydrophobin layer, the gaseous CO_2 will accumulate in this structure. **F**: The bubble is finally closed by the lateral force resulting from the Young-Laplace's law. **G**: The closed bottle contains nanobubbles stabilized by a layer of hydrophobin with a diameter of 63 nm at 4 bar (Deckers *et al.*, 2012a).

Contrary to Class II, Class I hydrophobin has not been reported to be a gushing inducer up to now. However, the mechanism described here seems to be the same as described by Wang *et al.* (2005) where the rigid film formed by Class I SC3 hydrophobin can stabilize oil droplets. However, in the case of gushing, the hydrophobic component is gaseous CO_2 which is unable to extract rodlet structures as oil can do in order to form stabilized nanobubbles. However, this statement needs further practical and computational experiments as several parameters can influence the surface properties.

II.4.2. Nanobomb theory

After nanobubble formation, the gushing phenomenon can be considered in 5 stages; decapping of closed glass bottle, disruption and explosion, nucleation, foaming and finally degassing. In closed bottles, the stabilization of gaseous CO_2 nanobubbles by a crystalline layer of hydrophobins insulates gaseous CO_2 from the beer. The internal pressure of these nanobubbles is similar to the pressure inside the bottle (*i.e.* around 4 bar) and these pressurized nanobubbles will be responsible for primary gushing when opening the bottle. When the bottle is opened, the pressure is released. The drop of pressure from 4 bar to 1 bar results in more volume of the gas and the nanobubble explodes (Yount *et al.*, 1984; Liger-Belair and Villaume, 2011). This is why the concept of nanobomb is introduced. This explosion provides the required energy for nucleation and release of dissolved CO_2 and can be compared to what happens when a shock is given to an opened beer bottle (Lubetkin, 2003). The bubble resulting from the explosion represents a local high concentration of gaseous CO_2 which will grow by diffusion of dissolved CO_2 as the beer is supersaturated (Hepworth *et al.*, 2003; Blatteau *et al.*, 2006; Yang *et al.*, 2007; Liger-Belair *et al.*, 2008; Stuart and Craig, 2011). As they ascend to the surface the growing bubbles attract proteins and create overfoaming (Polidori *et al.*, 2009). If overfoaming and the remaining beverage is left to be degassed at atmospheric pressure, nanobubbles stabilized by hydrophobin films will be reformed with a diameter equal to critical diameter of CO_2 at atmospheric pressure which is 100 nm (Deckers *et al.*, 2011).

II.5. Conclusion

MD simulations were carried out in order to give new insights on the biophysical details of the primary gushing mechanism. This technique allowed the description of the formation of stabilized CO_2 nanobubbles resulting from the hydrophobic interaction between CO_2 and the hydrophobic patch of Class II hydrophobins. The disruption of these nanobubbles results in vigorous overfoaming when the pressure is released.

Chapter III

Thermodynamic properties of primary gushing

By applying the different gushing tests reported in the brewing literature, the volume of overfoam is inconsistent and non repeatable from laboratory to laboratory. Thermodynamic considerations of the process reveal which parameters may be responsible. For gushing, energy is obtained from other sources than only from expansion of the nanobubbles. Thus, the explosion of the nanobombs results in vibration energy which breaks the weak hydrogen bond between CO_2 and water molecule resulting in the CO_2 release. We shall underline that primary gushing is mainly linked to CO_2 properties and is positively related to the liquid temperature (K) at opening, to the pressure (bar), to the CO_2 concentration (g/L) and to energy (J or N.m).

III. 1. Introduction

To test the gushing potential of malt or beer wort, it is common practice to add a malt extract or a wort sample to a carbonated beverage such as sparkling water or beer (Garbe *et al.*, 2007). However, the overfoaming volume ejected from the test bottles varies from laboratory to laboratory and differs sometimes even within a particular laboratory (Rath, 2008). Moreover, the overfoaming volume depends on the type of hydrophobin tested (Sarlin *et al.*, 2005), on the nature of the carbonated beverage used for the test (Sarlin *et al.*, 2011), on the extract preparation (Christian *et al.*, 2009b) and on the CO_2 concentration in the carbonated beverage used (Rath, 2008). Based on the mechanism described in the previous chapter, primary gushing would be induced by CO_2 bubbles stabilized at its critical diameter (100 nm at atmospheric pressure) by a self-assembly of Class II hydrophobin.

Sarlin *et al.* (2005) showed that a critical concentration of Class II hydrophobin is necessary to induce primary gushing. This implies that the quantity of nanobubbles is limited by the Class II hydrophobin concentration. The overfoaming volume also depends on the duration of shaking the bottles (Christian *et al.*, 2009c). Thus, the quantity of nanobubbles depends on the agitation (*i.e.* introduction of energy). We observed that the overfoaming volume is also affected when the liquid temperature at bottle opening is different (Figure 27). The overfoaming volume is also higher when the carbonation level is higher. The energy released at bottle opening thus clearly depends on opening temperature and on CO_2 concentration.

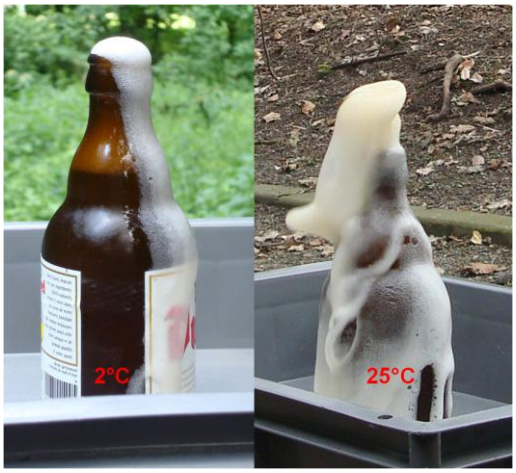

Figure 27: Visualisation of different overfoaming volume expelled from the bottle depending on the liquid temperature at opening: left, at 2°C where 10 g is expelled and right, at 25°C where 130 g is expelled.

To summarize, primary gushing in practice is related to a critical concentration of Class II hydrophobin, to the shaking energy brought to the closed bottle by manipulation (transport,…) and to the physico-chemical properties of soluble CO_2 at opening the bottle.

III. 2. Theoretical calculation

The critical diameter of CO_2 at atmospheric pressure is 100 nm (see Chapter II). It is then possible to determine its critical diameter at 4 bar by applying the Boyle-Mariotte's law as in equation 11 and 12

$$P_{1bar} \times V_{1bar} = constant \rightarrow P_{1bar} \times V_{1bar} = P_{4bar} \times V_{4bar} \leftrightarrow V_{4bar} = \frac{P_{1bar} \times V_{1bar}}{P_{4bar}} = 1.31 \times 10^5 nm^3$$

(Equation 11)

$$r_{4bar} = \sqrt[3]{3V_{4bar}/4\pi} = 31.5\ nm$$

(Equation 12)

The volume of one CO_2 molecule (V_{CO2}) was estimated to be 0.033 nm^3 using the van der Waals volume. Combining the volume of the bubble (V_{4bar}) and of the CO_2 molecules, the number of CO_2 molecules in one bubble was estimated as in equation 13

$$Number\ of\ CO_2\ molecules\ in\ one\ bubble = \frac{V_{4bar}}{V_{CO2}} = 3.9 \times 10^6 molecules$$

(Equation 13)

The first law of thermodynamics is applicable for the gushing phenomenon as it takes place in adiabatic conditions. If it is considered that this system is the atmospheric environment, that it is a closed system where the changes are negligible and that this system occurs at low pressure (4 bar), the equation of Avogadro (Equation 14) can be applied (only applicable to ideal gases, in this case to CO_2 as single and pure gas).

$$PV = nRT$$

(Equation 14)

where *P* is the pressure (Pa or N/m^2)

V is the volume occupied by the gas (m^3)

n is the quantity of matter (mol)

R is the universal constant of ideal gas (8.31 J/K mol)

T is the temperature (K)

As 1 mole of CO_2 contains 6.022×10^{23} molecules (Avogadro's number), the quantity of matter present in one bubble is determined (Equation 15).

$$n = \frac{3.9 \times 10^{6}}{6.022 \times 10^{23}} = 6.64 \times 10^{-18} mol/bubble \quad \text{(Equation 15)}$$

As n equals 6.64×10^{-18} mol, the energy (E) content in a bubble with a diameter of 63 nm at 25°C (*i.e.* 298 K) is determined by the equation of Avogadro (Equation 16)

$$PV = nRT = 6.64 \times 10^{-18} \times 8.31 \times 298 = 1.63 \times 10^{-14}\ J/bubble \quad \text{(Equation 16)}$$

In order to expel 200 mL or 200 g up to 15 cm height at **25°C**, the nanobubbles deliver the energy necessary for expulsion of the liquid by relaxation during depressurization (Equation 17).

$$Work = Energy = Pressure \times Volume$$
$$Work\ needed\ to\ expel\ 200\ mL\ up\ to\ 15\ cm\ height = 0.2 \times (15 \times 10^{-2})^2 = 4.5 \times 10^{-3} J$$
(Equation 17)

Combining the equations 16 and 17, the number of nanobubbles is determined as done in equation 18.

$$Number\ of\ bubble = \frac{4.5 \times 10^{-3}}{1.63 \times 10^{-14}} = 2.76 \times 10^{11} bubbles \quad \text{(Equation 18)}$$

Knowing the surface of one nanobubble (1.2×10^{4} nm²), the solvent accessible area of the hydrophobic patch of HFBII (7.4 nm²) and supposing that only 2/3 of the surface of the bubble is covered, the amount of hydrophobin monomers and the mass of hydrophobin covering the surface of all bubble is determined as done in equations 19 and 20

$$Amount\ of\ monomer\ of\ HFBII\ covering\ one\ bubble = \frac{2}{3} \times \frac{S_{4bar}}{S_{patch}}$$
$$= 1123\ monomers\ of\ HFBII$$

(Equation 19)

$$Mass\ of \frac{HBII}{bubble} = 7.2 \times 10^{3} \times 1.66 \times 10^{-18} \times 1123 = 1.34 \times 10^{-11} \mu g/bubble \quad \text{(Equation 20)}$$

Combining equations 18 and 20, the amount of hydrophobin needed to expel 200 mL up to 15 cm height can be determined with equation 21 and corresponds to 3.7 µg.

$$Concentration\ of\ hydrophobin = 2.76 \times 10^{11} \times 1.34 \times 10^{-11} = 3.7\ \mu g \quad \text{(Equation 21)}$$

Quantities as low as 10 µg/330 mL of HFBII are reported to be enough to induce a gushing overfoaming of 200 mL (Sarlin *et al.*, 2005). However, our calculations indicate that only 3.7µg would be enough to expel 200 mL. Also, we did not take account that the height is varying during the overfoaming. More the bottle is emptied, more the height to expell the liquid is increasing resulting in a higher energy requiring a higher number of nanobubbles and of hydrophobins. Our amount of hydrophobin is then underestimated. If we take in account the variation in the height, the amount of hydrophobins needed will be higher than the 10 µg observed in practice. Also, our calculations are valid if all energy comes from nanobubbles and if the 200 mL are expelled at 15 cm height. In practice, the height can be much higher than 15 cm. It means that extra energy needs to be liberated.

Moreover, if the same bottle is opened at 2°C (*i.e.* 275 K), the energy set free by 2.74×10^{11} is calculated as following:

$$6.64 \times 10^{-18} \times 8.31 \times 275 \times 2.76 \times 10^{11} = 4.2 \times 10^{-3} = 187\ mL \quad \text{(Equation 22)}$$

It means that 187 mL and 200 mL are expelled at 2°C and at 25°C respectively. Again, the calculation considers that all the energy comes from the nanobubbles. In practice, a much higher volume (about one third of the bottle volume) is expelled at 25°C in comparison with that at 2°C. It becomes obvious that energy is obtained from different sources than just from the expansion of the nanobubble. The difference in the volume expelled can be explained by the solubility of the gas depending highly on the temperature and by the nanobomb effect. The binding is higher at refrigerator temperature (*i.e.* 2°C) than at room temperature (*i.e.* 25°C). Considering the nanobomb theory, it is assumed that at bottle opening, the depressurization results in the explosion of the nanobubble stabilized by hydrophobic enveloppes. This explosion releases an initial amount of mechanical energy, under the form of vibrations or shaking energy in the liquid. This energy is responsible for breaking the weak bond linking CO_2 and liquid (*i.e.* hydrogen bond). Hydrogen bonds are attractive interactions of a hydrogen atom and an electronegative atom such as nitrogen, oxygen and fluorine present in another molecule or chemical group. The hydrogen has a polar bonding to another electronegative atom to create the hydrogen bond (Hill *et al.*, 2008). The electronic charge density in water molecule is higher at one extremity due to the higher electronegativity of the oxygen atom. The bond is polar, δ^- is on the oxygen atom and δ^+ on the hydrogen atom (Figure 28). The hydrogen is then considered as exposed. So an oxygen atom from a neighboring water molecule can approach the hydrogen atom and the oxygen atom from this neighboring molecule can share its electronic density and so on for the other atoms . The total number of hydrogen bonds of a water is up to four, one per hydrogen atom and two for the oxygen atom as it has two lone pair (Figure 29).

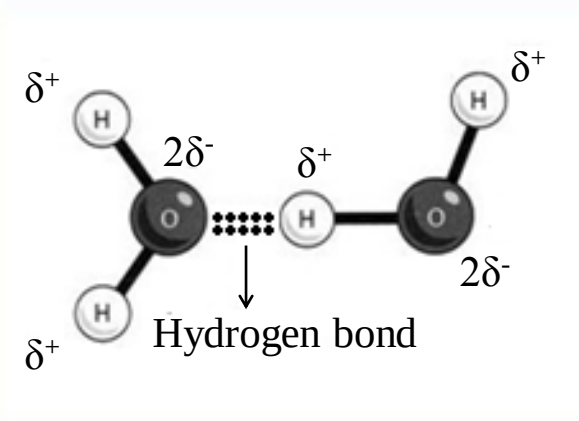

Figure 28: Hydrogen bond (Adapted from http://s2.e-monsite.com).

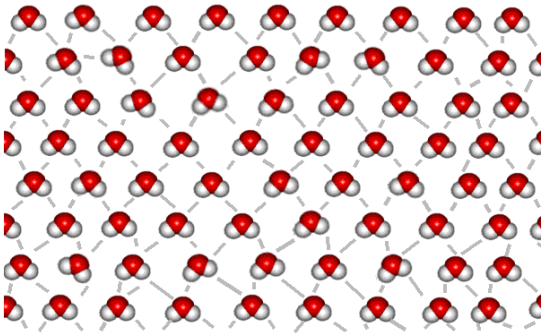

Figure 29: Hydrogen bonds formed between different water molecules (from Byrd and Perona, 1999).

As explained in the previous chapter, CO_2 in carbonated beverage is present under the dissolved form ($CO_{2(aq)}$) and not under the carbonic acid form (H_2CO_3). In fact, the oxygen atoms in CO_2 can make specific hydrogen bonding with water molecules (Chaplin, 2012). The CO_2 may form a hydration shell from a symmetrical dodecahedral arrangement of 18 water molecules where each CO_2 oxygen atom is bonded to three water molecules (Figure 30) (Chaplin, 2012).

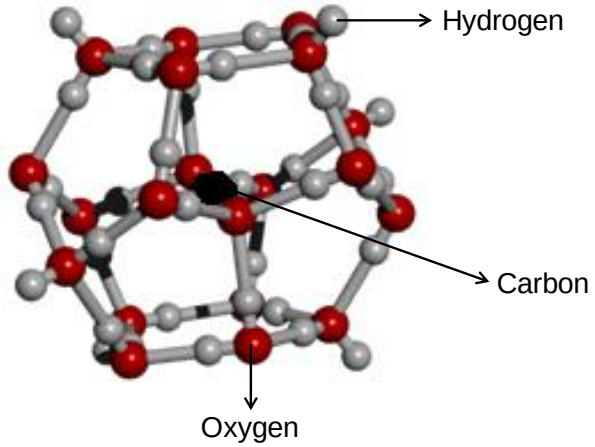

Figure 30: The CO_2-water cluster. The oxygen atoms are shown in red, the hydrogens in grey and the carbon in black (Adapted from Chaplin, 2012).

From these considerations, it can be assumed that at bottle opening (*i.e.* depressurization), the nanobubbles stabilized by Class II hydrophobin will explode resulting in the release of vibration energy (nanobomb effect). This energy is enough to break the hydrogen bonds between CO_2 and water and results in the liberation of CO_2 and in the overfoaming by CO_2 diffusion in the nucleation sites formed. A higher CO_2 concentration will result in higher overfoaming due to the higher pressure (*i.e.* nanobomb effect) and also to the higher CO_2 amount that wants to escape. The effect of the temperature is explained by its influence on the pressure (*i.e.* nanobomb effect) but also by its influence of the CO_2 solubility. It means that, at 25°C, after the nanobomb effect liberating vibration energy, more CO_2 will escape due to the lower solubility and it results in a higher overfoaming at 25°C in comparison with the opening at 2°C.

III.3. Conclusion

At the opening of the bottle, the pressure drops from 4 bar to 1 bar resulting in the expansion of the gas. The crystalline layer formed by the self-assembly of Class II hydrophobin around CO_2 bubbles is neither sufficiently solid nor sufficiently elastic to resist to such gas expansion. The stabilized nanobubbles explode with a release of energy under the form of vibration energy. This is referred to a nanobomb effect. This energy is enough to break the weak hydrogen bond between CO_2 and water molecule and is responsible for the potential abundant CO_2 release depending on the liquid temperature. Although it is also influenced by the hydrophobin (type and concentration) and the extraction method, this highlights the fact that the overfoaming volume is linked to CO_2 properties essentially! In fact, it is positively related to the liquid temperature (K) at opening, to the pressure (bar), to the CO_2 concentration (g/L) and to the energy release (J or N.m).

Chapter IV

CO_2-hydrophobin associated structure responsible for primary gushing: solid structures detectable at atmospheric pressure[2]

A method based on Dynamic Light Scattering (DLS) was developed for the detection of the gaseous CO_2 bubbles stabilized by hydrophobins which are responsible for primary gushing of carbonated beverages. This method allows discriminating between primary and secondary gushing of beverages, due to the detection of particles of approximately 100 nm in the former and not in the latter.

[2] This chapter is based on the following publication:
Deckers, S.M., Lorgouilloux, Y., Gebruers, K., Baggerman, G., Verachtert, H., Neven, H., Michiels, C., Derdelinckx, G., Delcour, J., Martens, J., (2011). Dynamic Light Scattering (DLS) as a tool to detect CO_2-hydrophobin structures and study the primary gushing potential of beer. *Journal of the American Society of Brewing Chemists* **69** (3), 144-149.

IV.1. Introduction

The disastrous effects caused by gushing of carbonated beverages become more and more frequent and explain why research in different countries such as Germany and Finland has been intensified. Research mainly focused on the development of methods to detect and predict the potential of raw material for primary gushing in the end product. Different methods based on a correlative factor (*i.e.* not measuring gushing but a factor correlated to it) were published such as standard plate counts, the ELISA test, a PCR-based method, a mycotoxin test and others (Garbe *et al.*, 2009; Shokribousjein *et al.*, 2011). Such microbiological tests based on the detection of raw material contaminants are expensive and time consuming (Denschlag *et al.*, 2012). More direct are tests based on adding a suspected sample to carbonated beverages and determination of the amount of overfoaming liquid after 3 days of shaking (Garbe *et al.*, 2007). However an inter-laboratory test-program showed the lack of reproducibility (Haikara *et al.*, 2005; Rath, 2008; Christian *et al.*, 2011). New ideas to quantify gushing more precisely were developed. It was proposed to determine the minimal volume of a wort needed to induce gushing but also the amount of a CO_2 hop extract to inhibit gushing (Christian *et al.*, 2009d and 2010b). Nüter and Harms reported the presence of particles of approximately 5 nm in gushing positive beer and suggested that particle size measurement can be used for final beverages to differentiate gushing positive from gushing negative samples (Nüter and Harms, 2009). At the same time, Christian *et al.* (2009a) reported that surface active particles in sizes of 1-2 nm are gushing inducers. These small particles could correspond to hydrophobin monomers (Hakanpää *et al.*, 2004; Christian *et al.*, 2009b). Christian *et al.* (2009a and 2009b) also detected particles with a diameter of approximately 100 nm but they did not comment their finding. The physical property of gaseous CO_2 (*i.e.* the critical diameter) and the physico-chemical property of hydrophobins (*i.e.* stabilization of a gaseous bubble by a crystalline self-assembly) prompted us to investigate whether the DLS method used for the determination of particle size in solution, can also be applied to detect the CO_2 bubbles stabilized by hydrophobins.

DLS is a method to determine the size distribution profile of small particles (in the range of submicron) undergoing Brownian motion in solution. The first microscopic observations of the rapid and erratic motion of small particles were made in 1827 by Robert Brown, an English botanist, examinating pollen grains of the plant *Clarkia pulchella* (Hunter, 2005). He noticed that if pollen grains are looked at in water through a microscope, the pollen jiggles about. He called this jiggling "Brownian motion" but he could not work out what was causing it. The motion was thought to be caused by the bombardment of the particles by the surrounding molecules of the solvent. The intensity of the bombardment would vary from moment to moment on one side or another of the particle thus causing erratic motion (Rogers, 2005). This phenomenon can be more

easily understood with the following metaphor. Consider a large balloon of 100 m diameter in a football stadium. The balloon is so large that it lies on top of many supporters. Due to their wild enthusiasm they hit balloon at different times and in different directions with the motion being completely random. In the end, the balloon is pushed in random directions, so it should not move on average. We might have 20 supporters pushing right, and 21 other supporters pushing left, where each supporter is exerting equivalent amounts of force. In this case, the forces exerted towards the left and the right are imbalanced in favor of the left. The balloon will move slightly to the left. This type of imbalance exists at all times, and it causes random motion of the balloon. Looking at this situation from far above, the supporters cannot be seen and the large balloon is seen as a small object animated by erratic movement. The Brownian motion of a particle in a liquid is thus due to the instantaneous imbalance in the combined forces exerted by collisions of the particle with the much smaller liquid molecules surrounding it. The first person to describe the mathematics behind the Brownian motion was Thorvald N. Thiele in a paper published in 1880 and was followed independently by Louis Bachelier in 1900. Albert Einstein and Marian Smoluchowski (1906) brought the solution of the problem to the attention of physicists (Rogers, 2005).

Einstein's theory consists of two parts (http://www.scienceisart.com). The first one consists in the formulation of a diffusion equation for Brownian particles, in which the diffusion coefficient is related to the mean square displacement of a Brownian particles and Einstein argued that the displacement of a Brownian particle is not proportional to the elapsed time but rather to its square root. The second part relates the diffusion constant to physically measurable quantities. Consider particles suspended in a viscous fluid in a gravitational field. Gravity tends to make the particles settle, whereas diffusion acts to homogenize them, driving them into regions of smaller concentration. Under the action of gravity, a particle acquires a downward speed of $v = \mu mg$ where m is the mass of particle, g is the acceleration due to gravity and μ is the particle's mobility in the fluid. George Stokes had shown that the mobility for a spherical particle with a radius r is $\mu = 1/(6\pi\eta r)$ where η is the dynamic viscosity of the fluid. Combining the distribution of particles into a state of dynamic equilibrium with the tendency of these particles to migrate to regions of lower concentration ruled by the Fick's law, a speed $v = Dmg/(k_BT)$ is found. This speed has to be equal to μmg.

Combining the two part of the Einstein's theory, a formula for the diffusivity is written:

$$\frac{\overline{x^2}}{2t} = D = \mu k_B T = \frac{\mu RT}{N} = \frac{RT}{6\pi\eta r N} \quad \text{(Equation 23)}$$

where x represents the mean square displacement of a Brownian particle, t the time, D the diffusion coefficient, μ the particle's mobility in the fluid, k_B the Boltzmann's constant, T the temperature, R the universal gas constant, N the Avogadro's number, η is the dynamic viscosity of the fluid, and r the radius of the spherical particle. Here the first equality follows from the first part, the second equality follows from the second part, the third equality follows from the definition of Boltzmann's constant as $k_B = R/N$, and the fourth equality follows from Stoke's formula for the mobility.

The scattering of light may be thought of as the redirection of light that takes place when an electromagnetic wave encounters an obstacle or non-homogeneity such as the scattering particle (Hahn, 2009). When the laser passes through the sample, the electromagnetic wave interacts with the particle and the electron orbits within the particle's constituent molecules are perturbed periodically. The oscillation or perturbation of the electron cloud results in a periodic separation of charge within the molecules, which is called an induced dipole moment (Hahn, 2009). As a consequence, the molecules provide a secondary source of light and subsequently scatter light (Sartor, 2010). When the particles are very small when compared with the wavelength of the light (typically less than $d=\lambda/10$), the intensity of the scattered light is uniform in all directions (Rayleigh scattering) (Malvern Technical note; http://www.brookhaven.co.uk). It is also supposed that the whole of the particle is subjected to the same electric field strength at each instant in time so there is a negligible difference in the phases of the scattered wave from different region of the particle (Hunter, 2005). The particle must also be separated from one another so that the scattering from one does not interfere with that from other particles (Hunter, 2005). As the particle size increases, the scattering pattern becomes still more complicated and, in the region $d\sim\lambda$, the theory developed by Mie must be used to properly describe the scattering pattern (Hunter, 2005; http://www.brookhaven.co.uk).

The DLS analysis is based essentially on two assumptions; the particles are in Brownian motion and are spherical in order to apply the Stokes-Einstein formula (Sartor, 2010). In DLS the speed at which the particles diffuse due to Brownian motion is measured. This is done by measuring the rate at which the intensity of scattered light fluctuates when detected using a suitable optical arrangement. The rate at which the intensity fluctuations occur will depend on the size of particles. The small particles cause the intensity to fluctuate more rapidly than the large ones (Figure 31) (Malvern Technical note). If it can be measured accurately it provides a means of determining the

diffusion coefficient of the particles (property of the velocity of Brownian motion) and consequently a mean diameter can be calculated using the Stokes-Einstein equation. As it will be seen later in the formula, the diffusion of the molecules is essentially controlled by the temperature, the viscosity of the solvent and the size of molecules (Instruction manual 90PLUS).

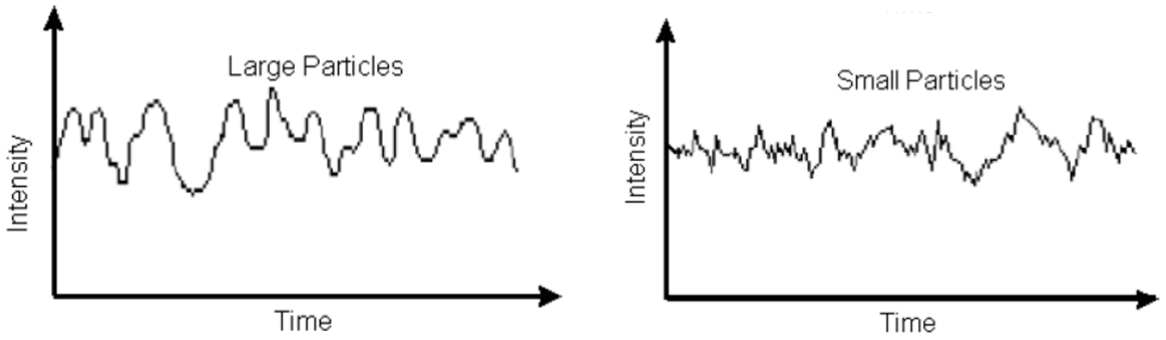

Figure 31: Typical intensity fluctuations for large (left side) and small (right side) particles. The large particles cause the intensity to fluctuate more slowly than the small ones (Malvern Technical note).

Before going further in the mathematical approach, it is important to note that the diameter (Figure 32) measured in DLS is a value that refers to how a particle diffuses within a fluid. Therefore, it refers to a hydrodynamic diameter. The diameter obtained is the diameter of a sphere that has the same translational diffusion coefficient as the particle (Malvern Technical note).

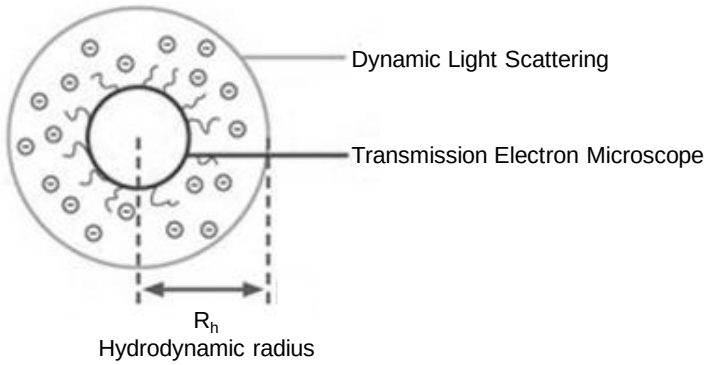

Figure 32: Hydrodynamic diameter. When a dispersed particle moves through a liquid medium, a thin, electric dipole layer adheres to its surface. Since this layer influences the movement of the particle, the diameter measured by dynamic light scattering is called hydrodynamic particle diameter and is above the diameter measured by a transmission electron microscope (Adapted from Crolly, 2012)

However, since the particles are all moving with different velocities, a solution will produce scattered light of different frequencies, this effect is obviously more pronouced in solution containing particles of different sizes (Hunter, 2005). So it is inefficient to do it and the more recent method of exploiting this particular phenomenon is to use photon correlation rather than the intensity comparison (Hunter, 2005). Photon correlation aims at calculating what is called the autocorrelation function of the scattered light (Hunter, 2005). A correlator is basically a signal comparator. It is designed to measure the degree of similarity between two signals, or one signal with itself at varying time intervals. If the intensity of a signal is compared with itself at a particular point in time and a time much later, then for a randomly fluctuating signal it is obvious that the intensities are not related in any way (*i.e.* there will be no correlation between the two signals). However, if the intensity of signal at time = t is compared to the intensity a very small time later (t+Δt) there will be a strong relationship or correlation between the intensity of the two signals. The two signals are strongly or well correlated. If the signal, derived from a random process such as Brownian motion, at t is compared to the signal at t+2Δt, there will still be a reasonable comparison or correlation between the two signals, but it will not be as good as the comparison at t and t+Δt. The correlation decays with the time. In DLS the total time over which a measurement is made is divided into small time intervals (nanoseconds or microseconds) called delay times (Malvern Technical note). These intervals are selected to be small compared with the time it takes for a typical fluctuation to relax back to the average. The scattered light intensity in each of these intervals, as represented by the number of electrical pulses registered during each delay time, fluctuates about a mean value. The intensity autocorrelation function is formed by averaging the products of the intensities in these small time intervals as a function of the time between the intervals (delay times). A computer automatically controls the buildup of the function including the choice of delay times. The fluctuating signal is processed by forming the autocorrelation function G(t), τ being the time delay. (Instruction manual 90Plus).

$$G(\tau) = \frac{\langle I_s(t) I_s(t+\tau) \rangle_t}{\langle I_s \rangle_t^2} \qquad \text{(Equation 24)}$$

If the signal intensity (I_S) at t is compared with itself then there is a perfect correlation as the signals are identical. Perfect correlation is indicated by unity (1) and no correlation is indicated by zero (0). If the signals at t+2Δt, t+3Δt, t+4Δt, etc are compared with the signal at t, the correlation at a signal arriving from a random source will decrease with time until at some time, effectively t=infinity, there will be no correlation. If the particles are large, the signal will be changing slowly and the correlation will persist for a long time. If the particles are small and moving rapidly then correlation

will reduce more quickly (Figure 33). The time at which the correlation starts to significantly decay is an indication of the mean size of the sample (Malvern Technical note; Hunter, 2005). The decay of the autocorrelation is described by an exponential decay function G(t) (Malvern Technical note). Each monodisperse population of particle sizes produces its own unique autocorrelation function – a single exponential decay. Mixtures of more than one size population produces sums of exponentials (http://www.bic.com).

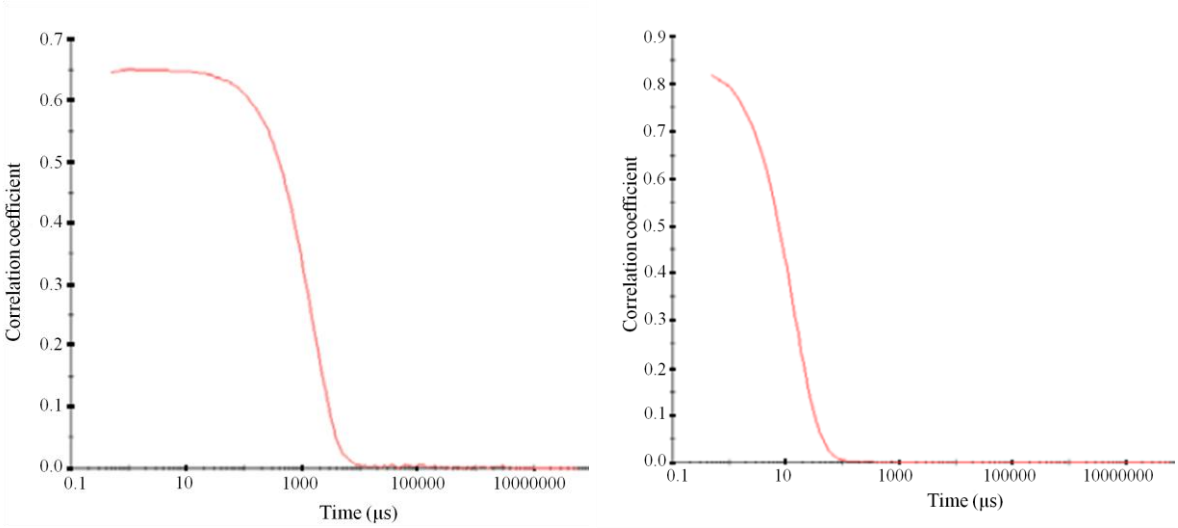

Figure 33: On the left, typical correlogram from a sample containing large particles in which the correlation of the signal takes a long time to decay. On the right, typical correlogram from a sample containing small particles in which the correlation of the signal decays more rapidly. (Malvern Technical note).

G(τ) relates the autocorrelation to the diffusion coefficient D and the wave vector q. By fitting the points of autocorrelation to the function G(t), the diffusion coefficient can be measured and related to the equivalent sphere of diameter d using the Stokes-Einstein equation (http://www.proteinchemist.com).

$$G(\tau) = Ae^{-2\Gamma\tau} + B \quad \text{(Equation 25)}$$

where *A* is the intercept of the correlation function, *B* is the baseline of the correlation function, τ is the time delay, and Γ, the decay rate is defined as in the following equation:

$$\Gamma = Dq^2 \quad \text{(Equation 26)}$$

$$D = \frac{k_B T}{3\pi\eta d} \quad \text{(Equation 27)}$$

$$q = \frac{2\pi n}{\lambda_0} 2 \sin\left(\frac{\theta}{2}\right) \quad \text{(Equation 28)}$$

$$d(H) = \frac{k_B T}{3\pi\eta D} \quad \text{(Equation 29)}$$

It is important to note that the autocorrelation function is the primary result measured by the instrument and all other information is computed from this curve. Available algorithms (Cumulant analysis, non-negative least square) can be used to extract "true" size distributions from complex samples (Malvern Technical note).

Dust is a generic term referring to a few, large particles that prevent a flat baseline. Without flat baseline, it is difficult to properly normalize the data and therefore to be confident with the results obtained. Dust can be a few, very large agglomerates coming from the sample itself, dust from air, or tiny bubbles (Instruction manual 90Plus). The Rayleigh approximation tells that the intensity of the light scattered is proportional to d^6 (d = diameter) (Malvern Technical note). It means that a 50 nm particle will scatter 10^6 or one million time as much light as a 5 nm particle (Malvern Technical note). There is therefore a danger that the light from larger particles will swamp the scattered light from the smaller one (Malvern Technical note). It is therefore essential to remove dust mechanically by filtration or centrifugation (Instruction manual 90Plus).

To summarize, a laser provides a light source to illuminate a sample contained in a cell. A detector is used to measure the light scattered by the particles present in solution and undergoing Brownian motion. The detector position is 90°. If too much light is detected, then the detector will become saturated. To overcome this, an attenuator is used to reduce the intensity of the laser source and hence reduce the intensity of scattering. For samples that do not scatter much light, such as very small particles or samples of low concentration, the amount of scattered light must be increased. In this situation, the attenuator will allow more laser light through to the sample. For samples that scatter more light, such as large particles or samples at higher concentration, the intensity of scattered light must be decreased. The appropriate attenuator position is automatically determined by the software. The scattering intensity signal from the detector is passed to a digital processing board called a correlator which compares the scattering intensity at successive time intervals to derive the rate at which the intensity is varying. This correlator information is then passed to a computer where the software will analyze the data and derive the size information (Malvern Technical note).

IV.2. Materials and Methods

IV.2.1. Materials and Chemicals

Still mineral water and sparkling water with a concentration of 7 g CO_2/L were kindly provided by Spadel S.A. (Spa, Belgium). The particle size analyzer 90Plus came from Brookhaven Instruments Corp. (Compiègne, France). The shaker (Bühler GmbH SM30) and the incubator hood (Bühler GmbH TH30) were purchased from Bühler (Berlin, Germany). A mycelium extract containing HFBI (at least 120 µg/mL mycelium extract) was obtained as described in the Chapter I in order to induce primary gushing. The buffer (Tris/HCl 170 mM, pH 9.0) was also used. Kieselghur and Mentos were used in order to induce secondary gushing.

IV.2.2. Methods

- Gushing test

2 mL of sparkling water (2°C) or still mineral water (2°C) were replaced by 2 mL of mycelium extract containing HFBI. Also 2 mL of sparkling water (2°C) were replaced by 2 mL of buffer (Tris/HCl). Secondary gushing was induced by introducing a Mentos pastille or 0.1 g of Kieselghur in sparkling water. The bottles were closed and shaken at 150 rpm in a horizontal position for 3 days at 25°C. After shaking, the bottles were weighed, left standing for 10 min and then manually turned upside down and right side up three times, with 10 sec of standing between each turn. After the last turn, the bottles were opened after 30 sec of standing. After the end of overfoaming, the bottles were weighed again to determine the amount of loss of liquid by overfoaming (Garbe *et al.*, 2007; Rath, 2008; Deckers *et al.*, 2011).

- Dynamic Light Scattering analysis

After the gushing test, 20 mL of the overfoaming were mixed with 30 mL of the remaining beverage and centrifuged (Beckman J2-21) at 4,000 × g for 10 min at room temperature. When there was no overfoaming, 50 mL of the beverage was used and centrifuged. The overfoam samples were then naturally degassed in a 100 mL volume beaker covered with a watch glass with a 4.5 cm diameter, till the CO_2 equilibrium concentration at atmospheric pressure and at room temperature (20°C) (1.66 g/L) was reached. Next, the (centrifuged and degassed) sample was homogenized by shaking and 4.5 mL was placed in a measurement cell (four optical slides), and the particle size was

determined by DLS with a particle size analyzer. To obtain the size particle distribution from the autocorrelation function, the algorithm non-negatively constrained least squares was applied but the refractive index of particles has to be known (Instruction Manual 90Plus). A refractive index of particles of 1.48 (*i.e.* refractive index of silica) was used as the refractive index of adsorbed protein layer is usually preset and its assumed value varies between 1.35 and 1.6 (Vörös, 2004). Five-1 min measurements were performed on each sample. To calculate the mean of five measurements each particle size distribution was simulated using Gaussian functions and the formule f(x):

$f(x) = a \times \exp[-(x - b)^2/2c^2]$, where *a* represents the height of the peak, *b* represents the position of its center (*i.e.* the mean value), and *c* represents the standard deviation. Standard deviation (c) is related to full width at half maximum (FWHM) by $FWHM = 2\sqrt{(2\ln 2)}c$. These three parameters were determined for each peak in each measurement by the least square method using the Excel (Microsoft Corp.) solver. For one sample, the mean value of each parameter (a, b, and c) was calculated simply as the arithmetic mean of the values determined for the five measurements. A representative sample is shown in Figure 34 (Deckers *et al.*, 2011). The reason why the results are expressed by a Gaussian curve in place of a cumulative curve will be discussed later on (see IV.3. Results and discussion).

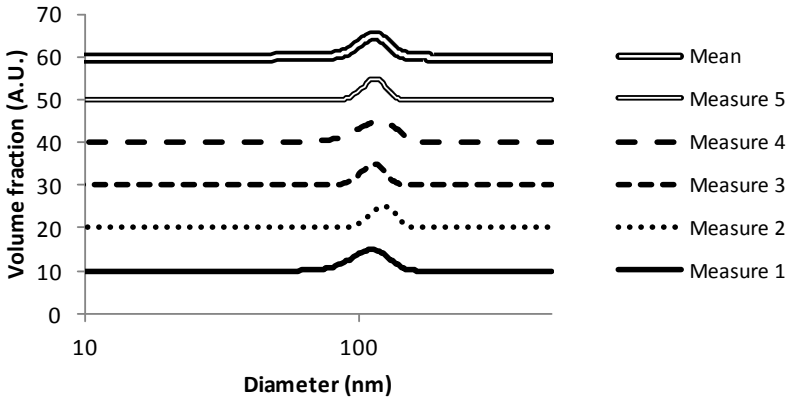

Figure 34: Example of the calculation of mean particle size distribution for sparkling water + 2 mL of mycelium extract. Experimental data obtained from five measurements performed on the same sample are indicated in the right part by Measure 1-5. For each of these measurements, a simulated Gaussian curve is shown. The average particle size distribution was calculated as the mean of the five simulated particle size distribution measurements (Deckers *et al.*, 2011).

IV.3. Results and Discussion

Before going into details through the results, the graphic expression of the results obtained by DLS has to be discussed. Some authors expressed the results by a cumulative curve (Christian *et al.*, 2009a) or by a Gaussian curve (Chiou *et al.*, 2005). For clarity, the first results obtained were

represented by both (Figure 35). In the cumulative curve, the result is graphically depicted as the volume sum distribution in dependency of the particle size. Existing particles are recognized by a slope in the graph, while a horizontal course represents absence of particle (Christian *et al.*, 2009b). However, later on, only the Gaussian representation will be used due to the fact that it is easier to be modelized it than a sigmoid and only the particles around 100 nm will be considered. It is the value of the critical diameter of CO_2 at atmospheric pressure. The method used to model the Gaussian curve is presented in the methods part. Further, in all studied samples, particles with approximately 1000 nm diameter were detected which will be discussed at the end of this chapter.

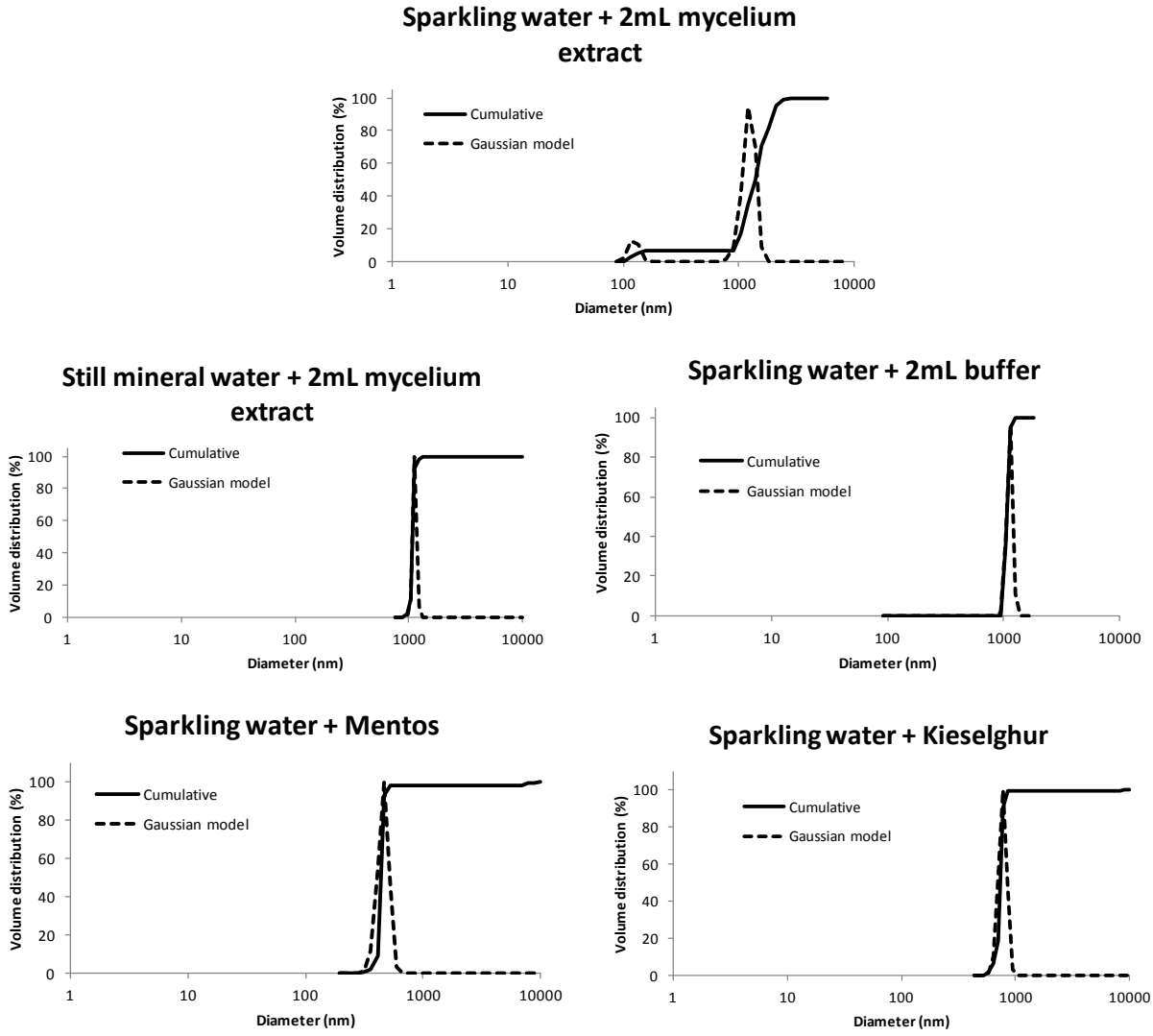

Figure 35: Volume sum distribution (continuous line) and volume size distribution (dashed line) of samples in five situations. Particles present in the sample are shown by a peak (dashed line) or by a vertical line (continuous line). When a mycelium extract containing hydrophobin is added to sparkling water, particles at 100 nm and at 1000 nm are detected. In still mineral water, only particles at 1000 nm are detected. Addition of the buffer used to extract hydrophobin in sparkling water leads to the presence of particles at 1000 nm. Addition of Mentos or Kieselghur results in the presence of particles below 1000 nm.

In order to study the importance of two key factors that determine primary gushing (carbon dioxide and hydrophobin), it was decided to choose still mineral water and sparkling water (7 g CO_2/L) as liquid matrix. From a 1 L bottle, samples were prepared from sparkling water by replacing 2 mL of sparkling water with either 2 mL of crude mycelium extract (in such a way, both carbon dioxide and hydrophobin are in the close bottle) or with 2 mL of extraction buffer (*i.e.* only carbon dioxide is present), or replacing 2 ml of still mineral water with 2 mL of mycelium extract (*i.e.* only hydrophobin is present). The results (Figure 36 (1)) show that without one of the two factors (carbon dioxide or hydrophobin) no gushing was observed. This means that to have gushing both carbon dioxide and hydrophobin are required. The results presented show also the particle size distribution (Figure 36 (2)). Most interesting is the appearance of particles by DLS with a diameter of approximately 100 nm in the degassed samples only when both CO_2 and hydrophobin were present in the experimental setup. This indicates a link between the observed gushing and the 100 nm particles. These particles may correspond to CO_2 bubbles with their critical diameter of 100 nm at atmospheric pressure which are stabilized by hydrophobin self-assembly, as described in a previous chapter.

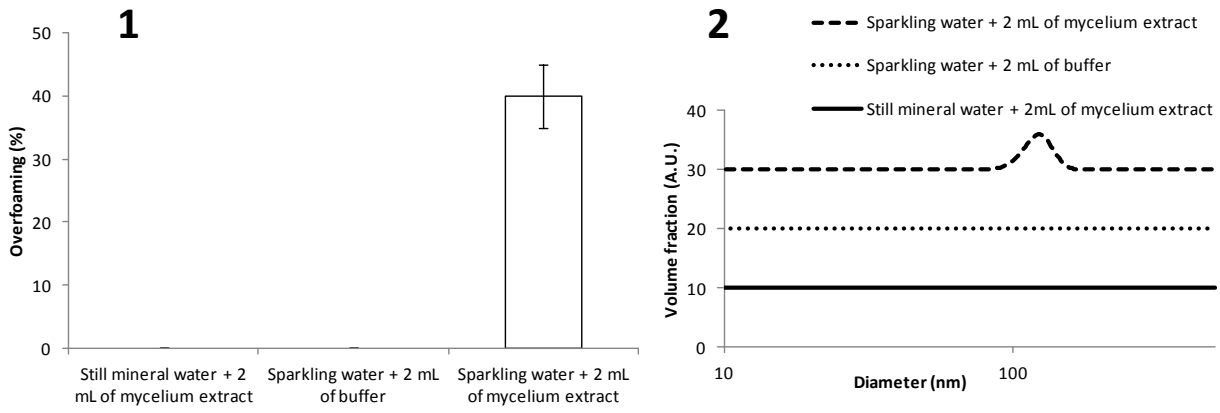

Figure 36: Determination of the overfoaming **(1)** and particle size distribution **(2)** of samples in three situations. Gushing is observed only when both hydrophobin and CO_2 are present (sparkling water + mycelium extract) but not when hydrophobin (sparkling water + buffer) or CO_2 (still mineral water + mycelium extract) is missing. In addition, particles at 100 nm are detected only when both key factors are present (sparkling water + mycelium extract). If hydrophobin (sparkling water + buffer) or CO_2 (still mineral water + mycelium extract) is missing, no particle at 100 nm is detected.

A DLS analysis was also performed on samples obtained by secondary gushing. Secondary gushing was induced by adding a Mentos pastille or Kieselghur (0.1 g) to the sparkling water instead of a 2 mL mycelium extract containing hydrophobin (Figure 37 (1)). The particle size distribution of these samples is shown in Figure 37 (2). Contrary to samples prepared by primary gushing no 100 nm diameter particles were found after secondary gushing.

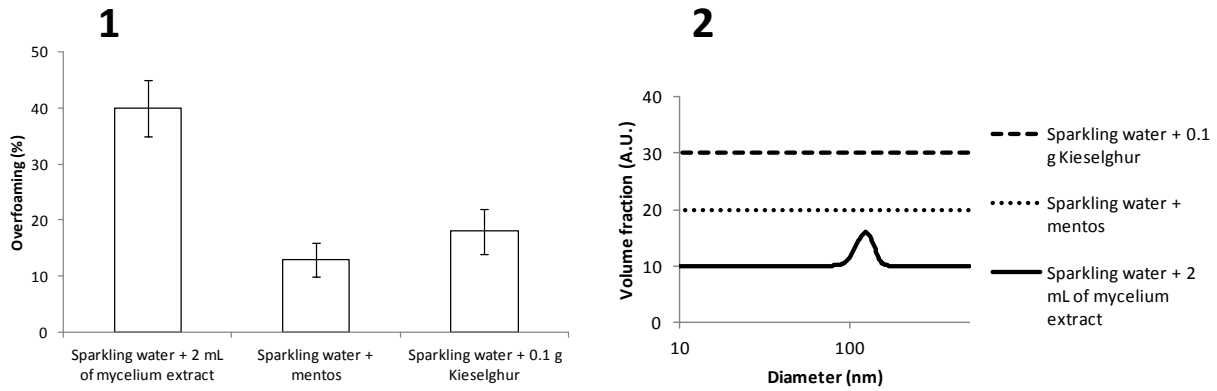

Figure 37: Determination of the overfoaming **(1)** and particle size distribution **(2)** of samples with primary or with secondary gushing opened at room temperature (25°C). Hydrophobin, mentos and kieselghur are able to induce gushing. However, only hydrophobin are able to stabilize CO_2 nanobubble at the critical diameter of 100 nm. Mentos and Kieselghur act as nucleation point and not as CO_2 stabilizer.

As observed in Figure 35, particles of approximately 1000 nm diameter were also detected in the samples. Their origin was analyzed by performing DLS analysis on de-ionized water, distilled water, still mineral water, degassed sparkling water, buffer, mycelium extract and sodium dodecyl sulfate dissolved in de-ionized water (1% w/v). For the water samples (de-ionized water, distilled water, still mineral water and degassed sparkling water), no particle was reported due to the bad autocorrelation function (*i.e.* no exponential decay) obtained (Figure 38). Therefore, the 1000 nm particles do not come from the watery matrix.

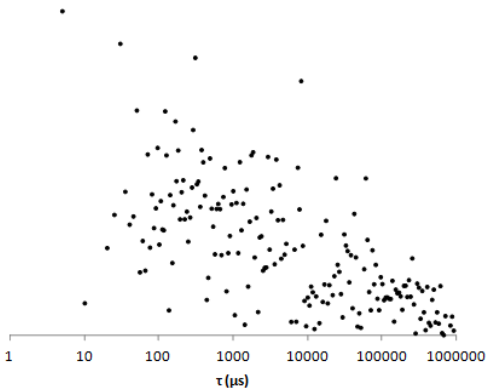

Figure 38: Autocorrelation function from de-ionized water. The function obtained is not an exponential decay and results most probably from the absence of particles.

As it can be seen (Figure 39), the particles originate from the buffer used to extract hydrophobin HFBI and probably from sodium dodecyl sulfate that was not completely removed by precipitation with KCl (Askolin *et al.*, 2001). Other results (Figure 39) show that a filter with pore size of 0.45 µm could remove the particles with 1000 nm diameter. Regarding the secondary gushing samples, Mentos and Kieselghur provide also particles around 1000 nm. (Figure 35).

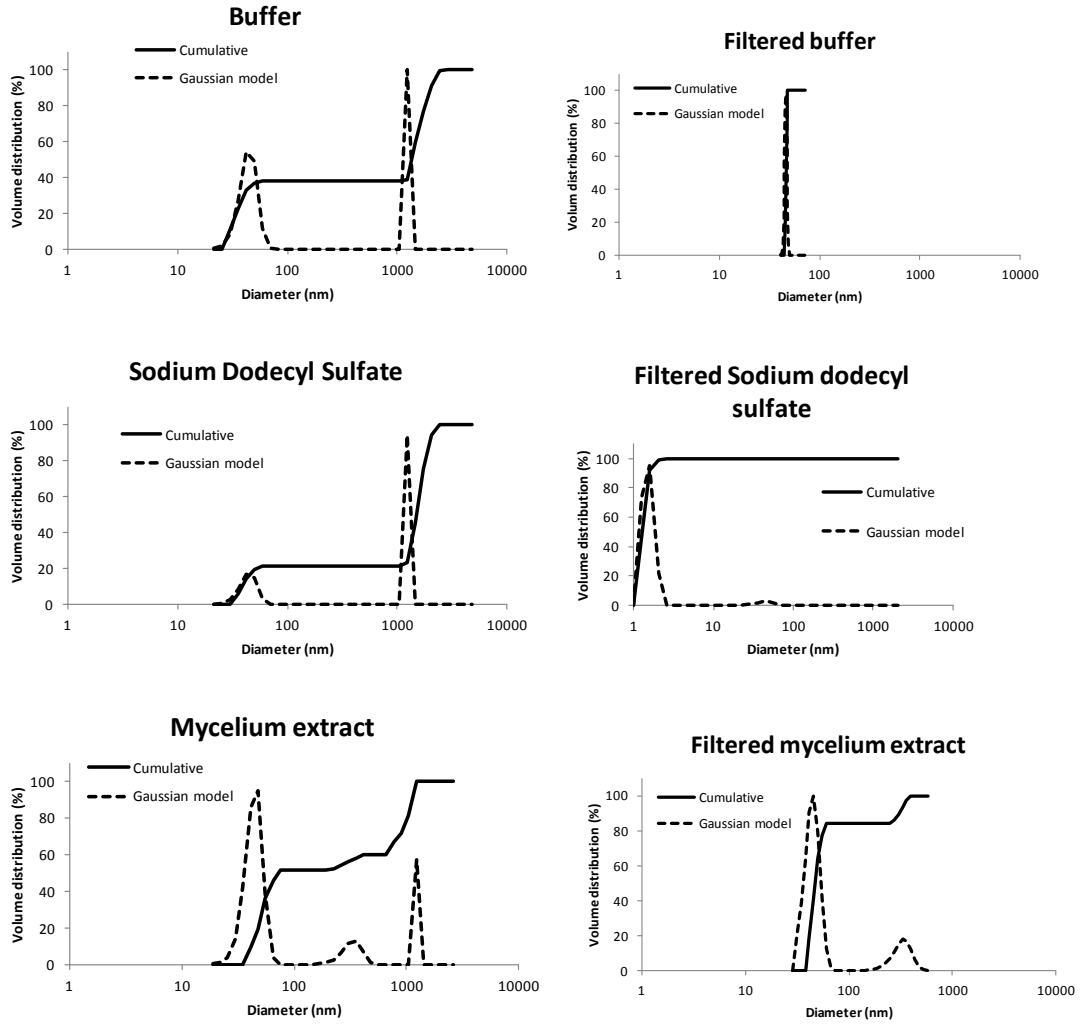

Figure 39: Volume sum distribution (continuous line) and volume size distribution (dashed line) of samples in six situations; buffer, buffer filtered on 0.45 µm, sodium dodecyl sulfate 1%, sodium dodecyl sulfate filtered on 0.45 µm, mycelium extract and mycelium extract filtered on 0.45 µm. The particles at 1000 nm in the mycelium extract come from the buffer containing sodium dodecyl sulfate used to extract the hydrophobin HFBI. A filtration (pore size of 0.45 µm) can remove these particles at 1000 nm.

The main advantage of the DLS method appears very interesting : the sample can be considered as primary gushing sample if and only if particles at 100 nm diameter are detected after shaking and storage under a saturated CO_2 atmosphere (1 bar) and as secondary gushing if overfoaming is observed without the detection of such particles.

IV.4. Conclusion

It was confirmed that for primary gushing the presence of both hydrophobin and carbon dioxide is necessary. The most interesting finding was that it is possible by DLS analysis to discriminate a primary gushing phenomenon from a secondary gushing or from non-gushing carbonated beverage after opening the container, degassing it at atmospheric pressure and treating it respecting the analytical rules described. DLS detects particles with a diameter of approximately 100 nm. These correspond to CO_2 nanobubbles stabilized by a hydrophobin self-assembled surface layer at 1 bar. These can never be formed in secondary gushing or in non-gushing samples.

Chapter V

DLS analysis: a new tool to predict the primary gushing potential of barley and malt and to distinguish primary from secondary gushing in beer[3]

The DLS method tuned and described in the previous chapter as a new tool to determine the nature of the gushing phenomenon in carbonated beverages (see Chapter IV) was used and found successful to predict and/or to confirm the primary gushing potential of barley and malt. It was also excellent to discriminate a beer with primary gushing from a beer with secondary gushing.

[3] This chapter is based on the following publication:

Deckers, S.M., Vissers, L., Gebruers, K., Shokribousjein, Z, Khalesi, M., Riveros-Galan, D., Schönberger, C., Verachtert, H., Neven, H., Delcour, J., Michiels, C., Ilberg, V., Derdelinckx, G., Titze, J., Martens, J., (2012). Doubly modified carlsberg test combined with dynamic light scattering allows prediction of the primary gushing potential of harvested barley and malt. *Cerevisia Belgian Journal of Brewing and Biotechnology* **37**, 77-81.

V.1. Introduction

As far as we know, no universal method is accepted in order to predict the primary gushing potential of barley and malt. Methods based on a correlative factor (Garbe *et al.*, 2009; Shokribousjein *et al.*, 2011), gushing tests (Garbe *et al.*, 2007) or on particle size analysis (Christian et *al.*, 2009a; Deckers *et al.*, 2011) were developed. Although gushing tests are mostly used in practice, they show a lack of reproducibility which is probably due to the number of parameters that can vary between analytical laboratories such as manipulation of the sample (grist size, method used,…), type of sparkling beverage (water, beer, …), conditioning of the bottle before opening (T opening, addition of sample, CO_2 concentration, …), shaking (orientation, speed,…), T opening … (Haikara *et al.*, 2005; Rath, 2008). Among the gushing tests, three "different" tests were developed. The first one, called Carlsberg test, consists of a water extract of malt added to a bottle of commercial beer. In 2010, Lutterschmid *et al.* observed that carbonated water is much more sensitive to hydrophobin gushing than beer, very likely because of the presence of substances in beer that restrict hydrophobin gushing and show a basic resistance to overfoaming. The beer viscosity can also be a reason. In the Modified Carlsberg test, the non-standardized beer matrix used in the Carlsberg test is replaced by sparkling water (7 g CO_2/L). In the third test, the doubly Modified Carlsberg test, fine malt grist is used for the preparation of a Congress wort and these worts are added to sparkling water (7 g CO_2/L). Garbe (2007 and 2009) reviewed the gushing tests and showed that the latter method was the best for a reliable prediction of gushing between six malts. In Germany, particle size analysis was used and showed the presence of particles around 5 nm diameter (Christian *et al.*, 2010a). As reported in the previous chapter we concentrated our study on the use of DLS and found that primary gushing is related to the presence of 100 nm particles (Deckers *et al.*, 2011). The objective of this chapter is to describe a reliable method for predicting the gushing potential of barley and malt. The results found with the combination of the doubly Modified Carlsberg test method and the DLS method for the analyses of harvested barley and malt samples are presented.

V.2. Materials and Methods

V.2.1. Materials

Barley gushing sample (variety Azurel) and non-gushing sample (variety Sebastian) were kindly provided by the Dingemans maltings (Stabroek, Belgium). Malt samples (gushing and non-gushing samples (variety Prestige)) were also kindly provided by Cargill (Herent, Belgium) and Dingemans (Stabroek, Belgium). Beer samples (gushing and non-gushing samples) were kindly provided by Duvel-Moortgat (Puurs, Belgium) (Beer Y) and Orval (Villers-devant-Orval, Belgium) (Beer Z) breweries. Sparkling water (7 g CO_2/L) was kindly delivered by S.A. Spadel (Spa, Belgium). The filters (Macherey-Nagel MN 614 ¼ 320 mm diameter) were purchased from FilterService (Eupen, Belgium).

V.2.2. Methods

V.2.2.1. Characterization of gushing potential of barley and malt by doubly Modified Carlsberg Test followed by DLS

- Extraction of hydrophobins from grains

In order to extract hydrophobins from grains, a standard laboratory Congress wort was produced according to Analytica-EBC method 4.5.1.(2004). Laboratory-scale mashing experiments were carried out in an automated mashing bath (LB8 Electronic mashing bath, Funke Gerber GmbH, Berlin, Germany). The grains were ground in a Bühler-Miag mill (Bühler-Miag, Minneapolis, MN, USA) set for fine grist coarseness (0.2 mm gap between the grinding discs). Fine grind (50.0 g) was mixed with 200 mL of water at 46°C. The composition of the grind is shown in Table 4. A temperature of 45°C was maintained in the mash for 30 min. The temperature was then raised at 1°C per min to 70°C before 100 mL water (70°C) were added. The temperature was maintained at 70°C for 1 h before cooling down to room temperature in 10-15 min (4°C per min). The mash was continuously stirred at 100 rpm. After adjusting the beaker content to 450 g, the contents were stirred thoroughly and emptied immediately and completely into a filter MN 614 ¼. The first 100 mL of the filtrate were returned to the funnel. The filtration was stopped when the cake appeared dry and the wort was obtained. Each combination (Table 4) was performed at least two times to produce a wort.

Table 4: Composition of the grind. Non-gushing barley is mixed with non-gushing or gushing malt in order to obtain a ratio from 0% till 50% of barley. Gushing barley was also mixed in the same ration with non-gushing malt. Gushing malt was mixed with non-gushing malt to obtain a ratio from 0% till 50% of gushing malt and also 100% gushing malt.

Non-gushing Barley – Non-gushing Malt							
NG Barley (%)	0	10	20	30	40	50	n.d.(*)
NG Malt (%)	100	90	80	70	60	50	n.d.
Gushing Barley – Non-gushing Malt							
G Barley (%)	0	10	20	30	40	50	n.d.
NG Malt (%)	100	90	80	70	60	50	n.d.
Non-gushing Malt – **Gushing** Malt							
NG Malt (%)	100	90	80	70	60	50	0
G Malt(%)	0	10	20	30	40	50	100
Non-gushing Barley – **Gushing** Malt							
NG Barley (%)	0	10	20	30	40	50	n.d.
G Malt (%)	100	90	80	70	60	50	n.d.

(*) n.d.: not determined

- Gushing test

For each testing of prepared wort, 20 mL of sparkling water (2°C) were replaced by 20 mL of wort (2°C). The bottles were crowned and shaken at 150 rpm (Bühler GmbH SM30, Berlin, Germany) in a horizontal position for 3 days at 25°C (Bühler GmbH TH30 incubator hoods, Berlin, Germany). After shaking, the bottles were weighed, left standing for 10 min and then manually turned upside down and right side up three times, with 10 sec of standing between each turn. After the last turn, the bottles were opened after 30 sec of standing. Once overfoaming ended, the bottles were weighed again to determine the amount of overfoaming that occurred (Garbe *et al.*, 2007; Rath, 2008; Deckers *et al.*, 2011).

- Dynamic Light Scattering analysis

After the gushing test, 20 mL of the overfoaming were mixed with 30 mL of the beverage remaining in the bottle and were centrifuged (Beckman J2-21) at 4,000 × g for 10 min at room temperature. 50 mL of the beverage was used and centrifuged if no overfoaming was observed. The samples were then naturally degassed in a 100 mL volume beaker with a 4.5 cm diameter which is covered by a watch glass, till the CO_2 equilibrium concentration at atmospheric pressure (1.66 g/L) (after 48h-72h) was reached. Next, the centrifuged and degassed sample was homogenized by shaking and 4.5 mL was placed in a measurement cell (four optical slides), and the particle size was determined by DLS with a particle size analyzer (90Plus, Brookhaven Instruments Corp.).
Three-1 min measurements were performed on each sample (Deckers *et al.*, 2011).

V.2.2. Characterization of gushing potential of finished beer by DLS

- Gushing test

Before opening, beer bottles were weighed and stored vertically at 25°C. The bottles were opened and weighed again to determine the overfoaming amount.

- Dynamic Light Scattering

The same method as described before was performed on the centrifuged and degassed beer samples.

V.3. Results and Discussion

Figure 40 (A1, B1, C1 and D1) shows the overfoaming (in % of the bottle content) observed after the gushing test. An overfoaming was observed only when contaminated raw material (barley and/or malt) was mixed in the grind for mashing. The DLS analysis (Figure 40; A2, B2, C2 and D2) confirmed by the detection of particles at 100 nm (Deckers *et al.*, 2011) that the gushing was due to the presence of hydrophobin. If we go in more details, it can be observed (Figure 40 B1) that only 10% of the gushing barley tested was enough to induce gushing but surprisingly when the percentage is increased (*i.e.* hydrophobin concentration is increased), no difference in the

overfoaming volume is observed. This means that the energy brought by the increased hydrophobin concentration is not enough to expel more liquid from the 1L-bottle. In fact the overfoaming is not directly proportional to the hydrophobin concentration (Sarlin *et al.*, 2005). In other words, if a concentration X is necessary to expel 50 mL, a concentration higher than 2X will be required to expel 100 mL. It is also possible that no gushing was detected on a barley infected by *Fusarium sp.* However, if this infected barley is malted, the malt will be gushing inducer as the hydrophobin concentration can increase during the malting process (Sarlin *et al*., 2007). So, a barley identified as gushing-negative does not mean that the resulting malt will be also gushing-negative ! It can be seen from Figure 40 C1 that only 10% of the contaminated malt in the sample is enough to induce gushing and from Figure 40 C1 and D1 that when the percentage of gushing malt is increasing (*i.e.* hydrophobin concentration is increasing) the overfoaming volume is also increasing. As the hydrophobin concentration is increased, more nanobubbles can be formed and more energy can be released at the opening resulting in a higher overfoaming volume. However, the percentage needed to induce gushing depends on the degree of infection, on the hydrophobin type and on the hydrophobin concentration as a minimal hydrophobin is required to induce gushing (Sarlin *et al.*, 2005). Moreover as demonstrated, the hydrogen binding of CO_2 with water plays also a major role in the quantity of liquid released (see Chapter III).

When barley and malt samples are found to be gushing potential positive (*i.e.* contaminated by hydrophobins), they can be returned to the malthouses before entering the final beer. These results show the extremely high utility of this technique as a preventive method to predict primary gushing potential of barley and/or malt.

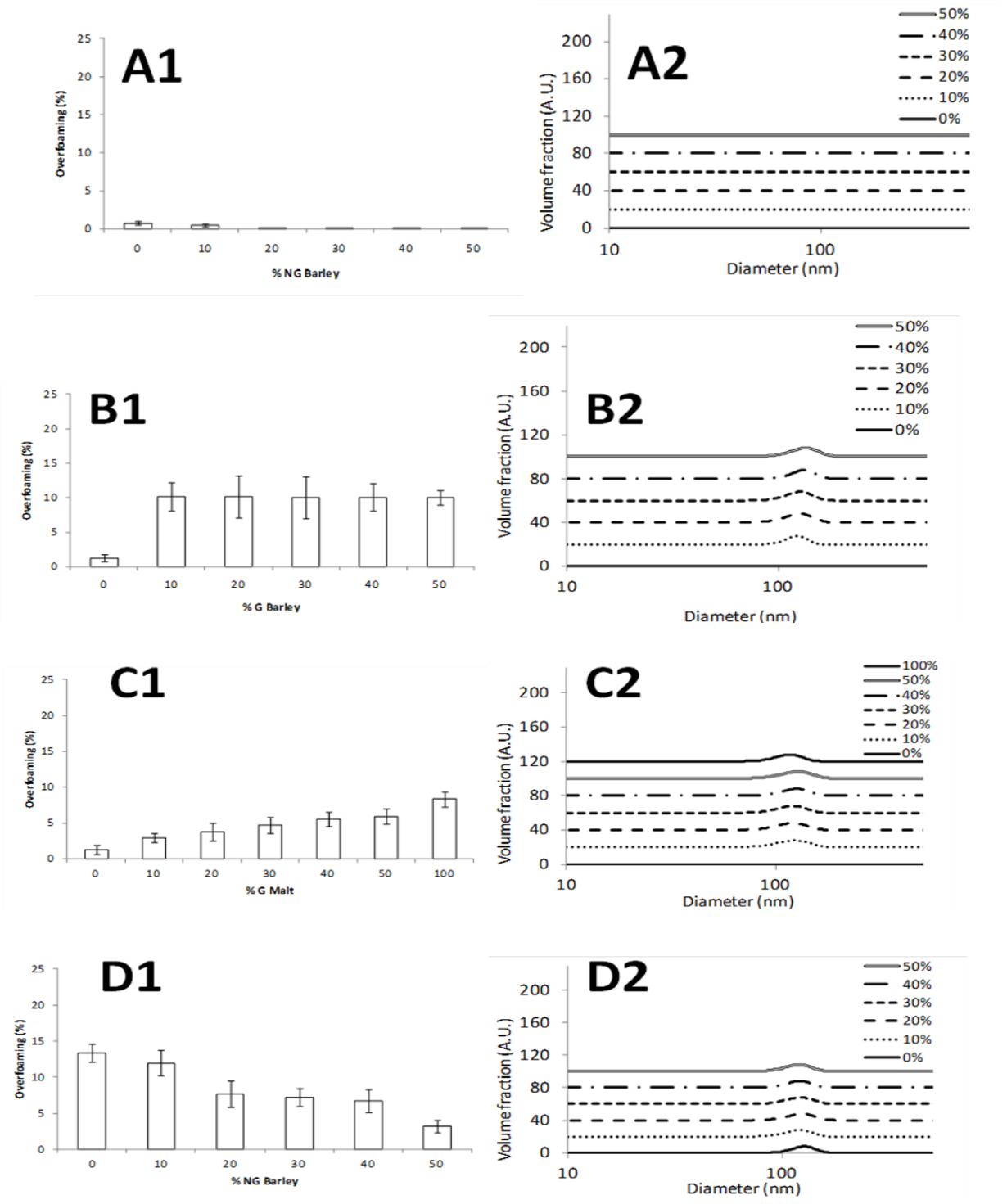

Figure 40: Determination of the overfoaming **(1)** and particle size distribution **(2)** of the different worts after the doubly Modified Carlsberg Test. **(A)** Wort produced with non-gushing barley and non-gushing malt. Gushing is observed when gushing barley is used and the DLS confirms the primary gushing. **(B)** Wort produced with gushing barley and non-gushing malt. Gushing is observed when gushing barley is used and the DLS confirms the primary gushing. **(C)** Wort produced with non-gushing malt and gushing malt. Gushing is observed when gushing malt is used and the DLS confirms the primary gushing. **(D)** Wort produced with non-gushing barley and gushing malt. Gushing is observed when gushing malt is used and the DLS confirms the primary gushing. The percentage are mentioned in Table 4. (Deckers *et al.*, 2012b).

This method was also tested on two commercial beers showing gushing. In Figure 41 (1) it can be seen that for Beer Y2 and Beer Z2 gushing is observed at 25°C. After DLS analysis (Figure 41 (2)), particles at 100 nm typical for primary gushing are only detected in gushing Beer Y2 but nor in the blank (Beer Y1 and Beer Z1) nor in gushing Beer Z2 (Figure 41 (2)). These results showed that this technique is useful to make the difference between a beer showing primary gushing (Beer Y2) and a beer with heavy gushing due to the presence of particles (solid nucleation sites) as in secondary gushing (Beer Z2).

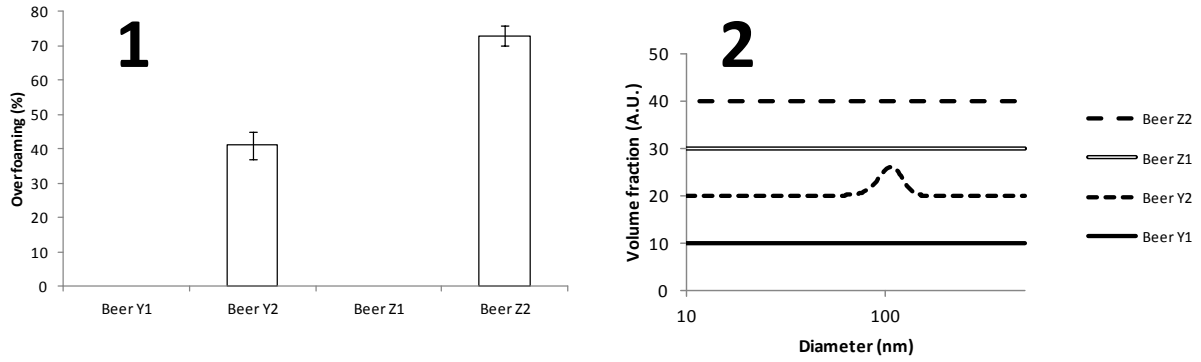

Figure 41: Commercial beers were tested. Gushing (1) is observed in the samples Y2 and Z2, but only the sample Y2 suffers of primary gushing as shown by the DLS (2) and the detection of particles at 100 nm (Deckers *et al.*, 2012b).

V.4. Conclusion

It is shown that the combination of the doubly modified Carlsberg test with the DLS method is confident and consistent to predict the primary gushing potential at the raw material level. It was also proved that it is possible to discriminate carbonated beverages showing primary gushing (particles at 100 nm) from one showing secondary gushing (no particle at 100 nm) using DLS analysis after opening the container.

General conclusions

Gushing is defined as a wild and uncontrolled overfoaming of carbonated beverages that appears at the bottle opening. Although many studies involving huge budgets were carried out for 25 years and although it is assumed that primary gushing is due to the presence of amphiphilic proteins as hydrophobins from molds and maybe ns-LTP from plant. Class II hydrophobins from fungal contaminations were assessed as the most probable causal agent but the mechanism of primary gushing was not at all clear. A better understanding of the phenomenon aiming at predicting and/or curing an economic unfavorable process was a priority of our research.

Chapter I

To study gushing two main responsible molecules must be at hand : CO_2 and a Class II hydrophobin. The CO_2 was available through the use of sparkling water specially and kindly carbonated at 7 g/L by Spadel S.A. To currently dispose of Class II hydrophobins it was decided to produce HFBI at lab-scale using a wild strain of *Trichoderma reesei*. Extraction from the mycelium, purification, detection, identification and sequencing were performed according to described methods, however with slight and appropriate modifications.

Chapter II

In order to understand in depth the gushing phenomenon the most important and essential physico-chemical properties of both CO_2 and Class II hydrophobins were reviewed. The main properties of CO_2 are its hydrophobicity and bubble critical diameter corresponding to 100 nm at atmospheric pressure. Regarding the hydrophobins, its special feature is the presence of hydrophobic aliphatic amino acids in what is called the "hydrophobic patch". Hydrophobins are produced by filamentous fungi to reduce the water surface tension by concentration and self-assembly at the hydrophobic-hydrophilic interface. They are known as strong surface-active molecules. Based on these properties and by performing molecular dynamics simulation, the detailed mechanism of primary gushing was highlighted and described in successive phases. In the closed container, the beverage contains hydrophobins contaminated during the carbonation step and/or non-contaminated hydrophobins. Due to their surface activity, hydrophobins migrate to the interface where they all become contaminated due to interaction with a pure CO_2 atmosphere. They are then concentrated at the interface where they reach locally the critical concentration required for crystallization. Once the crystalline structure is formed and if energy is incorporated to the system (*e.g.* shaking during transport), the Henry's equilibrium is imbalanced and it results in gas exchange. To return to equilibrium, CO_2 molecules provoke the bending of the crystalline structure of Class II hydrophobin due to the low surface tension (30 mJ/m^2). CO_2 accumulates inside and forms a bubble finally

closed by the Young-Laplace's law at the critical diameter corresponding to the pressure inside the closed bottle. Finally the carbonated beverage contains gaseous CO_2 nanobubbles stabilized by a crystalline layer formed by the self-assembly of Class II hydrophobin. At the bottle opening, the depressurization results in the expansion of the gas and the hydrophobin layer is nor solid nor elastic enough to resist, so that the nanobubble explode what is called the **nanobomb effect**. By explosion, vibration energy is given to the system resulting in the release of CO_2 and in the overfoaming. Although this mechanism is based on modelisation and on physico-chemical properties, it lacks the practical observation of the CO_2 nanobubble stabilized by the layer of Class II hydrophobin (see Chapter IV).

Chapter III

A thermodynamic approach of the gushing phenomenon was done in order to better understand why gushing tests failed in the inter-laboratory tests. It is explained that CO_2 is in fact bound to water molecules by hydrogen bonds. The vibration energy coming from the explosion of the stabilized nanobubble is enough to break these weak bonds to allow the CO_2 release. Although the CO_2 release is also influenced by the hydrophobin (type and concentration) and the extraction method, the thermodynamics highlights the fact that the overfoaming volume is mainly linked to the CO_2 properties. It is positively related to the liquid temperature at the bottle opening, to the pressure, to the CO_2 concentration and to the energy released.

Chapter IV

As the gushing tests, commonly used in the malt houses and in the breweries, showed a lack of reproducibility, a method based on the DLS technique was developed. This method is used to determine the size distribution of particles under Brownian motion in a liquid. The results showed that this method was able to detect the presence of particles of 100 nm in samples where gushing was artificially induced in sparkling water by addition of Class II hydrophobin produced at lab-scale. These particles correspond to gaseous CO_2 bubbles stabilized by Class II hydrophobin at their critical diameter of 100 nm at atmospheric pressure. Moreover, this method allowed the discrimination between primary and secondary gushing. In samples where secondary gushing was artificially induced by addition of kieselghur in sparkling water, no particles of 100 nm were detected. Kieselghur only acts as nucleation sites and not as a bubble stabilizer which is specifically obtained by Class II hydrophobins: thus primary gushing is specific by the presence of particles at 100 nm at atmospheric pressure.

Chapter V

A new method was developed using samples where gushing (primary or secondary) was artificially induced in sparkling water. It remained to find out whether this method could be used in practice to predict the gushing potential of barley and malt and to find out which type of gushing is involved in a gushing beer. For the analysis of grain samples, an extract must be made which is then added to sparkling water as done in the gushing tests. The Congress mash method was used in order to standardize as much as possible the parameters which can vary between laboratories and are responsible for the lack of reproducibility of the gushing tests. The DLS analysis was performed after the gushing test and the results showed that it was possible to predict the primary gushing potential of barley and malt by detection in Congress wort. However, care has to be taken when barley is analyzed. A gushing negative barley does not mean that the malt will be also gushing-negative. Barley can be contaminated but the hydrophobin level is lower than the concentration required to induce gushing and during the malting process, the concentration may increase to result in gushing positive raw material. Both barley and malt must be analyzed in gushing predictive tests. Regarding beer, only the DLS analysis can discriminate between primary and secondary gushing. This method will be submitted to the ASBC and EBC Analytical Committee for evaluation and potential inclusion in the Methods of Analysis after collaborative testing.

Perspectives

Our study shows that primary gushing is due to the interaction between CO_2 and the hydrophobic patch of Class II hydrophobins resulting in the stabilization of CO_2 bubbles by a crystalline hydrophobin layer. As the mechanism of primary gushing is described, it is important to continue the research work in order to find out the definite solution to prevent and cure primary gushing.

Contamination of barley by *Fusarium* and/or by other gushing-inducer fungi is of concern to malsters and brewers particularly in years when bad weather conditions favor the growth of toxicogenic and gushing-active *Fusarium* species (Lowe *et al.*, 2006). Various approaches and means might be considered to control *Fusarium head blight* (FHB), mould growth, mycotoxin and hydrophobin production. These include treatment with fungicides in the field, use of resistant barley cultivars, or biological fungal growth control during malting (Lowe and Arendt, 2004). Fungicide applied in the field may prevent the initial *Fusarium* infection and needs to be applied within narrow periods to be effective (Wolf-Hall, 2007) but application is often expensive and not applied as barley is a low-value crop (Lowe and Arendt, 2004). Although there is no truly FHB resistant barley cultivar, their development is being explored, but may take many years of breeding to achieve results. Even if the resistance is achieved, the new cultivars will also need to have characteristics that will command malting quality (Wolf-Hall, 2007). So, there are preferences for biopreservation, meaning the control of one organism by another one (Dalié *et al.*, 2010). The supply of moisture, the residence time and the temperature to which the cereals or other plants are subjected during the different steps of malting are favourable for the rapid growth and development of bacteria, yeasts and fungi, present naturally in barley and in the malting house and steeping is probably the most critical step at which proliferation begins (Boivin and Malanda, 1999; Lowe and Arendt, 2004). The application of starter cultures could inhibit the growth of undesirable moulds when applied to the steeping water in the early stage of malting due to the intensive growth of *Fusaria* during the very first hours of steeping (Lowe and Arendt, 2004). Yeasts (*Geotrichum candidum*) and lactic acid bacteria have been added during steeping to decrease fungal load (Boivin and Malanda, 1999; Laitila *et al.*, 2007; Barakat *et al.*, 2010). Boivin and Malanda demonstrated that the addition of specific, malt-derived *Geotrichum candidum* (teleomorph *Galactomyces geotrichum*) into the malting process restricted the fungal growth (Laitila *et al.*, 2007) of undesirable flora such as *Fusarium*, *Penicillium*, *Aspergillus*, and also the production of secondary metabolites such as mycotoxins and hydrophobins. Boivin and Malanda (1999) and Laitila *et al.* (2007) showed that *Pichia anomala* C565 added to the steeping water restricted *Fusarium* growth and suppressed the production of hydrophobin during malting and prevented beer gushing. The antifungal action of biocontrol yeasts is often due to several antagonistic mechanisms but no single

mechanism has been shown to be responsible for the whole antifungal action. The mechanisms are poorly understood and competition for nutrients and space has often been suggested as the main mode of the action mechanism (Laitila *et al.*, 2007). Lactic acid bacteria were employed as starter cultures for restricting the growth of *Fusarium* moulds to prevent gushing (Lowe *et al.*, 2006). Lactic acid bacteria not only produce antifungal compounds such as lactic acid, acetic acid, reuterin… and other uncharacterized agents (Barakat *et al.*, 2010), they also compete with other species by acidifying their environment and by rapidly depleting the nutrients (De Muynck *et al.*, 2004). However, relevant use of antifungal lactic acid bacteria requires thorough knowledge of the parameters that modulate their antifungal properties. Numerous parameters have been considered, including temperature, time of incubation, growth medium, pH and nutritional factors (Dalié *et al.*, 2010). The mode of action of many of these is not understood and the growth inhibiting effect of these cocktails is not predictable (Barakat *et al.*, 2010). Most publication on antifungal activity of lactic acid bacteria merely illustrate the activity, but rarely identify active compounds or other reasons for the inhibitory activity (Lowe and Arendt, 2004). Consequently before exploring the commercial application of the antifungal potentials of lactic acid bacteria cultures, more extensive work is required on these lines to know the exact nature and properties of antifungal substances produced (Lowe and Arendt, 2004) and to understand the biosynthetic pathway and mode of action of fungal inhibitors (Rouse *et al.*, 2008). Also to minimise the negative influence on organoleptic properties, several strategies are under investigations. The most promising method concerns the direct use of antifungal metabolites produced via fermentation by native or genetically-engineered organisms, purified and added to foods as pure chemicals (Dalié *et al.*, 2010). Purification of the substance is not always possible due to its instability, losing activity after two or three purification steps or after storage. It is also likely that the activity requires a combination of products (Lowe and Arendt, 2004). This strategy requires precise knowledge of the chemical structure and biosynthetic pathway of the concerned metabolites (Dalié *et al.*, 2010). Regarding this strategy, an antifungal protein, abundantly secreted by the filamentous fungi *Aspergillus giganteus*, appeared to be very efficient against the main fungal contaminants, mainly belonging to the genus *Fusarium*. It is a small cysteine-rich protein resistant to heat and protease degradation. Low amounts, in the micromolar range, are sufficient to compete fungal growth. Supplementation of antifungal protein to the steeping water, where a large amount of water is involved is not feasible under large-scale industrial settings. Its application during the malting process had no obvious negative impact on the quality of malt and wort (Barakat *et al.*, 2010). The transfer of knowledge obtained from laboratory experiments into real complex malting processes is a challenging area which definitely needs further studies (Laitila *et al.*, 2007). Biological control methods may be desirable due to the use of

natural inhibition, but the effects on quality will need to be evaluated (Wolf-Hall, 2007). Although microbiological methods show promise, the brewing and malting industries are looking for control of gushing as soon as possible in the whole malting and brewing process. (Wolf-Hall, 2007).

Regarding brewers, in order to avoid primary gushing when gushing-positive malt is used, a molecule which can interact with the hydrophobic patch of Class II hydrophobin could be looked after thus avoiding contact with CO_2. In this context research has focused on hop compounds (Outtrup, 1980; Hanke *et al.*, 2009; Christian *et al.*, 2009d; Müller *et al.*, 2010; Lutterschmid *et al.*, 2010 and 2011), but no universal compound to inhibit the interaction between CO_2 and Class II hydrophobin has been found. As yet the future must concentrate on finding a universal compound able to interact with hydrophobin without modifying the quality of the carbonated beverage. The mode, the time and the place of its addition must be investigated. The compound has to be well dispersed in order to bind all hydrophobin molecules present and the injection has to be done before carbonation because once the hydrophobin is contaminated by CO_2, it is difficult if not impossible to disturb this interaction. Regarding the nanobubble formation, a solution would be the production of bottle with hydrophobic internal surface. If the interaction between the hydrophilic glass wall and the Class II hydrophobins that helps for the formation of the stabilized nanobubbles is prevented, the primary gushing problem will be solved (Derdelinckx *et al.* Patent under examination GB1217972.7)

Although hydrophobins have a negative aspect regarding the gushing phenomenon, they were suggested for a number of positive applications due to their extraordinary surface properties. The self-assembly of hydrophobins makes them interesting for use as stabilizers of emulsions, foaming agents and targets for the immobilization of other components. The application of hydrophobins in biosensor developments, in surface property modification and in tissue engineering were studied as well (Khalesi *et al.*, 2012). Therefore, developing methods to detect, isolate and mainly to purify these valuable proteins at a high purity level in real scale is interesting for industries, especially those which are looking for products in the area of nano-biotechnology. Our investigations on gushing allows a better understanding of the binding of CO_2 with hydrophobins and led to the study of their purification by foam fractionation using CO_2 (Khalesi *et al.*, 2013) combined to a glass separatory funnel for their isolation (Derdelinckx *et al.* Patent under investigation ZL912012).

References

Alexandrov, N.A.; Marinova, K.G.; Gurkov, T.D.; Danov, K.D.; Kralchevsky, P.A.; Stoyanov, S.D.; Blijdenstein, T.B.J.; Arnaudov, L.N.; Pelan, E.G.; Lips, A.; (2012). Interfacial layers from the protein HFBII hydrophobin : dynamic surface tension, dilatational elasticity and relaxation times. *Journal of Colloid and Interface Science* **376** (1), 296-306.

Altschul, S.F., Madden, T.L., Schäffer, A.A., Zhang, J., Zhang, Z., Miller, W., Lipman, D.J., (1997). Gapped BLAST and PSI-BLAST: A new generation of protein database search program. *Nucleic Acids Research* **25**, 3382-3402.

Askolin, S., Nakari-Setälä, T., Tenkanen, M., (2001). Overproduction, purification, and characterization of the *Trichoderma reesei* hydrophobin HFBI. *Applied Microbiology and Biotechnology* **57**, 124-130.

Askolin, S., Turkenburg, J.P., Tenkanen, M., Uotila, S., Wilson, K.S., Penttilä, M., Visuri, K., (2004). Purification, crystallization and preliminary X-ray diffraction analysis of Trichoderma reesei hydrophobin HFBI. *Acta Crystallographica Section* **D60**, 1903-1905.

Askolin, S., Penttilä, M., Wösten, H.A.B., Nakari-Setälä, T., (2005). The *Trichoderma reesei* hydrophobin genes *hfb1* and *hfb2* have diverse functions in fungal developments. *FEMS Microbiology Letters* **253**, 281-288.

Bailey, M.J., Askolin, S., Hörhammer, N., Tenkanen, M., Linder, M., Penttilä, M., Nakari-Setälä, T., (2002). Process technological effects of deletion and amplification of hydrophobin I and II in transformants of *Trichoderma reesei*. *Applied Microbiology and Biotechnology* **58**, 721-727.

Bamforth, C.W., (2004). The relative significance of physics and chemistry for beer foam excellence: theory and practice. *Journal of the Institute of Brewing* **110** (4). 259-266.

Barakat, H.; Spielvogel, A.; Hassan, M.; El-Desouky, A.; El-Mansy, H.; Rath, F.; Meyer, V.; Stahl, U.; (2010). The antifungal protein AFP from *Aspergillus giganteus* prevents secondary groxth of different *Fusarium* species on barley. *Applied Microbiology and Biotechnology* **87**, 617-624.

Basheva, E.S.; Kralchevski, P.A.; Christov, N.C.; Danov, K.D.; Stoyanov, S.D.; Blijdenstein, T.B.J.; Kim, H-J.; Pelan, E.G.; Lips, A.; (2011). Unique properties of bubbles and foam films stabilized by HFBII hydrophobin. *Langmuir* **27**, 2382-2392.

Baur, J.E., Baur, M.B., Franz, D.A.; (2006). The ultrasonic soda fountain: a dramatic demonstration of gas solubility in aqueous solutions. *Journal of Chemical Education* **83** (4): 577-580.

Bayry, J., Aimanianda, V., Guijaro, J.I., Sunde, M., Latgé, J-P., (2012). Hydrophobins – unique fungal proteins. *PloS Pathogens* **8** (5), e1002700 (4 pages).

Bech, L.M., Vaag, P., Heinemann, B., Breddam, K., (1995). Through-out the brewing process barley lipid transfer protein 1 (LTP1) is transformed into a more foam-promoting form. Proceedings of the European Brewery Convention Congress, Brussels, Belgium, 561-568.

Blatteau, J-E., Souraud, J-B., Gemp, E., Boussuges, A.; (2006). Gas nuclei, their origin and their role in bubble formation. *Aviation, Space and Environmental Medecine* **77** (10): 1068-1076.

Bobalova, J., Chmelik, J., (2007). Proteomic identification of technologically modified proteins in malt by combination of protein fractionation using convective interaction media and matrix-assisted laser desorption/ionization time-of-flight mass spectrometry. *Journal of Chromatography A* **1163**, 80-85.

Boivin, P.; Malanda, M.; (1999). Inoculation by *Geotrichum candidum* during malting of cereals or other plants. United States Patent, Patent Number 5,955,070.

Bussi, G., Donadio, D., Parrinello, M.; (2007). Canonical sampling through velocity rescaling. *The Journal of Chemical Physics* **126**, 014101. doi:10.1063/1.2408420

Byrd, J.; Perona, M.; (1999). Surface tension and soap bubble. http://wwwchem.csustan.edu (13/08/2012)

Casey, G.P., (1996). Primary versus secondary gushing and assay procedures used to assess malt/beer gushing potential. *Technical Quaterly Master Brewers Association of the Americas* **33** (4), 229-235.

Chaplin, M.; (2012). Water structure and science, the CO_2-water cluster. http://www.lsbu.ac.uk (13/08/2012)

Chasan, R., (1991). Lipid Transfer Proteins: movig molecules? *The Plant Cell* **3**, 842-843

Cheung, D.L.; (2012). Molecular simulation of hydrophobin adsorption at an oil-water interface. *Langmuir* **28** (23), 8730-8736.

Chiou, H.; Fellows, C.M.; Gilbert, R.G.; Fitzgerald, M.A.; (2005). Study of rice-starch structure by dynamic light scattering in aqueous solution. *Carbohydrate Polymers* **61**, 61-71.

Christian, M.; Ilberg, V.; Aydin, A.A.; Titze, J.; Friess, A.; Jacob, F.; Parlar, H.; (2009a). New gushing mechanism proposed by applying particle size analysis and several surfactants. *Brewing Science* **62**, 100-107.

Christian, M.; Ilberg, V.; Titze, J.; Aydin, A.A.; Jacob, F.; Parlar, H.; (2009b). New cognitions on the gushing phenomenon. 32nd European Brewing Convention Congress, Hamburg, Germany, Poster 9.

Christian, M.; Ilberg, V.; Titze, J.; Friess, A.; Jacob, F.; Parlar, H.; (2009c). Gushing laboratory tests as successful methods for obtaining new cognitions on gushing. *Brewing Science* **62**, 83-89.

Christian, M., Ilberg, V., Titze, J., Parlar, H.; Jacob, F.; (2009d). New ideas for quantifying the gushing potential of malt. *Brewing Science* **62**, 164-170.

Christian, M.; Titze, J.; Ilberg, V.; Jacob, F.; (2010a). Combined particle analysis as a new tool to predict gushing shown with alcohol-free beverages products. *Brewing Science* **63**, 72-75.

Christian, M.; Titze, J.; Ilberg, V.; Jacob, F.; (2010b). New cognitions in the wort production process and in quantifying the gushing potential of malt. *Cerevisia Belgian Journal of Brewing and Biotechnology* **35**, 35-37.

Christian, M.; Titze, J.; Ilberg, V.; Jacob, F.; (2011). Novel perspectives in gushing analysis: a review. *Journal of the Institute of Brewing* **117** (3), 295-313.

Cox, A.R., Cagnol, F., Russel, A.B., Izzard, M.F.; (2007). Surface properties of class II hydrophobins from *Trichoderma reesei* and influence on bubble stability. *Langmuir* **23**: 7995-8002.

Cox, A.R.; Aldred, D.L.; Russel, A.B.; (2009). Exceptional stability of food foams using class II hydrophobin HFBII. *Food Hydrocolloids* **23**, 366-376.

Crolly, G.; (2012). Terms particle sizing – Hydrodynamic diameter. http://www.fritsch-sizing.com/index.php?id=990795 (22/08/2012).

Dalié, D.K.D.; Deschamps, A.M.; Richard-Forget, F.; (2010). Lactic acid bacteria – potential for control of mould growth and mycotoxins : a review. *Food Control* **21**, 370-380.

De Clerck, J., (1973). Manifestation d'hommage au Professeur Jean De Clerck. *Bulletin de l'Association Royale des Anciens Etudiants en Brasserie de l'Université de Louvain*, **2**, 25-47.

De Muynck, C.; Leroy, A.I.J.; De Maeseneire, S.; Arnaut, F.; Soetart, W.; Vandamme, E.J.; (2004). Potential of selected lactic acid bacteria to produce food compatible antifungal metabolites. *Microbiological Research* **159**, 339-346.

Deckers, S.M., Gebruers, K., Baggerman, G., Lorgouilloux, Y., Delcour, J.A., Michiels, C., Derdelinckx, G., Martens, J., Neven, H.; (2010). CO_2-hydrophobin structures acting as nanobombs in beer Part 1: a critical review of hypotheses and mechanisms. *Brewing Science* **63**: 54-61.

Deckers, S.M., Lorgouilloux, Y., Gebruers, K., Baggerman, G., Verachtert, H., Neven, H., Michiels, C., Derdelinckx, G., Delcour, J.A., Martens, J.; (2011). Dynamic Light Scattering (DLS) as a tool to detect CO_2-Hydrophobin structures and study the primary gushing potential of beer. *Journal of the American Society of Brewing Chemists* **69** (3): 144-149**.**

Deckers, S.M., Venken, T., Khalesi, M., Gebruers, K., Baggerman, G., Lorgouilloux, Y., Shokribousjein, Z., Ilberg, V., Schönberger, C., Titze, J., Verachtert, H., Michiels, C., Neven, H., Delcour, J., Martens, J., Derdelinckx, G., De Maeyer, M., (2012a). Combined modeling and biophysical characterisation of CO_2 interaction with Class II hydrophobins: new insight into the mechanism underpinning primary gushing. *Journal of American Society of Brewing Chemists* **70** (4), 249-256.

Deckers, S.M., Vissers, L., Gebruers, K., Shokribousjein, Z., Khalesi, M., Riveros-Galan, D., Schönberger, C., Verachtert, H., Neven, H., Delcour, J., Michiels, C., Ilberg, V., Derdelinckx, G., Titze, J., Martens, J., (2012b). Doubly modified carlsberg test combined with dynamic light scattering allows prediction of the primary gushing potential of harvested barley and malt. *Cerevisia Belgian Journal of Brewing and Biotechnology* **37**, 77-81.

Denschlag, C.; Vogel, R.F.; Niessen, L.; (2012). Hyd5 gene-based detection of the major gushing-inducing *Fusarium spp.* in a loop mediated isothermal amplification (LAMP) assay. *International Journal of Food Microbiology* **156** (3), 189-196.

Derdelinckx, G.; Deckers, S.M.; Khalesi, M.; Martens, J.; Rongé, J.; Gebruers, K.; Delcour, J.; Venken, T.; DeMaeyer, M. Patent ZL912012 Hydrophobin purification. *Under investigation*

Derdelinckx, G.; Deckers, S.M.; Khalesi, M.; Shokribousjein, Z.; Verachtert, H. Patent GB1217972.7 Bottle with means to prevent gushing. *Under investigation*

Douliez, J-P., Michon, T., Elmorjani, K., Marion, D., (2000). Structure, biological and technological functions of lipid transfer proteins and indolines, the major lipid binding proteins from cereal kernels. *Journal of Cereal Science* **32**, 1-20.

Dubreil, L., Gaborit, T., Bouchet, B., Gallant, D.J., Broekaert, W.F., Quillien, L., Marion, D., (1998). Spatial and temporal distribution of the major isoforms of puroindolines (puroindoline-a and puroindoline-b) and non specific lipid transfer protein (ns-LTP1) of *Triticum aestivum* seeds. Relationships with their in vitro antifungal properties. *Plant Science* **138**, 121-135.

Essmann, U., Perera, L., Berkowitz, M.L., Darden, T., Lee, H., Pedersen, L.G.; (1995). A smooth particle mesh Ewald method. *The Journal of Chemical Physics* **103,** 8577-8593. doi:10.1063/1.470117

European Brewing Convention, (2004). Analytica-EBC, section 4, method 4.5.1. Extract of malt: Congress Mash. Verlag Hans Carl Getränke-Fachverlag, Nürnberg, Germany.

Fan, H., Wang, X., Zhu, J., Robillard, G.T., Mark, A.E., (2006). Molecular dynamics simulations of the hydrophobin SC3 at a hydrophobic/hydrophilic interface. *Proteins* **64**, 863-873.

Fischer, S., (2001). Blasenbildung von in flüssigkeiten gelösten gasen. Dissertation, Technische Universität Munchen, Germany, 134p.

Flannigan, B., (2003). The microbiota of barley and malt. In: Brewing Microbiology. Priest F.G., Campbell, I. (eds). 3rd edition. New-York: Kluwer Academic/Plenum Publishers.

Flannigan, B., Okague, R.N., Khalid, R., Teoh, C.K., (1982). Mould flora of malt in production and storage. *Brewing and Distilling International* **12**, 31-37.

Garbe, L;-A., Nagel, R., Rauschmann, M., Lamers, M., Ehmer, A., Tressl, R., (2007). Correlation of deoxynivalenol, hydrophobins and gushing. *Proceedings of the European Brewery Convention Congress*, Venice.

Garbe, L-A., Schwarz, P.; Ehmer, A.; (2009). Beer gushing. In Beer: a quality perspective. C.W. Bamforth, I. Russell, G.G. Stewart, (Eds.), Elsevier: New-York, pp 185-212.

Gardner, R.J., (1973). The mechanism of gushing – a review. *Journal of the Institute of Brewing* **79**, 275-283.

Gorjanovic, S., (2007). Barley grain non-specific lipid-transfer proteins (ns-LTPs) in beer production and quality. *Journal of the Institute of Brewing* **113** (3), 310-324.

Gorjanovic, S., Suznjevic, D., Beljanski, M., Ostojic, S., Gorjanovic, R., Vrvic, M., Hranisavljevic, J., (2004). Effects of lipid-transfer protein from malting barley grain on brewers yeast fermentation. *Journal of the Institute of Brewing* **110** (4), 297-302.

Gorjanovic, S., Spillner, E., Beljanski, M.V., Gorjanovic, R., Pavlovic, M., Gojgic-Cvijanovic, G., (2005). Malting barley grain non-specific lipid-transfer protein (ns-LTP): importance for grain protection. *Journal of the Institute of Brewing* **111** (2), 99-104.

Gyllang, H., Kjellen, K., (1981). Evaluation of fungal contaminations on barley and malt. *Journal of the Institute of Brewing* **87**, 248-251.

Hahn, D.W.; (2009). Light scattering theory. Http://plaza.ufl.edu/dwhahn/Rayleigh%20and%20Mie%20Light%20Scattering.pdf (12/08/2012)

Haikara, A., Sarlin, T., Nakari-Setälä, T., Penttilä, M., (1999). Method for determining a gushing factor for a beverage. International Patent Application, WO 99/54725.

Haikara, A.; Sarlin, T.; Home, S.; (2005). Determination of gushing tendency of malt. *Journal of the Institute of Brewing* **111** (2), 247.

Hakanpää, J., Paananen, A., Askolin, S., Nakari-Setälä, T., Parkkinen, T., Penttilä, M. Linder, M.B., Rouvinen, J., (2004). Atomic resolution structure of HFBII hydrophobin, a self-assembling amphiphile. *The Journal of Biological Chemistry* **279**, 534-539.

Hakanpää, J., Linder, M., Popov, A., Schmidt, A., Rouvinen, J., (2006a). Hydrophobin HFBII in detail: ultrahigh-resolution structure at 0.75Å. *Acta Crystallographica* **D62**, 356-367.

Hakanpää, J., Szilvay, G.R., Kaljunen, H., Maksivainen, M., Linder, M., Rouvinen, J., (2006b). Two crystal structures of *Trichoderma reesei* hydrophobin HFBI-The structure of a protein amphiphile with and without detergent interaction. *Protein Science* **15**, 2129-2140.

Hanke, S.; Kern, M.; Herrman, M.; Back, W.; Becker, Th.; Krottenthaler, M.; (2009). Suppression of gushing by hop constituents. *Brewing Science* **62** (11/12), 181-186.

Heinemann, B., Andersen, K.V., Nielsen, P.R., Bech, L.M., Poulsen, F.M., (1996). Structure in solution of a four-helix lipid binding protein. *Protein Science* **5**, 13-23.

Hepworth, N.J., Boyd, J.W.R., Hammond, J.R.M., Valey, J.; (2003). Modelling the effect of liquid motion on bubble nucleation during beer dispense. *Chemical Engineering Science.* **58**, 4071-4084.

Hess, B., Kutzner, C., van der Spoel, D., Lindahl, E.; (2008). GROMACS 4: Algorithms for highly efficient, load-balanced, and scalable molecular simulation. *Journal of Chemical Theory and Computation* **4**, 435-447. doi: 10.1021/ct700301q

Hill, J.W.; Petrucci, R.H.; McCreary, T.W.; Perry, S.S.; (2009). Chapitre 8: Les états de la matière et les forces intermoléculaires. In: Chimie générale (2nd eds). Editions du Renouveau Pédagogique Inc. Canada, 360-424.

Hippeli, S., Elstner, E.F., (2002). Are hydrophobins and/or non-specific lipid transfer proteins responsible for gushing in beer? New hypotheses on the chemical nature of gushing inducing factors. *Verlag der Zeitschrift für Naturforschung* **57c**, 1-8.

Hippeli, S., Hecht, D., (2009). The role of ns-LTP1 and proteases in causing primary gushing. *Brauwelt International* **27**, 30-34.

Hub, J.S., de Groot, B.L.; (2006). Does CO_2 Permeate through Aquaporin-1? *Biophysical Journal* **91**, 842–848. doi:10.1529/biophysj.106.081406

Hunter, R.J.; (2005). Chapter V Particle size and shape. In: Foundations of Colloid Science (2nd edition). Oxford University Press Inc., New-York.

Instruction Manual 90 Plus. Brookhaven Instruments Corporation.

Jégou, S., Douliez, J-P., Mollé, D., Boivin, P., Marion, D., (2000). Purification and structural characterization of LTP1 polypeptides from beer. *Journal of Agricultural and Food Chemistry* **48**, 5023-5029.

Jones, S.F.; Evans, G.M.; Galvin, K.P.; (1999). Bubble nucleation from gas cavities – a review. *Advances in Colloid and interface Science* **80**, 27-50.

Jonsson, A.P., (2001). Review Mass spectrometry for protein and peptide characterisation. *Cellular and Molecular Life Sciences* **58**, 868-884.

Jorgensen, W.L., Chandrasekhar, J., Madura, J.D., Impey, R.W., Klein, M.L.; (1983). Comparison of simple potential functions for simulating liquid water. *Journal of Chemical Physics* **79**, 926-935. Doi:10.1063/1.445869

Jorgensen, W.L., Tirado-Rives, J.; (1988). The OPLS [optimized potentials for liquid simulations] potential functions for proteins, energy minimizations for crystals of cyclic peptides and crambin. *Journal of the American Chemical Society* **110**, 1657–1666. doi:10.1021/ja00214a001

Kader, J-C., (1996). Lipid-transfer proteins in plants. *Annual Review of Plant Physiology and Plant Molecular Biology* **47**, 627-654. Abstract.

Kader, J-C., (1997). Lipid-transfer proteins: a puzzling family of plant proteins. *Trends in plant science reviews* **2** (2), 66-70.

Kallio, J.M., Linder, M.B., Rouvinen, J., (2007). Crystal structures of hydrophobin hfbii in the presence of detergent implicate the formation of fibrils and monolayer films. *Journal of Biological Chemistry* **282** (39), 28733-28739.

Kastner, H., (1909). Das "Wildwerde," des Malzbieres. *Wochenschrift für Brauerei* **26**, 169-170.

Kaufmann, R., (1995). Matrix-assisted laser desorption ionization (MALDI) mass spectrometry: a novel analytical tool in molecular biology and biotechnology. *Journal of Biotechnology* **41**, 155-175.

Khalesi, M.; Deckers, S.M.; Gebruers, K.; Vissers, L.; Verachtert, H.; Derdelinckx, G.; (2012). Hydrophobins : exceptional proteins for many applications in brewery environment and other bio-industries. *Cerevisia Belgian Journal of Brewing and Biotechnology* **37** (1), 3-9.

Khalesi, M.; Venken, T.; Deckers, S.; Winterburn, J.; Shokribousjein, Z.; Gebruers, K.; Verachtert, H.; Delcour, J.; Martin, P.; Derdelinckx, G.; (2013). A novel method for hydrophobin extraction using CO_2 foam fractionation system. *Industrial Crops and Products* **43**, 372-377.

Kisko, K., Torkkeli, M., Vuorimaa, E., Lemmetyinen, H., Seeck, O.H., Linder, M., Serimaa, R., (2005). Langmuir-Blodgett films of hydrophobins HFBI and HFBII. *Surface Science* **584**, 35-40.

Kisko, K., Szilvay, G.R., Vaimio, U., Linder, M.B., Serimaam, R., (2008). Interactions of hydrophobins proteins in solution studied by small-angle X-ray scattering. *Biophysical Journal* **94**, 198-206.

Kovacs, K., Megyeri, L., Szakacs, C.P., Galbe, M., Zacchi, G., (2008). *Trichoderma atroviride* mutants which enhanced production of cellulase and β-glucosidase on pretreated willow. *Enzyme and Microbial Technology* **43**, 48-55.

Laitila, A., (2007). Microbes in tailoring of barley properties. Dissertation. University of Helsinki, Finland, 85p.

Laitila, A.; Sarlin, T.; Kotaviita, E.; Huttunen, T.; Home, S.; Wilhelmson, A.; (2007). Yeasts isolated from industrial maltings can suppress *Fusarium* growth and formation of gushing factors. *Journal of Industrial Microbiology and Biotechnology* **34**, 701-713.

Liger-Belair, G.; (2012). The physics behind the fizz in champagne and sparkling wines. *The European Physical Journal Special Topics* **201**, 1-88.

Liger-Belair, G., Polidori, G., Jeandet, P.; (2008). Recent advances in the science of champagne bubbles. *Chemical Society Reviews* **37**, 2490-2511

Liger-Belair, G., Villaume, S.; (2011). Losses of dissolved CO_2 through the cork stopper during champagne aging: toward a multiparameter modeling. *Journal of Agricultural and Food Chemistry* **59**, 4051-4056.

Linder, M.B., (2009). Hydrophobins: proteins that self-assemble at interfaces. *Current Opinion in Colloid Interface Science* **14**, 356-363.

Linder, M., Szilvay, G.R., Nakari-Setälä, T., Soderlund, H., Penttilä, M., (2002). Surface adhesion of fusion proteins containing the hydrophobins HFBI and HFBII from *Trichoderma reesei*. *Protein Science* **11**, 2257-2266.

Linder, M.B., Szilvay, G.R., Nakari-Setälä, T., Penttilä, M.E., (2005). Hydrophobins: the protein-amphiphiles of filamentous fungi. *FEMS Microbiology Reviews* **29**, 877-896.

Lindorff-Larsen, K., Lerche, M.H., Poulsen, F.M., Roepstorff, P., Winther, J.R., (2001). Barley lipid transfer protein, LTP1, contains a new type of lipid-like post-translational modification. *The Journal of Biological Chemistry* **276** (36), 33547-33553.

Lindorff-Larsen, K., Winther, J.R., (2001). Surprisingly high stability of barley lipid transfer protein, LTP1, towards denaturant, heat and proteases. *FEBS Letters* **488**, 145-148.

Lowe, D.P.; Arendt, E.K.; (2004). The use and effects of lactic acid bacteria in malting and brewing with their relationships to antifungal activity, mycotoxins and gushing : a review. *Journal of the Institute of Brewing* **110** (3), 163-180.

Lowe, D.P.; Ulmer, H.M.; Graser, K.; Arendt, A.K.; (2006). The influence of starter cultures on barley contaminated with *Fusarium culmorum* TMW 4.0754. *Journal of the American Society of Brewing Chemists* **64** (3), 158-165.

Lubetkin, S.D.; (2003). Why is it much easier to nucleate gas bubbles than theory predicts? *Langmuir* **19**, 2575-2587.

Lutterschmid, G.; Stübner, M.; Vogel, R.F.; Niessen, L.; (2010). Induction of gushing with recombinant Class II hydrophobin FcHyd5p from *Fusarium culmorum* and the impact of hop compounds on its gushing potential. *Journal of the Institute of Brewing* **116** (4), 339-347.

Lutterschmid, G., Muranyi, M., Stübner, M., Vogel, R.F., Niessen, L., (2011). Heterologous expression of surface-active proteins from barley and filamentous fungi in *Pichia pastoris* and characterization of their contribution in beer gushing. *International Journal of Food Microbiology* **147**, 17-25.

Malvern Technical note. Dynamic light scattering: an introduction in 30 minutes. http://www.malvern.com/common/downloads/campaign/MRK656-01.pdf (12/08/2012)

Marion, D., Bakan, B., (2009). Soluble proteins of beer. In: Beer in Health and Disease Prevention, 265-271.

Müller, M.P.; Schmid, F.; Becker, T.; Gastl, M.; (2010). Impact of different hop compounds on the overfoaming volume of beer caused by primary gushing. *Journal of the Institute of Brewing* **116** (4), 459-463.

Nakari-Setälä, T., Aro, N., Kalkkinen, N., Alatalo, E., Penttilä, M., (1996). Genetic and biochemical characterization of the *Trichoderma reesei* hydrophobin HFBI. *European Journal of Biochemistry* **235**, 248-255.

Nakari-Setälä, T., Aro, N., Ilmen, M., Munoz, G., Kalkkinen, N., Penttilä, M., (1997). Differential expression of the vegetative and spore-bound hydrophobins of *Trichoderma reesei* cloning and characterization of the *hfb2* gene. *European Journal of Biochemistry* **248**, 415-423.

Nelson, C.E.; (2009). Conditions for bubble formation in porous regions and narrow channels. http://www.nelsonresearchinc.com/Work-Bubbles/Bubble%20Formation%20in%20Porrous%20Regions.ppt (15/08/2009)

Neuhof, T., Dieckmann, R., Druzhinina, I.S., Kubicek, C.P., Nakari-Setälä, T., Penttilä, M., von Döhren, H., (2007). Direct identification of hydrophobins and their processing in *Trichoderma* using intact-cell MALDI-TOF MS. *The FEBS Journal* **274**, 841-852.

Noots, I., Delcour, J.A., Michiels, C.W., (1998). From field barley to malt: detection and specification of microbial activity for quality aspects. *Critical Reviews of Microbiology* **25** (2), 121-153.

Nüter, C.; Harms, D., (2009). Particle measurement in beverages-anew tool fors statement on gushing. 32nd Congress of European Brewery Convention, Hamburg, Germany, Abstract.

Oshchepkova, Y.I., Veshkurova, O.N., Rogozhin, E.A., Musolyamov, A.Kh., Smirnov, A.N., Odintsova, T.I., Egorov, Ts. A., Grishin, E.V., Salikhov, Sh.I., (2009). Isolation of the lipid-transporting protein ns-LTP1 from seeds of the garden fennel flower (Nigella sativa). *Russian Journal of Bioorganic Chemistry* **35** (3), 315-319.

Outtrup, H.; (1980). The relation between the molecular structure and gushing potential of dehydrated humulinic acid. *Carlsberg Research Communication* **45**, 381-388.

Paananen, A., Vuorimaa, E., Torkkeli, M., Penttilä, M., Kausanen, M., Ikkala, O., Lemmetyinen, H., Serimaa, R., Linder, M.B., (2003). Structural hierarchy in molecular films of two class II hydrophobins. *Biochemistry* **42** (18), 5253-5258.

Parrinello, M.; (1981). Polymorphic transitions in single crystals: A new molecular dynamics method. *Journal of Applied Physics* **52**, 7182–7190. doi:10.1063/1.328693

Pellaud, J., (2002). Gushing: State of the art. *Cerevisia Belgian Journal of Brewing and Biotechnolgy* **27** (4), 189-205.

Polidori, G., Jeandet, P., Liger-Belair, G.; (2009). Bubbles and low patterns in champagne. *American Scientist* **97**, 294-301.

Qin, M., Hou, S., Wang, L.K., Feng, X.Z., Wang, R., Yang, Y.L., Wang, C., Yu, L., Shao, B., Qiao, M.Q.; (2007). Two methods for glass surface modification and their application in protein immobilization. *Colloids Surfaces B: Biointerfaces* **60**, 243-249.

Rath, F., 2008. Investigations to improve the reproducibility of the "Modified Carlsberg Test". The Gushing Day, Brussels.

Ravve, A., Wilt, P.M.; (1982). Container having internal wall surfaces modified to reduce carbonation loss. US Patent 4311250.

Reichelt, W.H., Ek, J., Stensrud, M., Reichelt, K.L., (1998). Peptide excretion in celiac disease. *Journal of Pediatric Gastroenterology and Nutrition* **26**, 305-309.

Rogers, L.; (2005). Randomness and Brownian motion. http://nrich.maths.org/6127 (12/08/2012).

Rouse, S.; Harnett, D.; Vaughan, A.; van Sinderen, D.; (2008). Lactic acid bacteria with potential to eliminate fungal spoilage in foods. *Journal of Applied Microbiology* **104**, 915-923.

Sahu, K.K., Hazama, Y., Ishihara, K.N.; (2006). Gushing in canned beer: the effect of ultrasonic vibration. *Journal of Colloid and Interface Science* **302**, 356-362.

Sarlin, T.; Nakari-Setälä, T.; Linder, M.; Penttilä, M.; Haikara, A.; (2005). Fungal hydrophobins as predictors of the gushing activity of malt. *The Journal of the Institute of Brewing* **111** (2), 105-111.

Sarlin, T.; Vilpola, A.; Kotaviita, E.; Olkku, J.; Haikara, A.; (2007). Fungal hydrophobins in the barley-to-beer chain. *The Journal of the Institute of Brewing* **113** (2), 147-153.

Sarlin, T.; Kivioja, T.; Kalkkinen, N.; Linder, M.B.; Nakari-Setälä, T.; (2011). Identification and characterization of gushing-active hydrophobins from Fusarium graminerum and related species. *Journal of Basic Microbiology* **51**, 1-11.

Sartor, M.; (2010). Dynamic light scattering to determine the radius of small beads in Brownian motion in a solution. http:///physics.ucsd.edu/neurophysics/courses/physics_173_273/dynamic_light_scattering_03.pdf (12/08/2012)

Scholtmeijer, K., (2000). Expression and engineering of hydrophobin genes. Dissertation, University of Groningen, The Netherlands, 110p.

Shokribousjein, Z.; Deckers, S.M.; Gebruers, K.; Lorgouilloux, Y.; Baggerman, G.; Verachtert, H.; Delcour, J.A.; Etienne, P.; Rock, J-M.; Michiels, C.; Derdelinckx, G.; (2010). Hydrophobins, beer foaming and gushing. *Cerevisia Belgian Journal of Brewing and Biotechnology* **35**, 85-101.

Sorensen, S.B., Bech, L.M., Muldbjerg, T., Breddam, K., (1993). Barley lipid transfer protein 1 is involved in beer foam formation. *Technical Quaterly MasterBrewers Association of the Americas* **30** (4), 136-145. Abstract

Sossountzov, L., Ruiz-Avila, L., Vignots, F., Jolliot, A., Arondel, V., Tchang, F., Grosbois, M., Guerbette, F., Miginiac, E., Delseny, M., Puigdomenech, P., Kader, J-C., (1991). Spatial andtemporal expression of a maize lipid transfer protein gene. *The Plant Cell* **3**, 923-933.

Source 15RPC GE Healthcare amersham biosciences product data sheet. http://www.biocompare.com/ProductDetails/34970/SOURCE-15RPC-ST-46-100.html

Stuart, V., Craig, J.; (2011). Very small bubbles at surface – the nanobubble puzzle. *Soft Matter* **7**, 40-48.

Szilvay, G.R., (2007). Self-assembly of hydrophobin proteins from the fungus *Trichoderma reesei*. Academic Dissertation, VTT Technical Research Centre of Finland, Finland, 64p

Szilvay, G.R., Nakari-Setälä, T., Linder, M.B., (2006). Behavior of *Trichoderma reesei* hydrophobins in solution: Interactions, Dynamics, and multimer formation. *Biochemistry* **45** (28), 8590-8598.

Szilvay, G.R., Kisko, K., Serimaa, R., Linder, M.B., (2007a). The relation between solution association and surface activity of the hydrophobin HFBI from *Trichoderma reesei*. *FEBS Letters* **581**, 2721-2726.

Szilvay, G.R., Paananen, A., Laurikanen, K., Vuorimaa, E., Lemmetyinen, H., Petonen, J., Linder, M.B., (2007b). Self-assembled hydrophobin protein films at the air-water interface: structural analysis and molecular engineering. *Biochemistry* **46** (9), 2345-2354.

Valant, K-M.; (2005). Hétéronucléation des bulles dans les liquides sursaturés and CO_2. Université de Marne-la-Vallée, France, 162p.

Vinh, J., (1999). Etude et caractérisation structurale de modifications post-traductionnelles de la tubuline par spectrométrie de masse. Dissertation académique, Université Pierre et Marie Curie – Paris VI, 85 pp.

Vörös, J.; (2004). The density and refractive index of adsorbing protein layers. *Biophysical Journal* **87**, 553-561.

Wang, X., Shi, F., Wösten, H.A.B., Hektor, H., Poolman, B., Robillard, G.T., (2005). The SC3 hydrophobin self-assembles into a membrane with distinct mass transfer properties. *Biophysical Journal* **88**, 3434-3443.

Wessels, J.G., de Vries, O.M., Asgeirsdottir, S.A., Springer, J., (1991). The thn mutation of *Schizophyllum commune* which suppresses formation of aerial hyphae, affects expression of the Sc3 hydrophobin gene. *Journal of General Microbiology* **137**, 2439-2445.

Wilson, S.M., (1999). A study of gushing in ciders: its mechanism and causative effect. Dissertation, University of Guelph, Canada, 168p.

Winkelmann, L.; Hinzmann, E.; (2009). The gushing-puzzle – Parts are still missing. *Brauwelt International* **27**, 13-15.

Wolf-Hall, C.E.; (2007). Mold and mycotoxin problems encountered during malting and brewing. *International Journal of Food Microbiology* **119**, 89-94.**Wösten, H.A.B.,** (2001). Hydrophobins: multipurpose proteins. *Annual Review in Microbiology* **55**, 625-646.

Wösten, H.A.B., (2001). Hydrophobins: multipurpose proteins. *Annual Review in Microbiology* **55**, 625-646.

Wösten, H.A.B., de Vocht, M.L., (2000). Hydrophobins, the fungal coat unravelled. *Biochimica et Biophysica Acta* **1469**, 79-86.

Yang, J., Duan, J., Fornasiero, D., Ralston, J.; (2007). Kinetics of CO_2 nanobubble formation at the solid/water interface. *Physical Chemistry Chemical Physics* **9**, 6327-6332.

Yount, D.E., Gillary, E.W., Hoffman, D.C.; (1984). A microscopic investigation of bubble formation nuclei. *Journal of the Acoustical Society of America* **76** (5), 1511-1521.

Zapf, M.W., Theisen, S., Vogel, R.F., Niessen, L., (2006). Cloning of wheat LTP1500 and two *Fusarium culmorum* hydrophobins in *Saccharomyces cerevisiae* and assessment of their gushing inducing potential in experimental wort fermentation. *Journal of the Institute of Brewing* **112** (3), 237-245.

Zhang, X.L.; Penfold, J.; Thomas, R.K.; Tucker, I.M.; Petkov, J.T.; Bent, J.; Cox, A.; Campbell, R.A.; (2011). Adsorption behavior of hydrophobin and hydrophobin/surfactant mixtures at the air-water interface. *Langmuir* **27**, 11316-11323.

Zoecklein, B., (1999). A review of méthode champenoise production. Virginia Polytechnic Institute and State University (USA), Publication number 463-017.

http://s2.e-monsite.com (13/08/2012)
http://www.scienceisart.com/A_Diffus/DiffusMain_1.html (10/05/2010)
http://www.brookhaven.co.uk/dynamic-light-scattering.html (10/05/2010)
http://www.proteinchemist.com/dls/dls.html (10/05/2010)
http://www.bic.com/DLSBasics.html (10/05/2010)
http://blast.ncbi.nlm.nih.gov/Blast.cgi (03/03/2010)

List of publications

Publication in international peer-reviewed journals

Khalesi, M.; Venken, T.; **Deckers, S.M.**; Winterburn, J.; Shokribousjein, Z.; Gebruers, K.; Verachtert, H.; Delcour, J.; Martin, P.; Derdelinckx, G.; (2013). A novel method for hydrophobin extraction using CO_2 foam fractionation system. *Industrial Crops and Products* **43**, 372-377.

Deckers, S.M.; Venken, T.; Khalesi, M.; Gebruers, K.; Baggerman, G.; Lorgouilloux, Y.; Shokribousjein, Z.; Ilberg, V.; Schönberger, C.; Titze, J.; Verachtert, H.; Michiels, C.; Neven, H.; Delcour, J.; Martens, J.; Derdelinckx, G.; DeMaeyer, M.; (2012). Combined modeling and biophysical characterisation of CO_2 interaction with Class II hydrophobins : new insight into the mechanism underpinning primary gushing. *Journal of the American Society of Brewing Chemists* **70** (4), 249-256.

Deckers, S.M.; Lorgouilloux, Y.; Gebruers, K.; Baggerman, G.; Verachtert, H.; Neven, H.; Michiels, C.; Derdelinckx, G.; Delcour, J.; Martens, J.; (2011). Dynamic Light Scattering (DLS) as a tool to detect CO_2-hydrophobin structures and study the primary gushing potential of beer. *Journal of the American Society of Brewing Chemists* **69** (3), 144-149.

Deckers, S.M.; Gebruers, K.; Baggerman, G.; Lorgouilloux, Y.; Delcour, J.; Michiels, C.; Derdelinckx, G.; Martens, J.; (2010). CO_2-hydrophobin structures acting as nanobomb in beer. *Brewing Science* **63** (03/04), 54-61.

Publication in other journals with academic editorial board

Deckers, S.M.; Vissers, L.; Gebruers, K.; Shokribousjein, Z.; Khalesi, M.; Riveros-Galan, D.; Schönberger, C.; Verachtert, H.; Neven, H.; Delcour, J.; Michiels, C.; Ilberg, V.; Derdelinckx, G.; Titze, J.; Martens, M.; (2012). Doubly Modified Carlsberg Test combined with Dynamic Light Scattering allows prediction of the primary gushing potential of harvested barley and malt. *Cerevisia Belgian Journal of Brewing and Biotechnology* **37**, 77-81.

Khalesi, M.; **Deckers, S.M.**; Gebruers, K.; Vissers, L.; Verachtert, H.; Derdelinckx, G.; (2012). Hydrophobins: exceptional proteins for many applications in brewery environment and other bio-industries. *Cerevisia Belgian Journal of Brewing and Biotechnology* **37**, 3-9.

Shokribousjein, Z.; **Deckers, S.M.**; Gebruers, K.; Lorgouilloux, Y.; Baggerman, G.; Verachtert, H.; Delcour, J.; Etienne, P.; Rock, J-M.; Michiels, C.; Derdelinckx, G.; (2010). Hydrophobins, beer foaming and gushing. *Cerevisia Belgian Journal of Brewing and Biotechnology* **35**, 81-101.

Congress proceedings

Deckers, S.M.; Schönberger, C.; Titze, J.; Ilberg, V.; Derdelinckx, G.; (2012). Primary gushing : the explosive love story between CO_2 and hydrophobin. World Brewing Congress. Portland, Oregon, USA, 28th July – 1st August 2012. Oral presentation 21.

Deckers, S.M.; Vissers, L.; Riveros-Galan, D.; Derdelinckx, G.; Titze, J.; Ilberg, V.; Schönberger, C.; Shokribousjein, Z.; Verachtert, H.; Gebruers, K.; Neven, H.; Rock, J-M.; (2012). Thermodynamic properties of primary gushing of beer. World Brewing Congress. Portland, Oregon, USA, 28th July – 1st August 2012. Poster 110.

Herrmann, A.; Titze, J.; Schönberger, C.; **Deckers, S.M.**; Derdelinckx, G.; Ilberg, V.; (2012). Hop and hop substances – Induction, reduction or suppression of gushing? World Brewing Congress. Portland, Oregon, USA, 28th July – 1st August 2012. Poster 148.

Deckers, S.M.; Gebruers, K.; Shokribousjein, Z.; Khalesi, M.; Vissers, L.; Riveros-Galan, D.; Venken, T.; Verachtert, H.; Michiels, C.; Martens, J.; DeMaeyer, M.; Derdelinckx, G.; Delcour, J.; (2012). Beer primary gushing : the mechanism of a world wide major concern scientifically unraveled. Knowledge for Growth, Flanders Bio's annual life sciences convention. Gent, Belgium, 24th May 2010. Poster and oral presentation

Shokribousjein, Z.; Bajoulkakahi, F.; Riveros-Galan, D.; Gebruers, K.; **Deckers, S.M.**; Verachtert, H.; Michiels, C.; Delcour, J.; Derdelinckx, G.; (2012). Differences between hydrophobic patches of Class II hydrophobins – a review. 10th Trends in Brewing. Gent, Belgium, 1st – 5th April 2012. Poster presentation

Khalesi, M.; **Deckers, S.M.**; Gebruers, K.; Verachtert, H.; Martin, P.; Derdelinckx, G.; (2012). New approach to isolate hydrophobin HFBII. ChemCys. Blankenberg, Belgium, 1st – 2nd March 2012. Oral presentation

Deckers, S.M.; Shokribousjein, Z.; Khalesi, M.; Lorgouilloux, Y.; Gebruers, K.; Baggerman, G.; Martens, J.; Delcour, J.; Michiels, C.; Derdelinckx, G.; (2011). Application of dynamic light scattering technique to detect primary gushing potential from barley to finished beer. 74th ASBC Annual Meeting. Fort Myers, Florida, USA, 11th – 15th June 2011. Poster 50.

Deckers, S.M.; Khalesi, M.; Shokribousjein, Z.; Gebruers, K.; Lorgouilloux, Y.; Baggerman, G.; Verachtert, H.; Delcour, J.; Michiels, C.; Martens, J.; Derdelinckx, G.; (2011). Physico-chemistry and thermodynamic involved by primary gushing. 33rd International Congress of the European Brewery Convention. Glasgow, Scottland, 22nd – 26th May 2011. Poster 37.

Deckers, S.M.; Khalesi, M.; Shokribousjein, Z.; Gebruers, K.; Baggerman, G.; Verachtert, H.; Delcour, J.; Michiels, C.; Derdelinckx, G.; Martens, J.; (2011). Microbiology and Biochemistry of primary gushing. Annual Meeting of Belgian Nutrition Society. Brussels, Belgium, 29th April 2011. Poster presentation

Deckers, S.M.; Gebruers, K.; Baggerman, G.; Lorgouilloux, Y.; Martens, J.; Delcour, J.; Michiels, C.; Derdelinckx, G.; (2010). Primary gushing of over-carbonated beverages: Mechanism and new detection method. Ph.D. Symposium, Gent, Belgium, 20th December 2010. Poster presentation.

Deckers, S.M.; Gebruers, K.; Baggerman, G.; Lorgouilloux, Y.; Delcour, J.; Martens, J.; Michiels, C.; Derdelinckx, G.; (2010). Primary gushing of over-carbonated beverages such as Belgian specialty beers. LFoRCe Symposium, Leuven, Belgium, 19th November 2010. Poster presentation.

Deckers, S.M.; Gebruers, K.; Baggerman, G.; Lorgouilloux, Y.; Van der Vliet, P.; Delcour, J.; Michiels, C.; Derdelinckx, G.; Martens, J.; (2010). Are magnetic fields a technical opportunity to influence the structure of CO_2 nanobubbles responsible for primary gushing in beer? 73rd ASBC Annual Meeting. Providence, Rhodes Island, USA, 15th – 18th June 2010. Poster 47.

Deckers, S.M.; Gebruers, K.; Baggerman, G.; Lorgouilloux, Y.; Van der Vliet, P.; Michiels, C.; Delcour, J.; Martens, J.; Derdelinckx, G.; (2010). Contribution of magnetic fields on CO_2 binding in carbonated beverages and in beers. Knowledge for Growth, Flanders Bio's annual life sciences convention. Gent, Belgium, 20th May 2010. Poster presentation

Deckers, S.M.; Gebruers, K.; Baggerman, G.; Lorgouilloux, Y.; Delcour, J.; Martens, J.; Michiels, C.; Derdelinckx, G.; (2010). Understanding of the primary gushing mechanism in over-carbonated beverages. Ph.D. Interaction Day, Leuven, Belgium, 23rd April 2010. Poster presentaiton.

Deckers, S.M.; Gebruers, K.; Baggerman, G.; Lorgouilloux, Y.; Delcour, J.; Martens, J.; Michiels, C.; Derdelinckx, G.; (2010). A method for detection of beer gushing at brewing scale. 9th Trends in Brewing. Gent, Belgium, 13th – 16th April 2010. Poster presentation

Patent

Derdelinckx, G.; **Deckers, S.M.**; Khalesi, M.; Martens, J.; Rongé, J.; Gebruers, K.; Delcour, J.; Venken, T.; DeMaeyer, M. Patent ZL912012 Hydrophobin purification.

Derdelinckx, G.; **Deckers, S.M.**; Khalesi, M.; Shokribousjein, Z.; Verachtert, H. Patent GB1217972.7 Bottle with means to prevent gushing.